Modelling and Design Optimization of Low Speed Fuel Cell Hybrid Electric Vehicles

by

Matthew Blair Guenther
B.Eng. University of Victoria, 2001

A Thesis Submitted in Partial fulfillment of the Requirements for the Degree of

MASTER OF APPLIED SCIENCE

in the Department of Mechanical Engineering

Supervisors: Dr. Zuomin Dong

Supervisors: Dr. Zuomin Dong

ABSTRACT

Electric vehicles, as an emerging transportation platform, have been introduced over the past several decades due to various concerns about air pollution and the contribution of emissions to global climate change. Although electric cars and buses have been the focus of much of electric vehicle development, smaller low-speed electric vehicles are used extensively for transportation and utility purposes in many countries. In order to explore the viability of fuel cell - battery hybrid electric vehicles, empirical fuel cell system data has been incorporated into the NREL's vehicle design and simulation tool, ADVISOR (ADvanced Vehicle SimulatOR), to predict the performance of a low-speed, fuel cell - battery electric vehicle through MATLAB Simulink. The empirical fuel cell system data are obtained through systematic tests of a 1.2 kW Proton Exchange Membrane (PEM) fuel cell stack that is used as the power plant for a fuel cell - battery hybrid electric scooter. The modelling and simulation of the fuel cell electric scooter using new performance modules built using ADVISOR provide valuable feedback to the design, and a platform for the design optimization of the fuel cell power system. Various optimization methods, including a sampling based optimization algorithm, were used to explore the viability and options of a low cost design for urban use. This study serves as the foundation for further research on the modeling and design optimization of PEM fuel cell power system, and fuel cell powered, low speed electric vehicles.

TABLE OF CONTENTS

LIST OF TABLES

LIST OF FIGURES

ACKNOWLEDGEMENT

The authour would like to thank several people for their generous help in completing this thesis, first and foremost, my supervisor Dr. Zuomin Dong for choosing such an interesting area of research and providing me with excellent guidance over the course of my work at the University. I would also like to express my gratitude to Dr. Jean-Marc Le Canut for his patient education and troubleshooting of the fuel cell test stand and instrumentation system. Finally, the assistance of Greg Iuzzolino for his help transferring the fuel cell data into MatLab code and Sezer Tezcan's work with the vehicle dynamometer/test stand was invaluable.

CHAPTER 1 INTRODUCTION

1.1. General Background

Over the past decade, research and development of electric vehicles have attracted significant attention due to various concerns about air pollution and the contribution of emissions to global climate change. To overcome the inherent limitations of short range and long charge time, fuel cell powered electric vehicles have been considered as an ultimate and ideal solution over the traditional battery powered electric vehicles. Although electric cars and buses have been the focus of much of electric vehicle development, smaller vehicles are used extensively for transportation and utility purposes in many countries.

In order to explore the viability of fuel cell - battery hybrid electric vehicles, the system performance and simulation models of low speed fuel cell hybrid electric vehicles are introduced in this research. The introduced vehicle model was created based on the NREL's vehicle design and simulation tool, ADVISOR (ADvanced Vehicle SimulatOR), which consists of a modular framework that enables a wide variety of conventional and hybrid vehicles to be simulated on a personal computer. ADVISOR was modified to simulate fuel cell power plants based on a theoretical model developed at the University of Victoria (UVic) and experimental data obtained from an appropriately sized fuel cell stack. The empirical fuel cell system data are obtained through systematic tests of a 1.2 kW Proton Exchange Membrane (PEM) fuel cell stack that is used as the power plant for a fuel cell – battery hybrid electric scooter. With the verification of fuel cell tests, the fuel cell system and vehicle performance model is used as an accurate and effective design tool to explore the performance and cost envelope of these types of vehicles. Various optimization methods, including a sampling based optimization algorithm, are used to explore the viability and options of a low cost design for urban use. The results of the design optimization are presented in this thesis.

This study serves as the foundation for further research on the modeling and design optimization of PEM fuel cell power system, and fuel cell powered, low speed electric vehicles. There exist several reasons for the use of fuel cells as a vehicle power plant, although this research found that the most compelling often depends greatly on the point of view of the researcher. These arguments are somewhat inter-dependent, however they are split for convenience into the Air Pollution, Energy System and Global Climate Change sections.

1.1.1. Air Pollution

Interest in electric vehicles has increased in the past several decades due in part to several reasons. The initial motivation for the development of commercial electric vehicles came from the realization of the health problems associated with urban air pollution [1]. This caused a desire by many municipal and provincial governments to reduce the problem of urban air pollution, of which transportation is a major cause. As urban density and development has increased around the world, the issue of urban air quality deterioration due to transportation emissions has become a global problem. The regulatory pressure exerted on automobile manufacturers has resulted in higher fuel-efficiency engines, lighter and more aerodynamic cars and the widespread deployment of technologies such as the catalytic converter. Additionally it provided the impetus for research into the feasibility of producing electric cars to compete with and supplant those powered by internal combustion engines.

In a bid to completely eliminate automobile emissions several car manufacturers developed electric car prototypes, and although the on-road performance was acceptable they all suffered from problems with energy storage and replenishment. The initial designs used lead-acid and nickel-cadmium batteries to st ore energy, however they had a limited capacity compared to the amount of energy that could be stored in a conventional car using liquid gasoline. Furthermore, the time needed to replenish the energy in the car was dramatically longer, since batteries require a slow recharging process that can take hours while conventional automobiles can completely fill a tank of gasoline in minutes.

The ability of fuel cells to solve this particular technological problem of providing electricity while producing no harmful emissions has resulted in intense focus on using them as vehicle power plants. Automotive companies believe that if fuel cells can be made to work well enough they will be able to produce zero tailpipe-emission electric vehicles without the previously mentioned recharging time and range limitations.

1.1.2. Global Climate Change

In addition to the relatively localized problem of air pollution and quality, there is the somewhat controversial global problem of carbon dioxide produced climate change.

There has been a great deal of research into the effects of carbon dioxide emissions on the climate, at first independently under the label of global warming research, and then as further insights about the possible global effects were gained, as global climate change.

In 1995 under the auspices of the UN an international panel of scientists, the Intergovernmental Panel on Climate Change (IPCC) published [2] a study examining existing research and climate modelling to attempt to predict whether carbon dioxide emissions were having an effect on the climate and what types of changes that might bring in the future. Of their many determinations they found that anthropogenic carbon emissions were currently having a measurable effect on the temperature of the climate, and their predictions were that it would continue to do so unless action is taken to drastically reduce the level of emissions. Partially as a result of their findings, the Kyoto treaty was developed to attempt to get nations to start reducing their carbon dioxide emissions.

One of the major contributors to carbon dioxide emissions is the transportation sector, accounting for between 40-50%. Although there has been some progress in reducing the emissions of internal combustion vehicles through both improved engine technology and hybridization, this is at best a half-measure of decreasing transportation emissions. If further reductions are desired a promising approach would be the widespread adoption of electrical vehicles. Electrical vehicles utilizing batteries would satisfy a zero-emission requirement however currently they fall far short of reaching performance specifications

for a consumer automobile and there do not seem to be any technologies that could change this. Fuel cells running on hydrogen would enable automobiles to be zero-emission vehicles while retaining the endurance and refueling characteristics of current models. The transition to hydrogen would not eliminate all related carbon emissions, since the production of hydrogen generally still requires electricity from polluting sources. However the centralization of these emissions would still result in a net reduction due to efficiencies of scale while providing an avenue for further reductions through alternative electricity sources or hydrogen production methods.

1.1.3. Energy System/Hydrogen Economy

In addition to the potential for local air quality improvements, fuel cells are attractive as vehicle power plants for several more far-reaching reasons. The use of hydrogen as a vehicle fuel presents the potential for a number of interesting energy system infrastructure changes.

Currently our energy system is divided into two broad areas, the electricity grid which is used to power most of our stationary technology, and the transportation fuel infrastructure which provides energy for our mobile technology needs. There is some overlap in the realm of batteries but they have significant problems for most conventional transportation applications. Although we are able to provide electricity for our daily domestic, commercial and industrial needs from a variety of primary sources such as hydro, coal and nuclear we are essentially limited to oil for our transportation system.

Hydrogen presents the unique opportunity to greatly increase the overall flexibility of the energy system since it can readily be produced from water and electricity via electrolysis. Since the electricity can be obtained from a variety of sources this would have the effect of integrating the energy requirements for transportation into the current electrical grid. This concept has been developed by many including Scott et al. [3, 4] and termed the hydrogen economy. This scenario would help reduce reliance on foreign petroleum sources for transportation energy requirements, instead allowing for the most appropriate generation technology for a region satisfy the given need. Also the hydrogen economy

would create the opportunity for a partially hybrid electricity grid through the use of large-scale hydrogen storage.

The primary disadvantage to the hydrogen economy at the moment is the inefficiency of the electrolysis process, which increases the cost of electrolytic hydrogen relative to reformed hydrogen. However as electrolysis technology improves the potential remains for this cost difference to decrease and make a good case for a dual electricity-hydrogen energy system.

1.2. Hydrogen Fuel Cells - an Alternative Solution

Fuel cells are electrochemical devices that convert the chemical energy of a fuel stream directly into electricity. Although the recent focus on them as a potential source of vehicle power plants has resulted in the popular perception that they are new technology, they were first developed by Sir William Grove in 1839. As one of the initial pioneers of electrochemistry, Grove had the insight that it might be possible to modify an electrochemical cell to use inert electrodes and use an external supply of reactant to produce electricity without changing the structure of the cell. Although they were demonstrated, the technical problems relative to simpler cells relegated them to a laboratory curiosity.

Fuel cells did not find any major practical use until the U.S. space program started to use them to power their spacecraft. When faced with the problem of powering the spacecraft fuel cells were brought up as a possible solution. They could use the two reactants already carried on a spacecraft for propulsion, hydrogen and oxygen, produce electricity to run the ship and as a byproduct provide drinking water for the crew. In addition they provided a higher power density relative to existing batteries, which is an important constraint on space-bound technologies. Although successful in the space program, they remained confined to that limited application afterwards for several decades.

Presently, the capacity and recharging limitations of batteries for powering vehicles resulted in a technological niche that fuel cells are uniquely suited to. As electrochemical devices, when run on hydrogen they can produce electricity via direct energy conversion

at high efficiency with no harmful emissions. However, they solve the largest problems with batteries by allowing refueling instead of recharging which greatly decreases turn around time. Additionally the use of a fuel to store energy increases the energy storage capacity and the range of the vehicle.

The desire to find a fuel cell suitable for use in vehicles has led to the rapid development of the Polymer-Electrolyte Membrane (PEM) fuel cell. Where most early fuel cells designs relied on a liquid electrolyte (e.g. the alkaline fuel cells used in the Apollo missions), the electrolyte for PEM fuel cells is based on a polytetrafluoroethelyne (PTFE) membrane. The use of a solid polymer electrolyte resulted in a cell that was able to operate at lower temperatures and without many reliability issues that occurred with liquid electrolytes.

Despite this development, fuel cells still require a great deal of progress before they will be competitive with conventional automobile power plants. Current commercially available fuel cell designs are able to produce electricity at a density of approximately 26 W/L and 92 W/kg [6], including the balance of plant necessary to operate the fuel cell. In contrast, modern internal combustion engine power densities are on the order of 500 W/kg or higher. The durability of fuel cells is also much lower than conventional alternatives, the current lifetimes of 1500 h of continuous operation do not meet the 5000 h that is generally seen for engines used in consumer automobiles.

1.3. Low Speed Electric Vehicles

1.3.1. Definition, Scope and state of the art

For the purposes of this thesis, low-speed electric vehicles consist of transportation or utility vehicles designed for use in urban driving conditions or slower, such as scooters, golf carts and indoor forklifts. These vehicles are very widespread although they do not have the high visibility of mass transportation applications such as automobiles and buses. Despite the potential for niche utility applications the range and recharging turnaround time limitations of battery energy storage have prevented more widespread adoption and general use of these vehicles.

1.3.2. Vehicle Performance Characteristics

The typical performance capabilities of this category of vehicle vary depending on application, but tend to share several characteristics due to the limits of the technology. Generally power plants vary in size from 1 to 10 kW, with the small energy sources used for light duty use such as bicycles and scooters, while the larger range of power plants are used by utility vehicles. This power plant generally propels the vehicle at a maximum speed of between 30 to 50 km/h, although this is dependent on the typical duty cycle of the vehicle. Due to the characteristics of the electric motors used in the drive train, these vehicles exhibit high low-end torque which results in high acceleration capability. Powerful acceleration is an important attribute that is required by the typical duty cycles encountered by low-speed vehicles and is another reason why they have become popular in certain niche markets.

The other major characteristics exhibited by battery powered electric vehicles are their limited endurance and long turnaround time. Depending on the type of onboard battery pack, vehicles can often only operate continuously for a few hours before requiring an eight or twelve hour recharge. Additionally memory effects can degrade the performance of the battery if careful charging and discharging precautions are not taken. This can result in additional maintenance costs and require the replacement of the battery after a short period of service. Due to these factors the energy storage system has an overwhelming influence on the design and performance of the vehicle. Typically battery powered vehicles are heavier and bulkier than conventional alternatives due to the weight of the energy storage system. However for many applications the unique qualities of these vehicles with zero emissions and quiet operation are necessary enough to warrant the extra expense and complexity.

1.4. Hybrid Vehicles

Hybrid vehicles represent a revolutionary change in vehicle design. The fundamental difference is the addition of a large scale energy storage system to the vehicle. In concert with the addition of the energy storage system, the internal combustion engine is decoupled from the drive train and instead used to drive a generator. This modification

creates an electrical drive train that integrates the gasoline engine and battery into a functionally single power source. By using the energy storage system as a buffer, the engine can be operated at its most efficient condition and reduced in size while maintaining the overall performance of the vehicle. As a consequence of the reduced size and more efficient operating condition, the fuel usage and emissions of the vehicle are dramatically lower than comparable conventional vehicles.

In addition to the obvious benefits of reduced emissions for hybrid designs, another benefit of hybridization is the change of the drive train architecture. Although early internal combustion hybrid designs retained a conventional drive layout (i.e. a driveshaft and differential to the drive wheels), the nature of the hybrid design led to the possibility of a completely electrical drive train. Transferring power via electrical means offers increased flexibility in vehicle design, which is being exploited by a number of vehicle designs. GM's Hi-Wire concept car illustrated a number of these ideas, with independent hub wheel motors and a modular chassis design that would reduce manufacturing costs and enable rapid customization.

1.4.1. Energy Storage

The major innovation of hybrid vehicle design is the use of a large energy storage system to act as a buffer between the power demands of the drivetrain and the output of the electrical generator. It can also be used in conjunction with the generator to provide short duration boosts of high power such as those experienced during acceleration. The principle of an energy buffer has been used in conventional vehicles for many years with engine flywheels; however the more flexible electric drivetrain enables much larger amounts of energy to be stored in batteries and ultracapacitors.

Battery

Most energy storage systems for modern hybrid vehicles use some form of electrochemical battery due to their considerable storage capacity and well-understood behavior. Advanced types of rechargeable batteries such as nickel-metal hydride or lithium-ion cells are commonly used. Due to the imposed duty cycle, it is important that the type of battery chosen has a high tolerance for being repeatedly charged and

discharged without adverse effects on performance. Physical dimensions and weight are also important considerations as the batteries often represent a major portion of the mass and bulk of the vehicle.

Ultracapacitor

A new alternative to conventional batteries has recently been developed which involves using a new type of capacitor to store energy from the engine. These capacitors use a different design that shares some characteristics with batteries, allowing them to store a much larger charge than ordinary capacitors. Although they do not have quite as large a capacity as batteries, ultracapacitors have significantly better dynamic performance and do not have any memory effects that can hamper their long term performance. Given the duty cycle of frequent and rapid charging and discharging that is imposed on hybrid energy storage systems, ultracapacitors are ideally suited for this application. However they are relatively new technology and therefore tend to be more expensive than batteries for an equivalent energy capacity requirement.

1.4.2. Motor

Hybrid vehicles require some form of electric motor to transfer the power generated in the rest of the vehicle to the wheels. The motor has a direct effect on the performance of the vehicle since it determines the acceleration and maximum speed as well as affecting other values such as the overall fuel efficiency. Once the motor is selected based on the given vehicle performance requirements, it becomes possible to determine the size of fuel cell and battery required to supply it with electricity.

The type of motor used can vary depending on the power system of the vehicle and its size. Current internal combustion hybrid cars tend to use AC induction motors due to both the power requirements and the generally increased efficiency over commutated DC motors. However for smaller low-speed vehicles the desire would be to use some form of DC motor to decrease the overall complexity of the vehicle. The use of a DC motor would reduce the power conditioning requirements by eliminating the need for an inverter from DC to AC power. Despite being slightly less efficient, the reduced expense

and balance of plant obtained by using DC motors makes them more suitable for low-speed hybrid vehicles.

1.5. Hydrogen Fuel Cell Vehicles

Fuel cell vehicles are still being prototyped by various car and vehicle manufacturers. The motivation for their design has resulted primarily from the poor endurance of battery-powered electric vehicles. Fuel cells are capable of providing DC electric power like batteries while having lower weight and greater vehicle range through the use of a fuel for energy storage.

Fuel cell vehicles are also well-suited to hybrid technology since they already require an electric drivetrain. Hybridization can bring similar benefits to those experienced by internal combustion vehicles, since the energy storage system allows the fuel cell to operate closer to its ideal operating point while the energy demands of the vehicle vary. Since fuel cells have generally been proposed for urban use, some method of compensating for the rapidly changing power demands of the drivetrain would be beneficial to the fuel cells performance and lifetime.

The use of a hybrid design in the vehicle also creates the potential for a significant reduction in the size of the fuel cell, and the investment cost of the vehicle. The periods of highest power demand for a vehicle only occur during acceleration, however with a hybrid design the battery can be used to compensate for these peak loads while the fuel cell can be sized for the smaller base cruising load. Since the cost of fuel cells is still quite high, anything that can reduce its size will have the effect of significantly reducing the overall cost of the vehicle. Although the batteries are an additional cost to a hybrid design over a conventional powertrain, the fuel cell is such a disproportionately.

1.5.1. Fuel Storage

Fuel storage poses a considerable challenge with the current fuel cell vehicles. Although hydrogen has a high energy density by mass, as a gas its volumetric density is very poor. Depending on the operation of the vehicle just over 500 grams of hydrogen is required to

provide enough fuel for a range of 100 km. However at atmospheric pressure this hydrogen would occupy approximately 6340 L. There are two currently viable storage techniques for vehicular hydrogen, compressed and metal hydride cylinders.

Compressed Storage

Compressed hydrogen is the traditional technique for storing gases, and is commonly used in many hydrogen storage applications. The main advantages are the relative simplicity of the storage system, and the generally low weight of the cylinder. Disadvantages include the energy cost needed to compress the gas to the required storage pressure and the safety issues encountered when storing compressed gas.

Current storage cylinders store the hydrogen at a pressure of between 172 and 206 bar (2500 to 3000 psi), which requires a cylinder of between 39.4 - 33.5 L for 500 g of hydrogen. Although this is dramatically smaller than the volume at atmospheric pressure, it remains difficult to accommodate in a small vehicle. Recent technology has been developed to allow storage at pressures up to 5000 psi, which would further reduce the volume to 21.7 L. Storage at higher pressures is possible but the difficulty lies in producing a pressure vessel that is economical and does not weigh so much that it eliminates the benefits of the increased pressure. Lightweight composite cylinders have been developed by companies such as Dynetek for storage pressures of up to 10000 psi in mobile applications; however they are still more expensive than conventional cylinders.

Liquefied Storage

Liquefied hydrogen storage is a mechanical storage technique similar to compressed hydrogen, however due to the phase change can achieve higher storage densities. Although currently not favoured due to the difficulties of liquefying hydrogen, this method is being pursued by many since it has both high volumetric density and low mass. Additionally liquid storage would reduce the risk of explosion or ignition of the hydrogen, since it is not flammable in a liquid phase. However the reduced explosion risk is somewhat offset by the hazards of storing and transporting a cryogen which could cause severe skin damage or asphyxiation if the container were breached in a crash.

Metal Hydride Storage

Metal hydride storage is an interesting alternative to conventional storage methods, utilizing chemical rather than mechanical properties to increase the storage density of the hydrogen. The storage system works by filling a container with a powdered alloy, usually made up from various metals such as titanium, iron, manganese *etc.* When exposed to hydrogen the metal tends to bond with it in a reversible reaction:

$$M + H_2 \leftrightarrow MH_2 \tag{1.5.1}$$

The reaction produces a metal hydride, which can store hydrogen at a very high volumetric density due to the compact atomic structure of the metal. Several types of metal hydrides can reach a volumetric storage density higher than that of liquefied hydrogen. Unfortunately the mass the storage system is much greater than either compressed or liquefied alternatives due to the quantities of metal required.

The filling procedure is straightforward. Hydrogen is supplied to the container at slightly elevated pressure (approx. 2 bar), which causes the hydride formation reaction to proceed, producing a small amount of heat in the process. To recover the hydrogen the pressure is reduced and heat is supplied to the metal hydride, causing the storage reaction to reverse. The amounts of heat involved are generally small, and can be obtained from the waste heat of the fuel cell during operation.

In addition to the increased volumetric storage density, metal hydrides have other attractive features for use as a vehicular hydrogen storage system. The energy required to store the hydrogen is minimal compared to that for conventional compressed hydrogen storage. Also the low pressure and chemical storage mechanism decreases the risks of storing hydrogen on a vehicle by limiting the escape of the gas from the container in the case of an accident causing the tank to be breached.

Alternate Fuel Storage

A final alternative to directly storing the hydrogen is to use a different chemical as fuel. Petrochemicals such as methane and methanol are often used, since they can be reformed into hydrogen for use in the fuel cell. There are also several fuel cell designs that are

capable of operating directly on these alternative fuels. As a fuel storage approach the benefits vary with the chosen fuel, however in general it improves the volumetric density while reducing the energy density. If a liquid fuel such as methanol is used the storage becomes essentially identical to conventional gasoline or diesel liquid fuel storage methods. This has advantages of familiarity, both in the storage method and safety considerations. The disadvantage is that there is often reduced performance relative to direct hydrogen fuel cells. The reduced performance can be the result of additional required equipment such as reformers and filters, or it can be a function of the direct use of a fuel other than hydrogen. However the performance cost may be preferable for applications where existing hydrogen storage techniques are determined to be inadequate.

1.5.2. FC Hybrid Vehicles

Fuel cell hybrid electric vehicles are based on the same architecture as conventional internal-combustion hybrids, however with a fuel cell stack instead of an ICE/generator as the primary source of electrical power for the vehicle. This design offers many of the same benefits to fuel cell vehicle designers; the hybrid design reduces the power plant size and increases vehicle fuel efficiency. However where hybrids are primarily motivated from an emissions perspective with internal-combustion, cost reduction is often a major motivation with fuel cell designs.

Fuel cell hybrid vehicles are still in early prototype development phase similar to other fuel cell powered vehicles. However they are rapidly being developed by a number of companies due to the perceived potential to provide a more economical platform for marketing fuel cell vehicles. A variety of applications are being developed ranging from niche-market utility vehicles to full-sized commuter automobiles.

CHAPTER 2 FUEL CELL POWER SYSTEM MODEL

Due to the central nature of the fuel cell power plant in the vehicles under consideration, the model of the fuel cell must receive a commensurate amount of attention. Modelling fuel cell behavior is a field of study unto its own, however for the vehicle model the overall characteristics of the stack were the primary concern. Parameters such as the gross and net power output of the stack, the parasitic losses to compressors and pumps, fuel and oxidant usage are all typical examples of desired information. A detailed simulation of the reactions occurring within the fuel cell is not required to accurately model the performance of a vehicle.

2.1. Fuel Cell Theory

Fuel cells are based on the same electrochemical principles that govern batteries and similar energy-conversion devices. The primary difference with respect to a fuel cell is the role the electrodes play in the reaction. In batteries electrodes serve as both reactant supplies for the chemical reaction in the cell as well as the conductor that connects the cell to an external circuit. In a fuel cell the reactant is supplied as fuel from an external source, and the electrodes are inert in the reaction.

The basic chemical reaction that governs the vast majority of fuel cells is hydrogen oxidization:

$$H_2 + \frac{1}{2}O_2 \rightarrow H_2O \tag{2.1.1}$$

Which for PEM cells consists of the following half reactions:

At the anode:

$$H_2 \rightarrow 2H^+ + 2e^- \tag{2.1.2}$$

At the cathode:

$$2H^+ + 2e^- + \frac{1}{2}O_2 \rightarrow H_2O \qquad (2.1.3)$$

Since fuel cells are electrochemical devices based upon batteries the physical structure is very similar. There are essentially seven components to a single fuel cell:

- The anode flow plate
- The anode
- The anode catalyst layer
- The electrolyte
- The cathode catalyst layer
- The cathode
- The cathode flow plate

Although there are many different fuel cell types, the major differences tend to be in the materials of the various components.

The electrodes are usually constructed from a porous material to enable reactants to diffuse from flow channels to reaction sites at the catalyst layer, while simultaneously conducting electrons from the reaction sites to an external circuit. For PEM cells these electrodes are some form of carbon graphite weave, while for high temperature cells they can be metal or ceramic.

The catalyst layer material primarily varies depending on the operating temperature of the fuel cell, since the temperature determines the activation energy from the molecules involved have to initiate the reaction. Low temperature cells require effective catalysts such as platinum but high temperature cells can use common metals such as nickel.

Flow plates exist to distribute reactants on both the anode and cathode side to the entire electrode so that reactions take place in a generally uniform fashion. In many designs they also have the dual function of conducting electrons from the electrode to an external circuit.

The major difference between different types of fuel cell is the electrolyte used. Most early cell designs such as alkaline and phosphoric acid fuel cells utilize a liquid electrolyte, however newer cells have relied on the use of solid electrolytes. Although liquid and solid electrolytes serve the same purpose, solid ones have the advantage of being easier to assemble and maintain, as well as helping to reduce the physical size per kilowatt. This is one of the chief developments that has enabled PEM fuel cells to be seriously considered as a vehicle power plant where all three factors are critical for a competitive product.

2.2. Types of PEM Fuel Cell Model

Due to the complexity of fuel cells, there are a multitude of different models available to simulate their behavior.

2.2.1. Empirical Model

The most straightforward approach to modelling a fuel cell in a computer is to use an experimental data based model. By measuring the polarization curve of the fuel cell along with the balance of plant component power requirements, a reasonably accurate simulation of the fuel cell can be obtained.

This type of model has the advantage of requiring very little in the way of computational resources and while producing accurate results. The accuracy of the results is only limited by the instrumentation and experimental procedure used to obtain the data. However the disadvantage is that the model is only accurate for a specific type of fuel cell and stack design under static and ideal working conditions. Although it is possible to apply a scale factor to the model, without a theoretical basis or further data it is impossible to guarantee accuracy. Many of the components in a fuel cell stack do not scale linearly, greatly complicating attempts to adapt the model to other types or sizes of fuel cell stacks. Additionally, it can be difficult to obtain measurements for all the independently operating components of a fuel cell stack, which further limits the flexibility of the model.

2.2.2. Theoretical Model

An alternative approach to the empirical model is the theoretical model. This approach attempts to use mathematical relationships to determine the performance of the fuel cell from various physical parameters used to describe it. The complexity of the model can vary widely from CFD models which attempt to predict performance from channel geometry and fluid dynamics to one-dimensional more thermodynamic based models.

Compared to the empirical models, theoretical models are generally more easily adaptable to different fuel cell stack types and sizes. However despite being more adaptable, these models tend to be less accurate overall. Determining a formula that is universally applicable is very difficult due to the non-linear nature of the fuel cell. As well, theoretical models are more computationally intensive which reduces the performance of any overall system models it is incorporated into.

2.2.3. Partially Empirical Model

A hybrid approach to stack modelling leads to the alternative chosen for this thesis. By combining the accuracy of an empirical model with the flexibility of a theoretical model, a more useful result is obtained. Experimental data is obtained from a fuel cell stack, which is used to provide a reference point for the theoretical relations. This approach is beneficial because the formulas can account for the varying power requirements of the balance-of-plant components which improves the models ability to scale to different sizes.

The fuel cell model developed at UVic by Dr. Zuomin Dong and colleagues was adapted to MatLab and changed to interoperate with ADVISOR. The stack model was utilized with the experimental polarization curves to produce a theoretical/empirical model. The model calculates the power costs of the major auxiliary components required by the stack for operation.

2.3. Fuel Storage

In this work, fuel storage is not modelled in detail due to the simplicity of the system in real applications. A metal hydride storage system is assumed, which simplifies the modelling requirements by rendering any weight change due to the use of fuel largely irrelevant. The only dynamic aspect of the metal hydride system that requires some attention is the temperature increase necessary to initiate the reaction to release fuel from the tank. This can be accounted for as a parasitic electrical load or considered to be obtained from the waste heat from the stack. Due to the small size of the power plant and storage tank under consideration the use of waste heat was assumed.

CHAPTER 3 FUEL CELL TESTING

In order to create a simulation of a Fuel Cell Hybrid Electric Vehicle (FCHEV), accurate models of several critical components are required, the most apparent of which is the fuel cell power plant. Although the vehicle simulation package contains a fuel cell model, it was intended for simulated commuter automobiles requiring a power plant on the order of 50 kW. This power plant was too large to scale to the 1-3 kW applications considered in this study, so there was an obvious need for a more appropriately scaled fuel cell model. To remedy this, a 1200 W PEM fuel cell was obtained from Palcan Fuel Cell Power Systems Inc. in Vancouver, British Columbia. Experiments were performed on fuel cell test station to characterize the performance of the fuel cell stack over a wide variety of operating conditions.

3.1. Technical Information on the Palcan PC6 Stack

The Palcan PC6-1200 stack is a Polymer-Electrolyte Membrane based fuel cell stack. It consists of 25 cells in a conventional plate-and-frame arrangement. Inlet and exhaust ports for fuel, oxidant and water are accessible from both ends of the stack for manufacturing and installation versatility. Its dimensions are approximately 15 cm × 19 cm × 21 cm, with a total active area of 96 cm^2 and an approximate weight of 1.5 kg. Each cell in the stack is fitted with terminals to enable convenient monitoring of the individual cell voltages. It is designed to operate at pressures slightly above atmospheric (3 psi gauge) and a temperature of 45 °C producing a maximum power output of 1200 W.

3.2. Test Setup

The test equipment used was a Ballard Test and Humidification stand; along with a Ballard (by ASA Automation) load bank and an in-house data acquisition system (DAQ) using Labview and National Instruments instrumentation.

3.2.1. Test Stand

The test stand is a 1996 design from Ballard Power Systems which consists of a test stand, humidification station and a 3 kW load bank.

The test stand is capable of monitoring and regulating the oxidant and fuel reactant streams into and out of the fuel cell, as well as providing a coolant circuit to control the temperature of the stack during operation. The test stand utilizes external compressed gas sources for both oxidant and fuel, with valves that allow for quick changes between several gases for either side of the fuel cell.

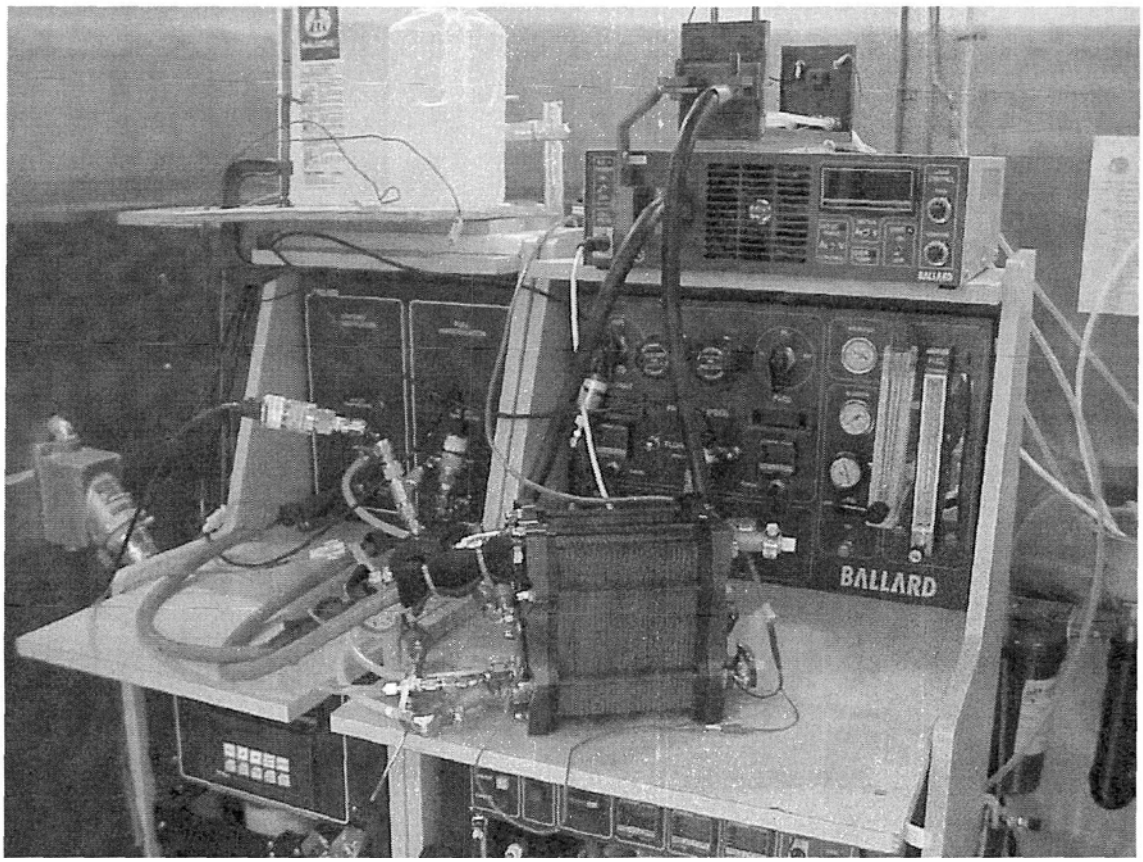

Figure 3.1: Test and humidification stands setup

The reactant gas enters the test stand at high pressure and initially passes through a digital mass flow meter. These mass flow meters are calibrated for each gas; both fuel (hydrogen) and oxidant (air), and enable the volumetric flow rate to be determined regardless of pressure fluctuations in the external gas source. Once through the flow

meter, the gas travels through a pressure regulator which lowers the pressure to the desired operating pressure of the stack. The operating pressure is measured at the output of the regulator and displayed on a digital readout on the front panel of the test stand. From the regulator the gas leaves the test stand for the humidification stand.

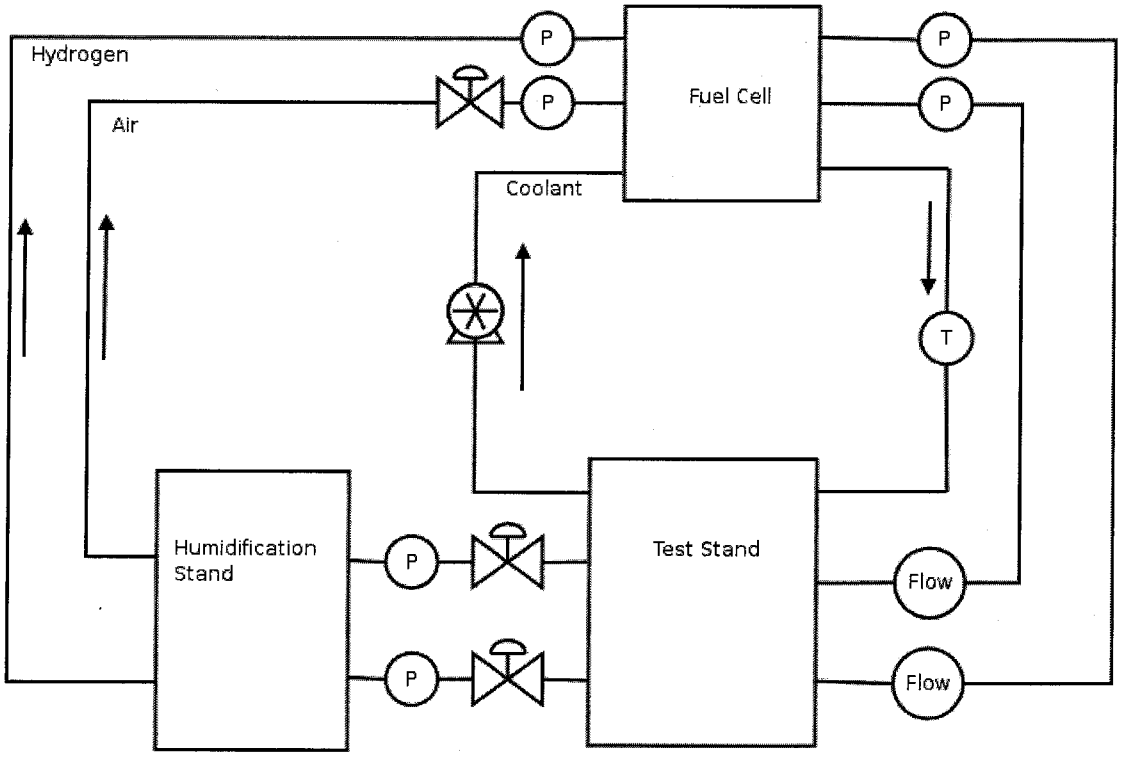

Figure 3.2: Fuel cell test station instrumentation setup schematic

The humidification stand is a separate unit that is connected to the test station and the fuel cell which is designed to fully humidify and adjust the temperature of the reactant gases. Each gas stream is humidified independently, such that they exit the station at 100% relative humidity at a set temperature. The separate humidification unit ultimately allows the relative humidity of each side of the fuel cell to be altered independently. The gases then exit the humidification station and travel via insulated and heated tubing to the fuel cell stack. This heated tubing is used to prevent condensation of the water vapour entrained in the gas on the insides of the tubes before it reaches the stack. Care must be taken when working around the humidification as these tubes can get very hot despite the insulation.

After passing through the fuel cell stack, the gases exit through exhaust ports on the stack, which are connected back to the test stand. After entering the test stand the gases pass through scavenging tanks which condense some of the water out of the gas streams and return it to the humidification stand. Finally, the gases pass through a rotameter where the flow can be accurately throttled before traveling out an exhaust vent.

The major difference between the oxidant and fuel circuits is the use of a second regulator on the oxidant lines, placed just before the fuel cell itself. This was put in place to allow the oxidant circuit upstream of the fuel cell to be run at a higher pressure than the fuel. The regulator before the stack inlet reduces the pressure down to the same level as the fuel, bypassing the pressure drops from the test and humidification stands and boosting the flow rate through the stack.

To test the stack a resistive load bank is also integrated into the apparatus, which is capable of dissipating a maximum of 3 kW of power. However due to the characteristics of the load bank, a water-cooled resistor was required to reduce the voltage to a manageable level for the currents involved. The load bank is capable of providing a current or voltage load; however it was only used to draw current in these tests. In addition to providing the test load it also had the secondary function of acting as a backup voltmeter. This functioned as a useful independent measurement for verification of the DAQ readings on the computer.

3.2.2. Instrumentation

The instrumentation system is a custom developed solution designed to integrate the diverse set of equipment available in the lab with the maximum amount of flexibility. All of the electronic instruments are linked together and logged using a National Instruments data logger and LabView program.

The main areas of instrumentation are the electronic performance of the stack, the conditions of the reactant gas streams, and the temperature of the stack and gases. The power generated by the stack was measured via several means including the load bank, the DAQ and manually using a volt meter. This redundancy provides a useful cross-

check on the accuracy of the various instruments involved. For example, the DAQ suffered from some type of signal interference that caused the voltage readings to fluctuate where the load bank and voltmeter indicated a steady potential. The final recorded values used for the polarization curves were therefore obtained from the portable Fluke multimeter.

The test stand is also outfitted with 14 cell voltage sensors to record the individual cell potentials in a stack during operation. These were not utilized for these tests since the stack had 25 cells to monitor and the individual cell performance was not considered a critical parameter.

In addition to the electrical output of the stack, the reactant inputs were measured to ensure the accuracy and repeatability of the results. These measurements principally included the pressure and flow rate. The pressures of the gases both entering and leaving the stack were of interest, and were measured at several locations. The inlet pressure of the reactants were measured at the outlet of the primary regulators, which was good for a estimated pressure range, however the sensor's accuracy at the low pressures of the test was too poor for useful measurements. Another set of pressure sensors were situated just before the inlets to the fuel cell stack, these were much more accurate due to their design for low pressures and their location. The outlet pressures were measured by another set of sensors located at junction between the exhaust lines and the fuel cell test station.

The regulator pressure sensors displayed their values on the front panel of the test stand, while the more accurate low pressure sensors sent their results to the DAQ where they were logged and displayed. As a result, the pressure values from the DAQ were used almost exclusively in the experiments, as they were more accurate and were continually recorded. The only disadvantage to the computer readouts was the longer sampling time involved with the LabView interface, other than that they were superior in every way to the panel readouts. An additional pressure gauge was also used to monitor the inlet pressure of the cooling water to the fuel cell stack. This sensor was a manual dial gauge, which was used instead of another integrated electronic sensor since the pressure was set

via the pump motor speed at the beginning of the tests and did not change at all during the tests.

The test stand was also instrumented with a variety of thermocouples for measuring temperatures of the fuel cell stack and reactant gases. However since the temperature was not a dependent variable in these tests they were not utilized. Thermal control of the stack was accomplished by measuring the coolant water temperature exiting the fuel cell using a thermocouple. The measurement was sent to a control circuit in the test stand and a digital display on the front panel. The desired stack temperature was set on the same digital readout and the test stand control system would then attempt to maintain the given temperature. Some difficulties with this system were encountered during the tests; it did not function properly at the temperatures most of the tests occurred at. In particular, the solenoid valve that regulated the flow of cooling water through the main heat exchanger would stay closed despite the temperature rising above the set point. To compensate, for many of the tests a manual bypass valve was used to throttle the flow through the heat exchanger and control the temperature of the stack. It was generally possible to reliably control the stack temperature to within 0.5 °C. However, once the stack was generating 800-900 W the cooling system capacity would be reached and the temperature would begin to rise above the baseline operating temperature. However this temperature rise was only several degrees at peak load.

3.2.3. Test Procedure

The test procedure used was as follows:

1) Start the test stand, including cooling loop and opening gas solenoids. The cooling loop will help heat the stack to the desired operating temperature while the rest of the test equipment is started.

2) Start the humidification station

3) Open the hydrogen, nitrogen and air valves in the fume hood.

4) Open the hydrogen and nitrogen valves outside the fume hood and from the control panel.

5) Launch the DAQ on the computer and enter the test information

6) Start the DAQ

7) Crack open the hydrogen and air rotameters and pressurize the fuel and air circuits to the desired operating pressures.

8) Measure the open circuit voltage of the stack and check the individual cell voltages to ensure no problems are occurring within the stack.

9) Once the stack temperature has reached the desired operating temperature, record the stack potential.

10) Increase the current draw from the load bank to the next desired measurement point and adjust the reactant flow rates.

11) Adjust the cooling water flow to keep the stack temperature at its set point.

12) Wait for the stack potential to stabilize, and then record the voltage.

13) If a further load point remains to be tested return to step 10

14) Reduce the load on the stack to ~10 A, reduce the pressure of the reactant streams and reduce the flow rate. Let the stack potential stabilize and check cell voltages to ensure no damage occurred during the test.

15) Turn off the load, and then close the oxidant and fuel regulator valves. Allow the pressure of both sides to reduce to zero, and then close the flow meters. The purge valves on the test stand can be used to reduce the pressure of both streams at the same rate.

16) Turn off the cooling system and humidification system, then stop the data acquisition system and shut down the test stand.

3.3. Test Results

The tests on the fuel cell were designed to explore the performance envelope of the stack. By varying the operating parameters of the stack in a systematic manner the effect of each factor on the overall performance can be isolated and recorded. Since there were a myriad number of parameters that could be modified, the following subset were used:

- Fuel and oxidant flow rate
- Fuel and oxidant pressure
- Stack temperature
- Reactant humidity

Palcan provided a specification listing the baseline operating values for these parameters, along with minimum and maximum tolerated values. All parameters were varied ± 40% from the given baseline values, with additional intermittent steps of ± 20%, 10% and 5% for the flow rate and pressure measurements.

Table 3.1: Fuel cell testing varied operating parameters

Parameter	Baseline	Minimum	Maximum
Oxidant Pressure (psi)	3	1.8	4.2
Fuel Pressure (psi)	3	2	5
Oxidant Humidification Temperature (°C)	45 °C (100%)	27 °C (60%)	63 °C (140%)
Fuel Humidification Temperature (°C)	40 °C (88%)	24 °C (53%)	56 °C (123%)
Stack Temperature (°C)	45	27	63

The first several tests were conducted at baseline conditions in order to establish the basic performance of the fuel cell stack and attempt to quantify the variability of the instrumentation setup. The polarization and power curves were found to vary by 6% on average, but with a median variance of 4%. The greatest variance occurred at high load, with a maximum of 13% just before the stack potential dropped to zero volts.

During the testing, additional details were noticed that did not appear in the data. In particular, the stack seemed to have water management difficulties, with excess liquid

water visible at the exhaust ports for both the fuel and air. Some of this liquid water was likely due to condensation from the temperature change upon exiting the stack, however occasionally it seemed to build up inside the stack as well. This usually manifested itself in a potential drop or increase in voltage variability. Using a ball valve to pass a quick burst of inert gas through the stack was enough to dislodge any droplets of water blocking channels within the stack and remedy the problem.

Additionally some problems were encountered with cell voltage reversal and drying, which were related to the orientation of the fuel cell stack. Although not detailed in the documentation provided with the stack, the cooling channels of the bipolar plates are arranged in such a way that the orientation of the stack is important to ensuring even cooling. The initial setup had the stack lying on one side, which when combined with parametric tests under high-load conditions heated a localized area of the membrane. This had the effect of accelerating the drying process which rapidly progressed to a localized burn-through. However the problem was quickly identified and the damaged membranes were replaced. The test series underway at the time of the accident were repeated with the repaired stack to ensure consistency.

3.3.1. Oxidant Pressure and Flow Rate

The oxidant pressure has a noticeable effect on the performance of the cell, dramatically influencing the stack potential at high load levels, and to a lesser extent at lower load levels (< 0.8 A/cm^2). However the actual performance change due to the pressure at high loads is difficult to separate from the effect of the variation in flow rate due to pressure drop across the stack. This is primarily due to the pressure drop through the stack in combination with the back pressure of the test station. The test stand was not designed with large low pressure stacks in mind, with the result that most of the internal piping has a smaller diameter than the air inlet and exhaust diameters. When combined with the 2 psi pressure drop through the stack at moderate flow rates of 2 cfm (cubic feet per minute), operation at high flow rates necessitates using pressures above the baseline of 3 psi.

When the air pressure was reduced 40% the stack voltage was unaffected at open circuit and low loads, but quickly reached starvation at a load of 0.5 A/cm^2. With -20% and -10% air pressure the performance was similar, but with the onset of starvation shifted to increased current densities of approximately 0.7 A/cm^2.

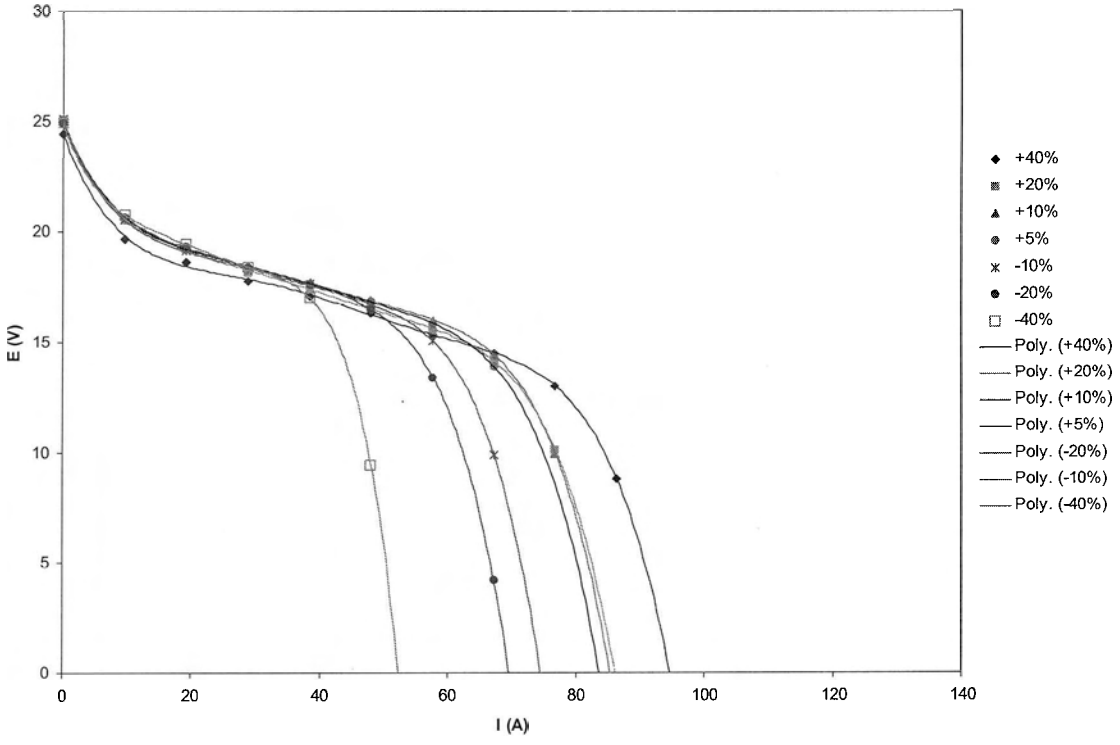

Figure 3.3: Effect of Oxidant pressure on fuel cell performance

In order to test the flow rates, a baseline reactant pressure of 5 psi was used instead of the normal 3 psi. The overall effect of the pressure drop through the test station could then be limited and allow both higher and lower than baseline flow rates to be tested. The results obtained from this test are somewhat problematic, as the persistent negative potential mentioned above developed during the last of these tests, when the stack was operating in an oxidant starved condition.

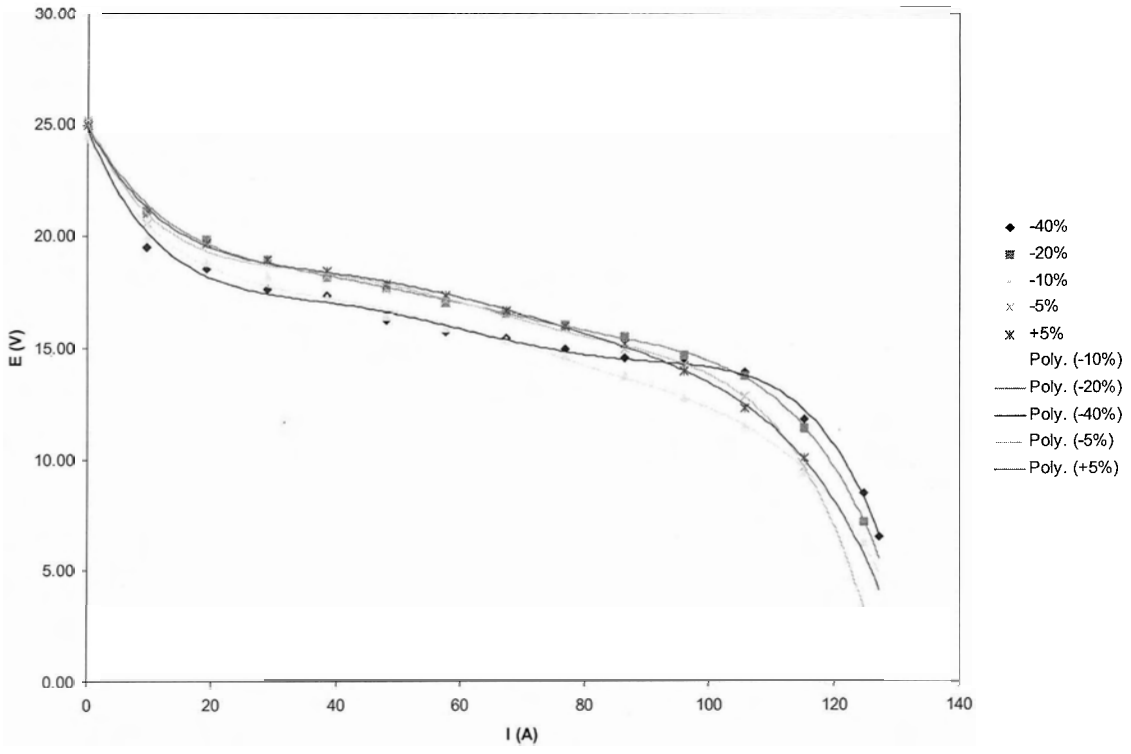

Figure 3.4: Effect of oxidant flow on fuel cell performance

At pressures above the baseline higher flow rates could be achieved, which due to the previous results we know has a separate effect from the pressure alone. The performance from the lower load points on all curves shows a slight trend of decreasing stack potential with decreased pressure. Unfortunately, this result is not consistent or large enough in magnitude that it can be easily separated from the measured variation of the instruments.

3.3.2. Fuel Pressure and Flow Rate

The fuel flow rate seemed to have little effect on the overall power generation capacity of the fuel cell stack, although there seemed to better load following performance at higher fuel flow rates than when using stoichiometric rates.

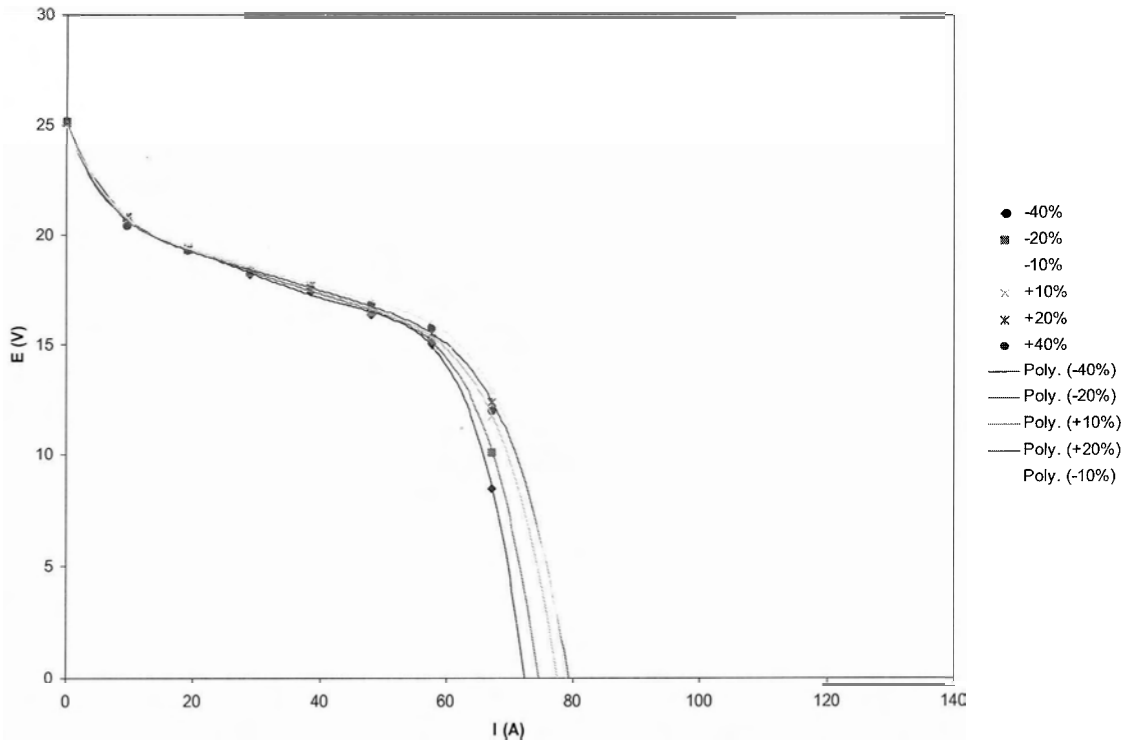

Figure 3.5: Effect of fuel pressure on fuel cell polarization curve

With baseline fuel flow rates the stack potential would drop sharply when the load was increased, then gradually return to a higher steady-state level. With excess fuel at higher pressure the initial drop was smaller and the recovery faster. This behavior is not easily quantifiable via polarization curves, although it is visible in the time-series data files initially obtained from the DAQ.

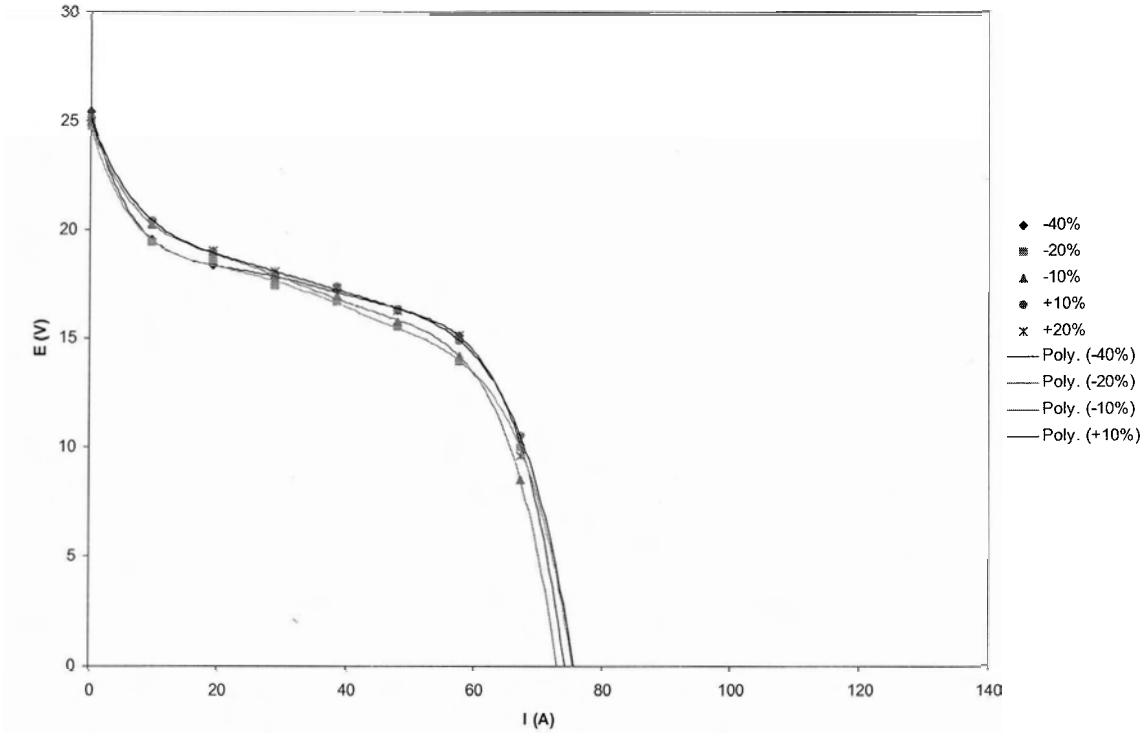

Figure 3.6: Effect of fuel flow rate on fuel cell polarization curve

The figures below illustrate the difference in dynamic performance, with Figure 3.7a showing the potential trace for a fuel-starved condition. At each load increase the potential dives sharply by nearly 3 V before rising to its steady state level over a period of approximately two minutes. On the other hand, for the supplementary fuel test the load changes result in the potential dropping only slightly below the eventual steady-state level, and the recovery occurs over a period of 15-30 seconds. Although this occurred with the different flow rates, it does not show up with varying pressures.

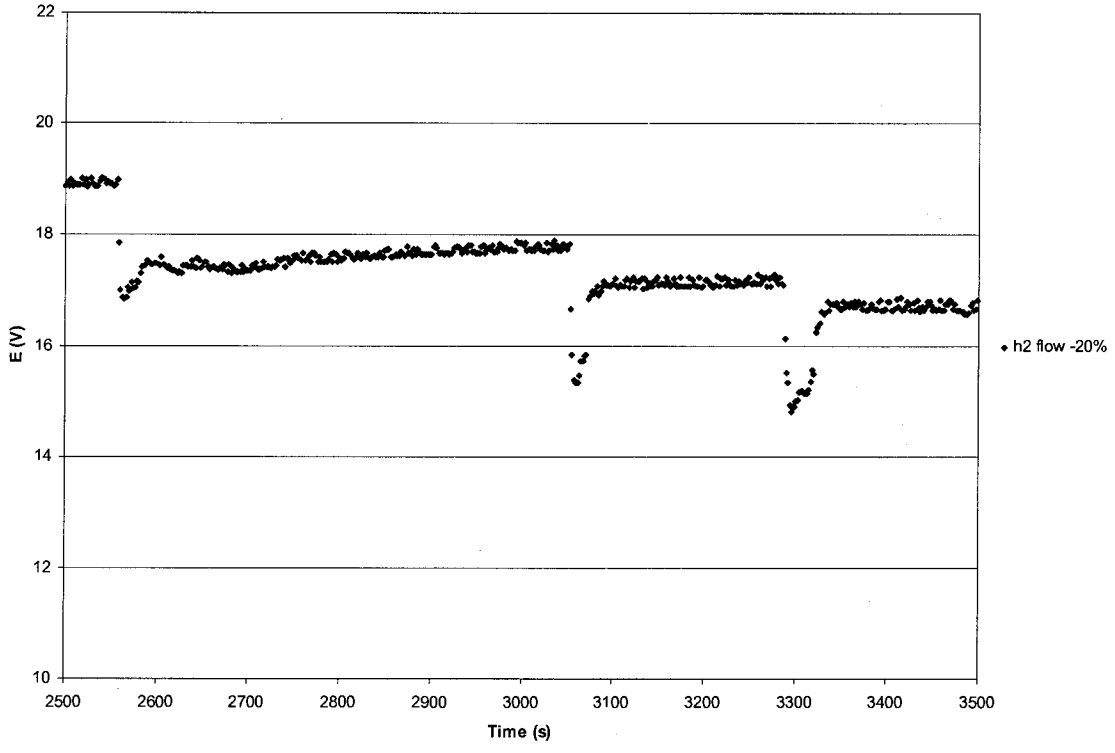

(a)

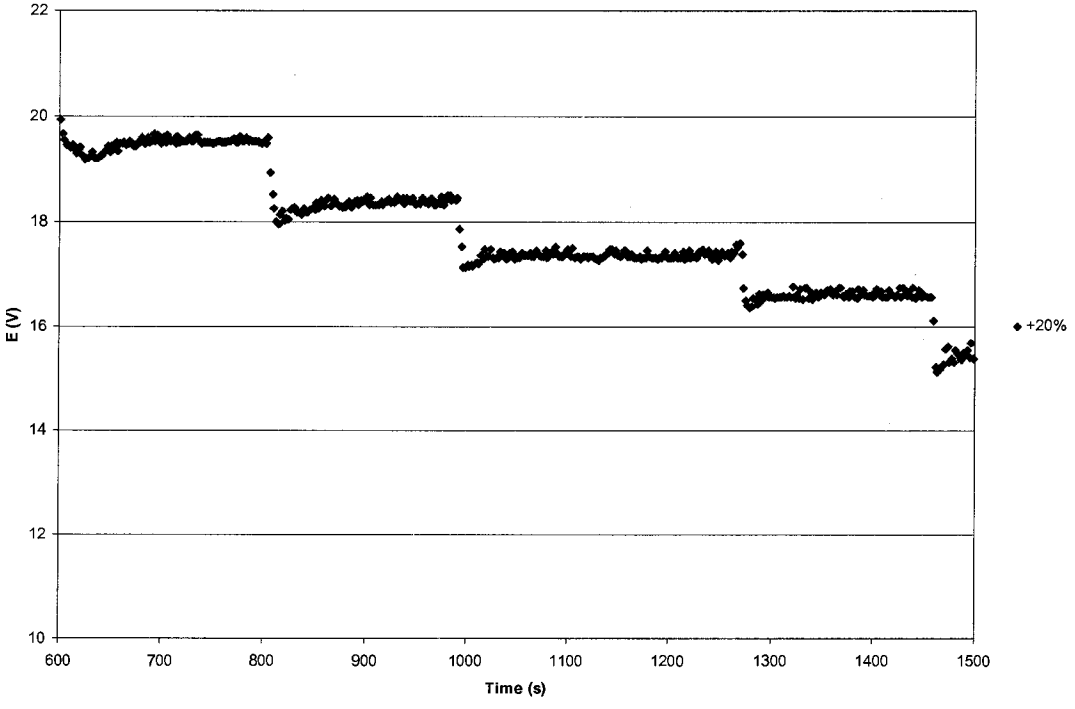

(b)

Figure 3.7: Stack potential vs. time at (a) -20% & (b) +20% flow

Testing of the stack with surplus fuel was only performed up to +20% in order to conserve our limited supply of hydrogen. Since the +10% and +20% cases were nearly identical, with an average absolute deviation of only 1.5%, further testing of this condition was not considered a priority.

3.3.3. Oxidant Humidity

Varying the oxidant humidity had no measurable effect on the stack voltage level and power output. However it did seem to affect the amount of liquid water exiting the stack via the oxidant exhaust line, with increased humidity there was a marked increase in the liquid condensing in the exhaust line. Flooding did not seem to occur outright in the cell at high loads, as the voltage did not exhibit a decrease relative to the baseline measurements. An effect that did not show up on the polarization curves was the increased variability of the stack potential measurements, especially at high loads. This could have been a result of partial and/or intermittent flooding of areas of the stack; however there was no way to determine for certain what was occurring.

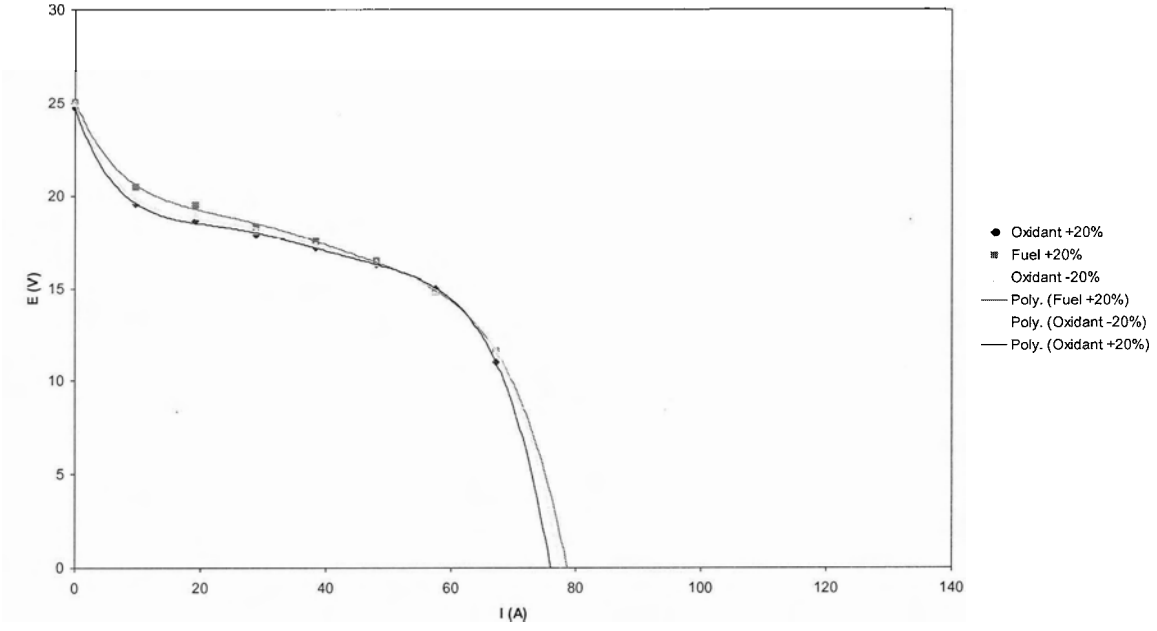

Figure 3.8: Oxidant and Fuel Humidity

3.3.4. Fuel Humidity

Fuel humidity somewhat surprisingly did seem to have a noticeable impact on the stack voltage, but unlike most of the parameters measured here it was more pronounced at lower loads. An average 3% increase over base performance was measured for a 20% increase in humidity at low loads, however the effect was especially noticeable at low loads, where the increase was close to 5%. Due to the risk of drying and damaging the cell membranes the test was only performed for an increased humidity.

3.3.5. Stack Temperature

The stack temperature was tested only at extremes as observations during the stack activation and previous tests, suggested the temperature would only have a minor effect on the potential. The two tests were performed at a stack temperature +40% and -40% of the baseline temperature, 27 °C and 63 °C respectively. Theoretical calculations estimated at most a 1 V difference in stack potential between the two cases. At these temperatures the variation from the steady-state curves is only on the order of 1% until the stack reaches starvation conditions. At this point the two cases deviate, with the cooler stack potential dropping below that of the warm stack.

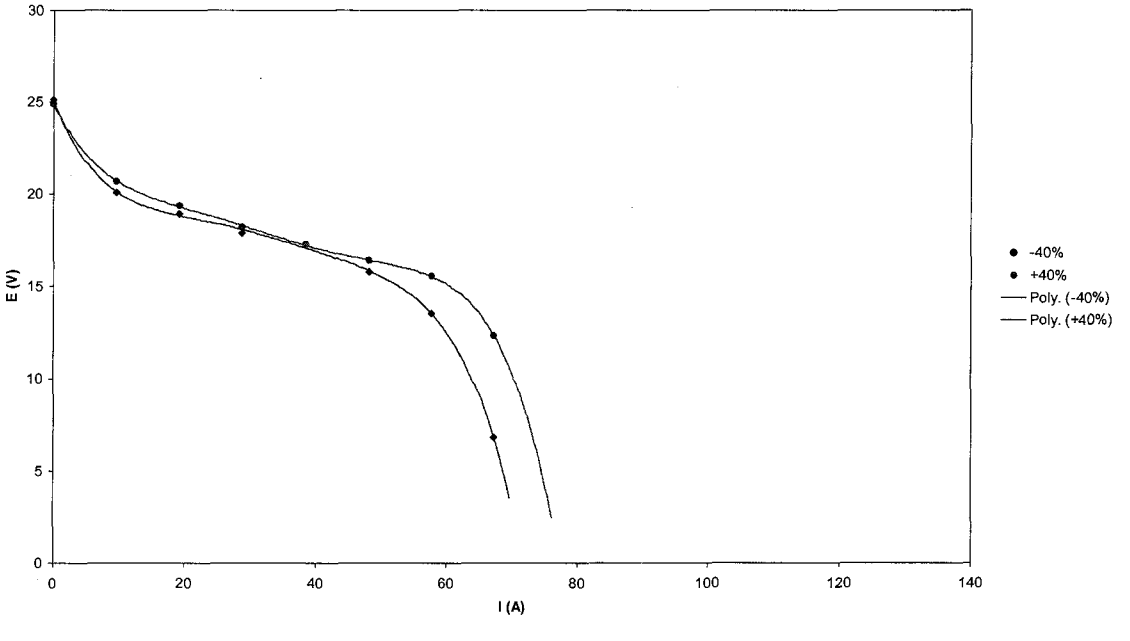

Figure 3.9: Effect of stack temperature on potential

However it is interesting to note that the data points of the test at 27 °C are all lower than the baseline curve, while those of the test at 63 °C are largely above it (with only two exceptions). Although quantifying the magnitude of the effect of temperature on the stack voltage is difficult because of its small magnitude, the measurements clearly show that the effect does exist.

3.3.6. Overall Reactant Pressure

An additional test was performed to test the maximum power output of the stack and to attempt to characterize the performance of the stack if higher flow rates and pressures could be sustained. Tests were performed with both the oxidant and fuel at inlet pressures of 5 and 6 psi. The improvement in performance was substantial, with the maximum load jumping from ~0.7 A/cm^2 to 1.0-1.3 A/cm^2, and the maximum power from 860 W to 1000-1100 W. Similarly to the other pressure and flow rate variation tests the effect at low loads was minimal.

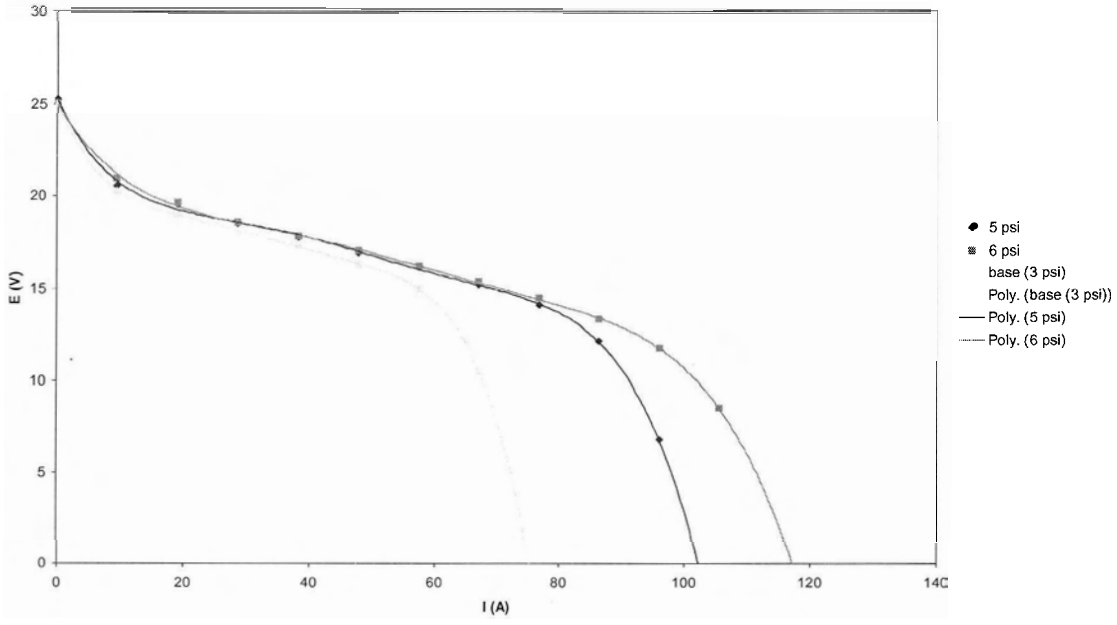

Figure 3.10: Effect of reactant pressure on fuel cell performance

3.4. Test Analysis & Discussion

Generally, with the exception of varying the oxidant flow, the fuel cell performance was relatively stable in the face of changing operating conditions. Although variations in other parameters seemed to correlate to changes in the loads that could be supported, they remained relatively minor relative to the differences that occurred when the oxidant flow was altered.

3.4.1. Oxidant and Fuel Pressure and Flow Rate

Altering the fuel flow rate and pressure did not result in large changes in the measured data for the polarization curve; however it did have other effects. Among these was a noticeable improvement in the dynamic load response of the stack. The stack voltage followed the load with less time needed for the voltage to stabilize to a steady-state reading after each change. In addition, the voltage exhibited less variability at higher current loadings, until the load reached the point when the cells in the stack became starved for oxygen. This dynamic performance has not been thoroughly investigated; however it could play an important role in the suitability of a stack design for use in a vehicular power plant.

The oxidant flow rate and pressure had a large effect on the overall performance of the fuel cell stack, and seem to be the major limiting factor in many cases. At 2.5 times the required flow rate, the stoichiometry of the oxidant is much higher than necessary. However, reducing it below this quickly resulted in escalating transport losses and a massive reduction in the stack potential. Altering the pressure had an effect, but since that effect also changed the flow rates through the cell it is difficult to completely separate which effect is a result of which parameter change. Unfortunately the pressure drop through the fuel cell stack is large enough to prevent the use of higher flow rates at baseline pressures.

Despite the fact that the back pressure from the test apparatus was only 1 - 1.5 psi, the stack was unable to reach a peak performance beyond 1500 W at the given inlet pressure due to insufficient flow. Given the pressure drops likely required in a fuel cell power plant exhaust system, it is unlikely that the stack will be able to provide the specified

power without changes to either reduce the pressure drop or handle higher pressures. A reduced pressure drop would be preferable as 3 psi operation presents a number of balances of plant and cost benefits.

The problems experienced during testing with cell voltage reversal were unexpected, as they were not detailed in the documentation provided with the stack or the testing equipment. A quick survey of available industry contacts indicated that this is a known, if poorly-understood problem. Some published literature was found on cell reversal occurring in rechargeable batteries and during tests of another low-pressure fuel cell design [7]. These suggest that negative voltages seem to be related to uneven distribution of reactants to certain cells. It is hypothesized that this imbalance can sometimes cause one of the starved cells to be driven in reverse by the other cells in the stack, with the result of reversing the normal reaction and an observed negative voltage. This causes rapid damage to the electrolyte as the water in the membrane is depleted, reducing the performance of the cell and potentially leading to a burn through.

In light of the potentially dangerous damage that was done to the stack, further investigation of this effect would be prudent. The start-up sequence of a fuel cell seems to be a previously identified trouble area, but high-load induced reactant starved conditions may also be a potential cause of problems.

3.4.2. Oxidant and Fuel Humidity

The humidity settings did seem to have a consistent effect on the overall polarization curve, however it was minor relative to the overall power output of the stack at any given point. There were some observed differences in the dynamic performance of the stack where the overall variability of the stack potential at high loads was increased with higher humidity. This variability may occur because of partial or intermittent flooding within the stack; however we do not have a way to determine whether this was in fact the case.

The limited sensitivity of the stack to humidity and temperature changes would seem to be beneficial. Control of temperatures and humidity within the stack can be difficult due to its thermal mass and the lack of instrumentation required to measure humidity.

Although these tests show little effect on the raw performance of the stack, this study did not attempt to perform any long-term tests in which these parameters might play a role in determining the lifetime performance of the stack.

3.4.3. Stack Temperature

Varying the stack temperature seems to have a largely deterministic effect, however similarly to the humidity changes, the magnitude is limited relative to the overall power output of the fuel cell. Additionally, the ability to accurately control the temperature uniformly throughout the cell is limited, due to the dynamics of the various internal fluid flows. The effect of temperature on the fuel cell has a more important function on influencing the humidity of the reactants and the water content of the membrane.

3.4.4. Overall Reactant Pressure

The overall reactant pressure tests were undertaken as a consequence of the poor power output seen during the single-parameter variation tests. The performance improvements obtained by increasing the reactant pressure by a minor amount are quite substantial, with peak power improving by over 260 W. However the parasitic power increase required to achieve the higher pressure has not been factored into that increase. Examining several data sheets from various vendors suggests that the increase will result in roughly a 100 W increase in motor power required for the compressor.

As this will result in a net power gain it would seem to be a valid tactic to use to easily improve the performance of the stack. However for practical applications several other factors need to be considered including any possible detrimental effects to the safety or durability of the stack and any additional financial costs of increasing the power of the compressor.

There is an upper limit to the marginal performance improvement that can be obtained from increased pressures as they are limited by the diminishing returns achieved as the pressure reaches higher values. Regardless, modest increases in the operating pressure or the reduction of the pressure drop through the system seem to be an interesting area for future investigation.

3.5. Incorporating Experimental Data into Fuel Cell System Model

The stack polarization curve data was then incorporated into an existing partially empirical model previously developed at the University of Victoria. The fuel cell model is based on empirical data for the fuel cell polarization curve and some tuning parameters, but also uses theoretical relations to determine predicted balance-of-plant losses to accessories required to operate the stack. The major components considered for parasitic losses from the PEM stack were the reactant air compressor and coolant pump.

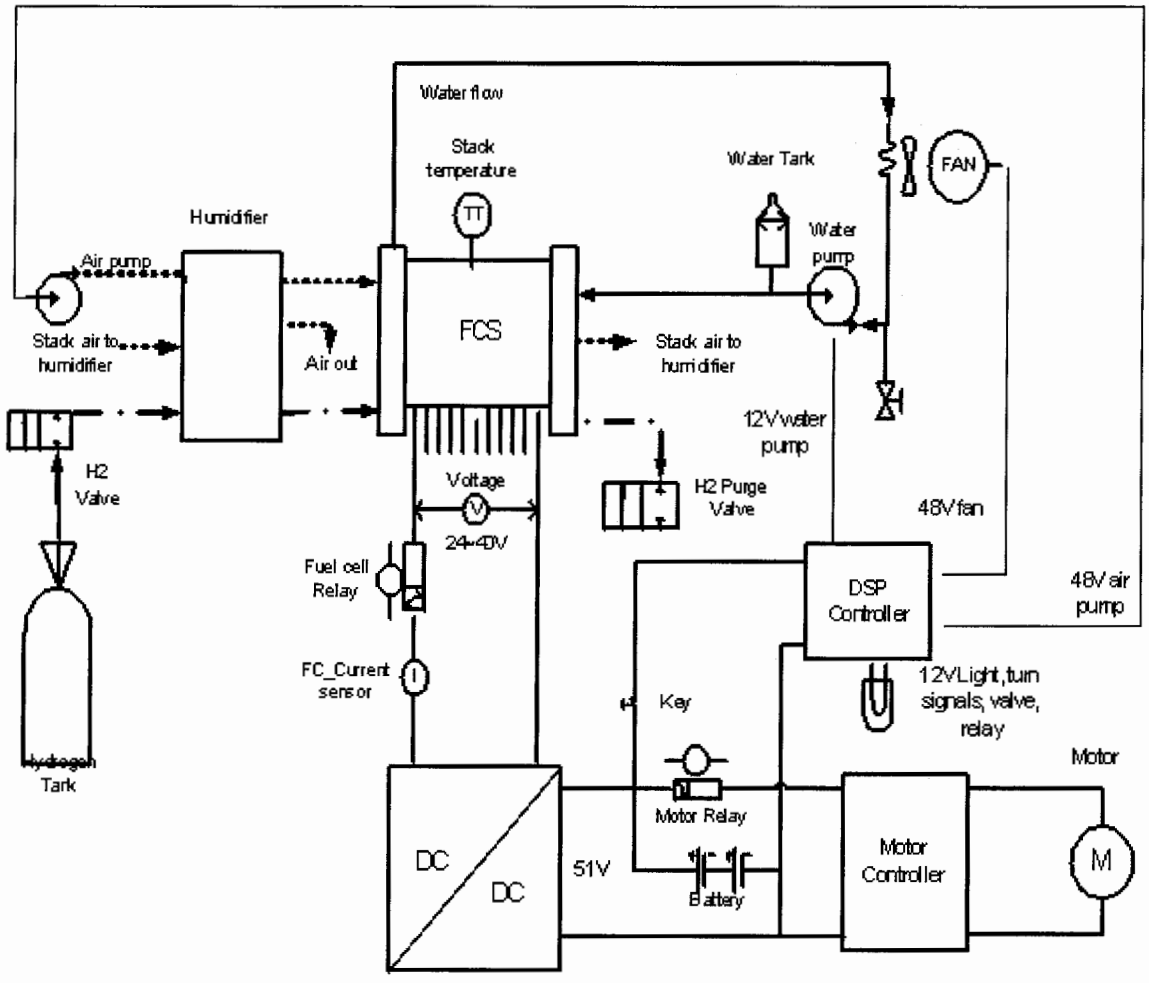

Figure 3.11: Palcan scooter fuel cell plant schematic

The total power required by the air compressor to provide sufficient air for the reaction to take place was modelled by the expression:

$$W_{compressor} = \frac{0.00433 \times P_{in} \times \dot{Q}_{airflow} \times N \times \left[\left(\frac{P_{out}}{P_{in}} \right)^{\frac{0.231}{N}} - 1 \right]}{E_{fd} \times E_{fm} \times 1000} \tag{3.5.1}$$

Where the drive efficiency is E_{fd} and E_{fm} is the motor efficiency. Values for both coefficients were determined from an empirically-derived relation in Xue and Dong (1998). With known reactant flow rates and pressure drops for the given operating points a curve describing the compressor power as a function of fuel cell current density was generated.

The Palcan stack utilized a water-based cooling system, it was modelled with the assumption that the active cooling system would account for 80% of the rejected heat while passive convection and radiation accounted for the remainder. Values for heat loss at each operating point were determined from the experimental data. The power required to pump the necessary coolant was given by

$$W_{cooling\ system} = \frac{\dot{m}_{H_2O}}{\rho_{H_2O}} \cdot P_{drop} \cdot \frac{FoS}{\eta_{pump} \cdot \eta_{motor}} \tag{3.5.2}$$

Where the pressure drop of coolant through the system was measured as 2 psi, combined with approximate pump (η_{pump}) and motor (η_{motor}) driving efficiencies and a factor of safety (FoS) of 1.5 an expression for the pumping losses was obtained.

From the combination of the gross power curve and the combined accessory losses a reasonable net power curve for the stack was created which could be integrated into ADVISOR. Other parameters such as the dimensions and mass were modified in the ADVISOR model to determine the amount of convective cooling.

Accounting for the fuel storage is also performed in the fuel converter (in this case fuel cell) component model in ADVISOR, so modifications were also required in this area. In the modeled fuel cell electric scooter, a removable metal-hydride hydrogen storage canister was used. The canister represents a reasonably dense and robust storage method with flexible replenishment options through either refueling or replacement cylinders.

The primary effect of the storage system on the vehicle model is limited to the mass added to the vehicle. Accounting for other effects such as the thermal management power requirements or changes to weight distribution were considered minor and abstracted as a constant parasitic power load or neglected. Calculations for the mass added to the vehicle were incorporated into the component model so the fuel storage would scale appropriately with any scaling of the power output of the model itself. A desired range of 100 km was used when estimating the amount of fuel capacity required for the storage system.

CHAPTER 4 DESIGN & ANALYSIS OF FUEL CELL HYBRID ELECTRIC VEHICLES

Although there are a number of computer models for simulating the performance of conventional consumer automobiles and trucks, there are few for the small scale low-speed vehicles. To develop one, we modified an existing system that was initially designed for modelling hybrid cars and trucks so that it could accurately handle the smaller scale. To do this many different components had to be accounted for and modelled before the entire vehicle could be accurately represented.

4.1. Vehicle Modelling Tools

Vehicle modelling is a technology that has become increasingly common as modern vehicles have become more complex and competitive pressures have reduced the time available to bring new concepts to market. Automotive engineers have found that it is far more effective to explore early design decisions in computer simulations than via traditional prototype testing methods. Although some prototyping is still required, by using a vehicle model the number of prototypes and amount of testing required can be reduced.

In addition to the ability to prototype new designs, computer vehicle simulations are also useful in existing vehicle testing. Simple tests such as acceleration and skid-pad tests are easy to perform, however they also do not provide much insight into the overall performance of the vehicle. More complex tests that can provide more information generally involve driving the vehicle along a track at a set of velocities over time in an approximation of a duty cycle for the vehicle. This type of drive-cycle test is used to determine attributes such as fuel economy and can be performed physically; however the tests are time-consuming and can require expensive instrumentation. Vehicle models play a role by simulating performance in both simple and complex tests in a fraction of the time required for a physical test.

There are two general modelling approaches used for vehicle simulation, which are distinguished by the direction of control information flow. A "forward facing" feedback model uses the control signals from the driver as the main input to the model, from which the response of the vehicle is calculated. The simulated response includes the behavior of each of the drivetrain components as well as the ultimate vehicle speed.

In contrast to the forward modelling approach the input to a "backwards facing" model is instead the desired velocity of the vehicle, which is converted to a power request. The request is propagated back through the drivetrain until it reaches the power bus. Depending on the vehicle configuration being simulated the power bus will attempt to satisfy the demand using the engine, energy storage system or combination thereof. If the velocity request can not be reached the feedback loop in the model progressively lowers the requested speed until an achievable velocity is found.

Each approach has different advantages and disadvantages which tend to steer their use to different applications. Due to the simple architecture, forward facing models are well suited to investigating the dynamic performance of a vehicle. Since information flows through the model in a way that closely resembles the arrangement in an actual vehicle, it can be used to create interactive driving simulators. Generally backwards-facing models are quasi-steady-state with corrections made for dynamic effects. Although this approach lacks the accurate dynamics of a forward facing model it is ideally suited for drive-cycle simulations where the vehicle velocity is the input parameter and known for the entire duty cycle. Forward facing models are capable of accurately simulating drive cycle performance, however they tend to require greater computational resources to translate the given drive cycle velocity into a control input to the vehicle.

Due to the complexity of modern vehicles, the modelling tools are advanced pieces of software. There are few publicly available vehicle modelling tools, which have been developed by primarily government and educational institutions. These include the ADVISOR and PSAT packages, which have been developed by the U.S. Department of Energy at the Argonne National Lab and National Renewable Energy Laboratory.

4.2. ADVISOR

The ADVanced VehIcle SimulatOR (ADVISOR) is a vehicle simulator built on the MatLab/Simulink software platform. It was initially created by the Department of Energy's National Renewable Energy Laboratory (NREL) in the United States to help investigate the design and performance of hybrid internal combustion vehicles [9]. Befitting its purpose as a research tool, it was built with expandable capabilities in mind and released with a relatively liberal license which encouraged modification and contribution to the existing model. As such, it has a very modular design with the vehicle simulation tasks divided into numerous subsystems ranging from the power plant to the wheels. Each of these systems is independently changeable so that a wide variety of vehicle types can be simulated. As a result ADVISOR has been modified to simulate not only consumer automobiles but heavy trucks and utility vehicles. Initially designed for internal combustion power plants, the base system has since been modified to allow the simulation of fuel cells as the primary power source in both non-hybrid and hybrid layouts.

The main computation engine of ADVISOR is based on Simulink, a graphical programming module most commonly used to simulate control systems. Individual component models are a combination of algorithms programmed in Simulink and data files that store various tuning parameters for the algorithms. The separation of fundamental model logic from the equipment data creates a flexible system that can easily integrate models for new components from equipment specifications and test data. In addition, the modular approach also increases the flexibility of the modelling software by allowing the inclusion of several algorithms for the same type of component. These vary from purely theoretical component models to those based entirely on empirical data.

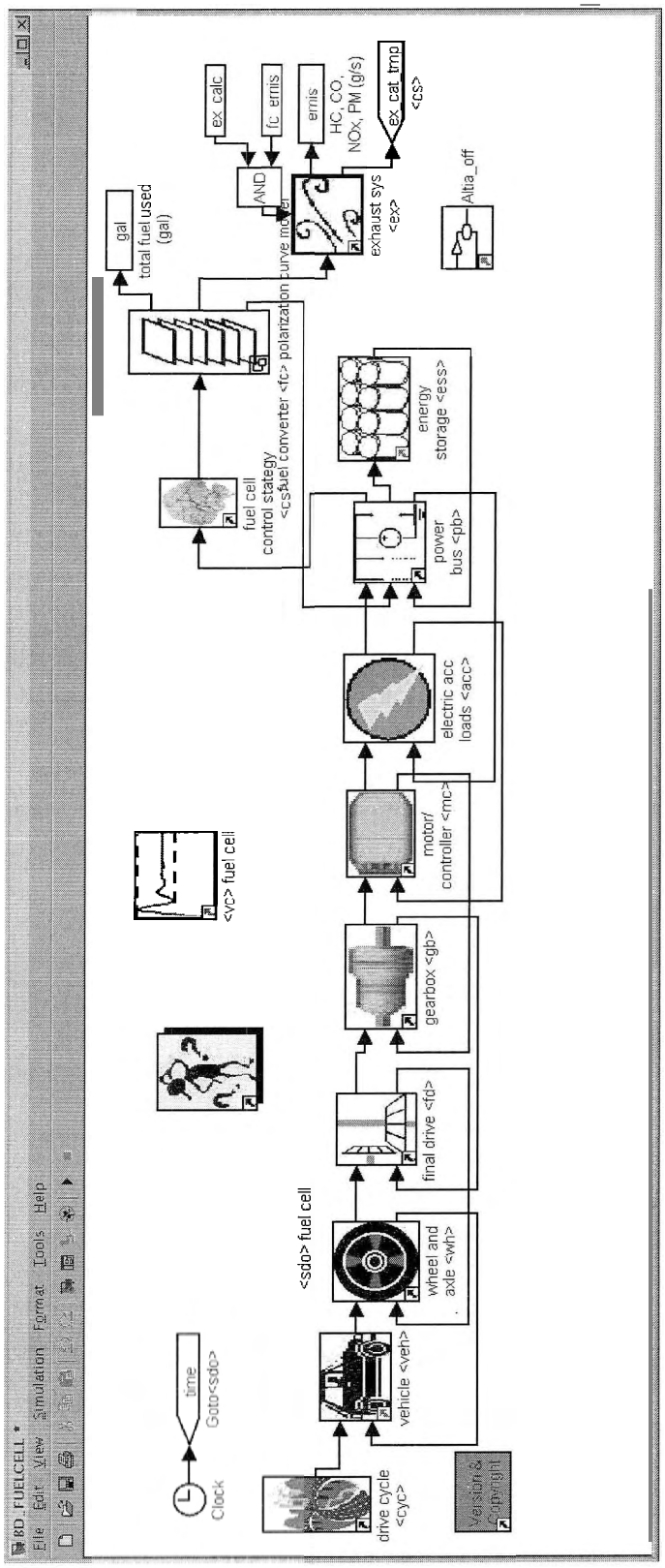

Figure 4.1: Overall vehicle Simulink diagram

The backward-facing nature of the ADVISOR model is visible from the above diagram, with velocity input moving from left to right through the drivetrain and achievable power feeding back from right to left. Each block represents a component model of the vehicle, containing the generic logic for each type of component which is tuned for each component using the easily edited data-files.

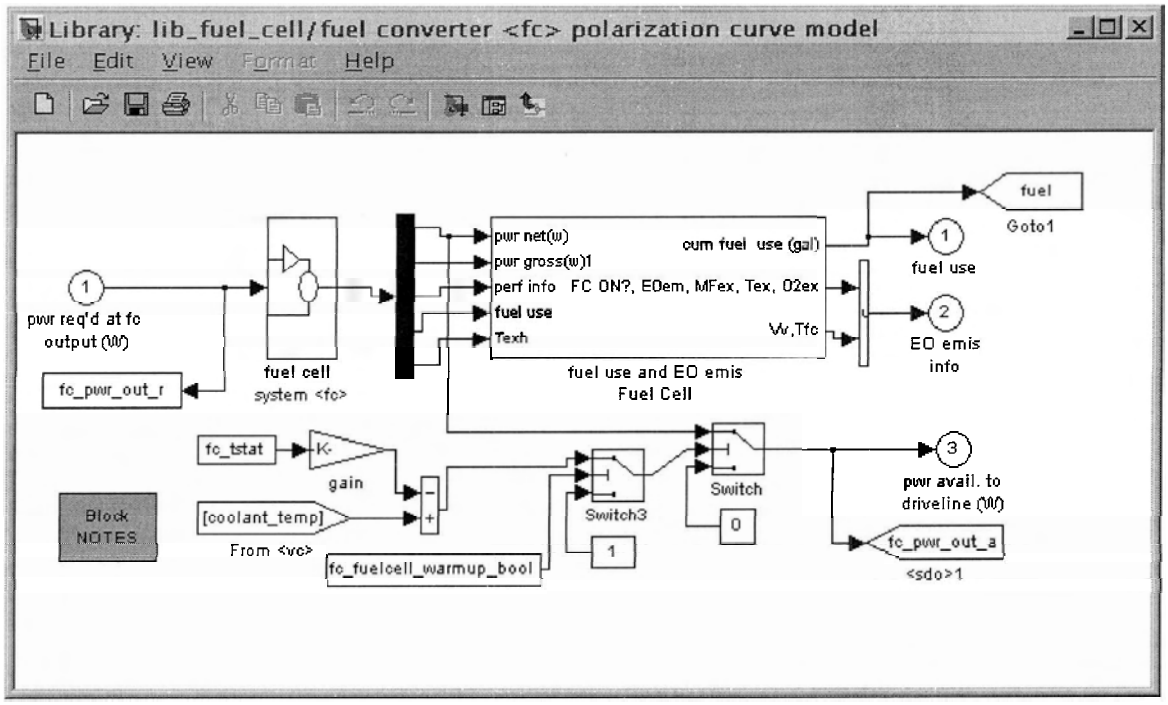

Figure 4.2: An example of a typical component model Simulink block

Creating a vehicle model involves specifying the vehicle powertrain architecture from the variety of available templates including conventional internal-combustion vehicles, internal-combustion hybrids or electric vehicles. Each template consists of an arrangement of expected component models which vary depending on the type of vehicle. A specific model is then selected for each component from either the choices included with ADVISOR or custom created component models. By default the package comes with a relatively broad selection of component models for sedan sized vehicles that have been obtained via testing of existing hybrid vehicles from the major automobile manufacturers. For larger vehicles there are some component models related to work on hybrid SUVs and busses, however there are far fewer models developed for smaller vehicle powertrains. Simple scaling can be done to many of the parameters used to

describe particular systems from the vehicle specification file. However if this is not sufficient it is relatively straightforward to create a new model by either using existing code as a starting point or writing a model from scratch.

Once a vehicle model is completely specified ADVISOR offers a variety of scenarios with which to measure the performance of the simulated automobile. Basic measures such as acceleration times to and from different velocities can be computed, and grade climbing ability can be explored in detail. However the primary tests performed on the modelled vehicles in ADVISOR revolve around simulating their performance while attempting to follow a given velocity over time. These profiles are referred to as drive cycles and many are used with actual vehicles for standardized emissions and fuel economy testing by government bodies. ADVISOR is especially useful because it enables the inspection of many internal and external performance characteristics at each time step as the model traverses the drive cycle. Some examples include how closely the vehicle is able to follow the drive cycle, the power into and out of all the drive train components and energy storage system and the rate and distribution of the emissions from the fuel converter. In addition ADVISOR compiles aggregate performance indicators such as fuel mileage and utilization at the end of the simulation.

In addition to running single simulations, ADVISOR has a limited capacity to perform parameter sensitivity analysis and auto-size components for simple objective functions. However these optimization routines can be enhanced using algorithms from MatLab's optimization toolbox or other external optimization programs. All of the adjustable input factors in the graphical interface can be manipulated directly in the MatLab workspace and any of the tests can be performed on the resulting model. The raw data from these tests can then be used for further analysis of the vehicle performance and stored for later comparison with other designs. This flexibility in both model construction and analysis was what lead to it being used as the research platform for exploring the parameters of low power fuel cell vehicle performance.

4.2.1. User Interface

The ADVISOR interface consists of a series of windows that progress through selecting and specifying a model, setting test parameters and displaying the results from the test.

When the program is launched from within MatLab an initial dialog is presented that gives a choice of unit systems to work in. Following that choice selection, a vehicle model setup window is displayed. The setup window shows the currently selected vehicle model along with a simple schematic and a list of its constituent component models on the right. Each of the component models that is associated with a scaling factor such as the fuel converter or energy storage system has an entry for adjusting the characteristic parameter of the model. A facility also exists for individually tuning any of the component model parameters if variations on saved vehicle models are to be tested. The current overall mass of the vehicle model is displayed, along with a selection of graphs showing characteristics of the selected component models such as the power/efficiency curves for the fuel converter.

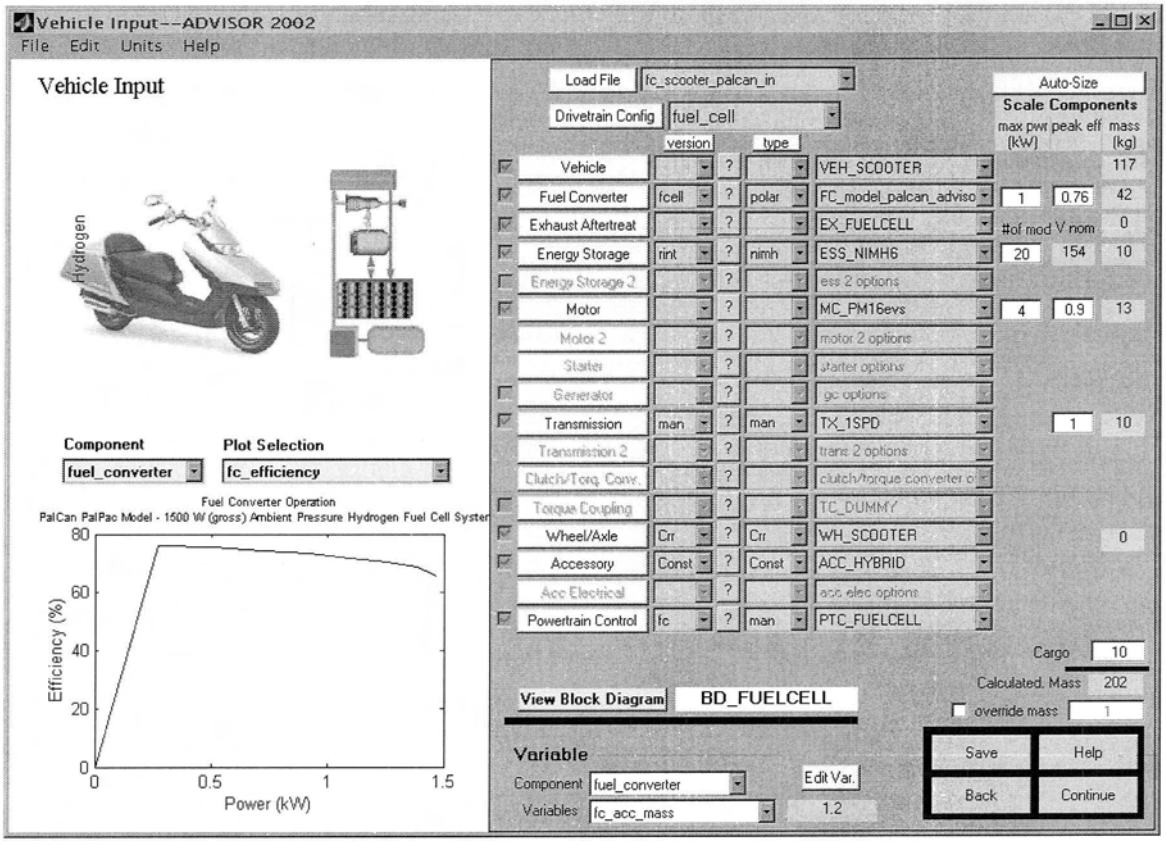

Figure 4.3: ADVISOR vehicle model selection/setup screen

Once the vehicle is set up to the users' satisfaction, ADVISOR moves to the testing screen. Here it is possible to specify the drive cycle to be simulated, along with any

additional acceleration or grade tests. A graph of the drive cycle is displayed along with some characteristic stats such as time, distance, mean velocity and a velocity histogram. The initial conditions can be set, as well as whether to run the test using a "zero-SOC" criterion and the tolerances for the test. The acceleration and grade tests have their own configuration dialogs where the settings for the desired speeds and grades can be adjusted. Optionally, the a parametric study of the vehicle can be specified here as well, which will use the aforementioned test settings while changing up to three component model scaling variables over a set range.

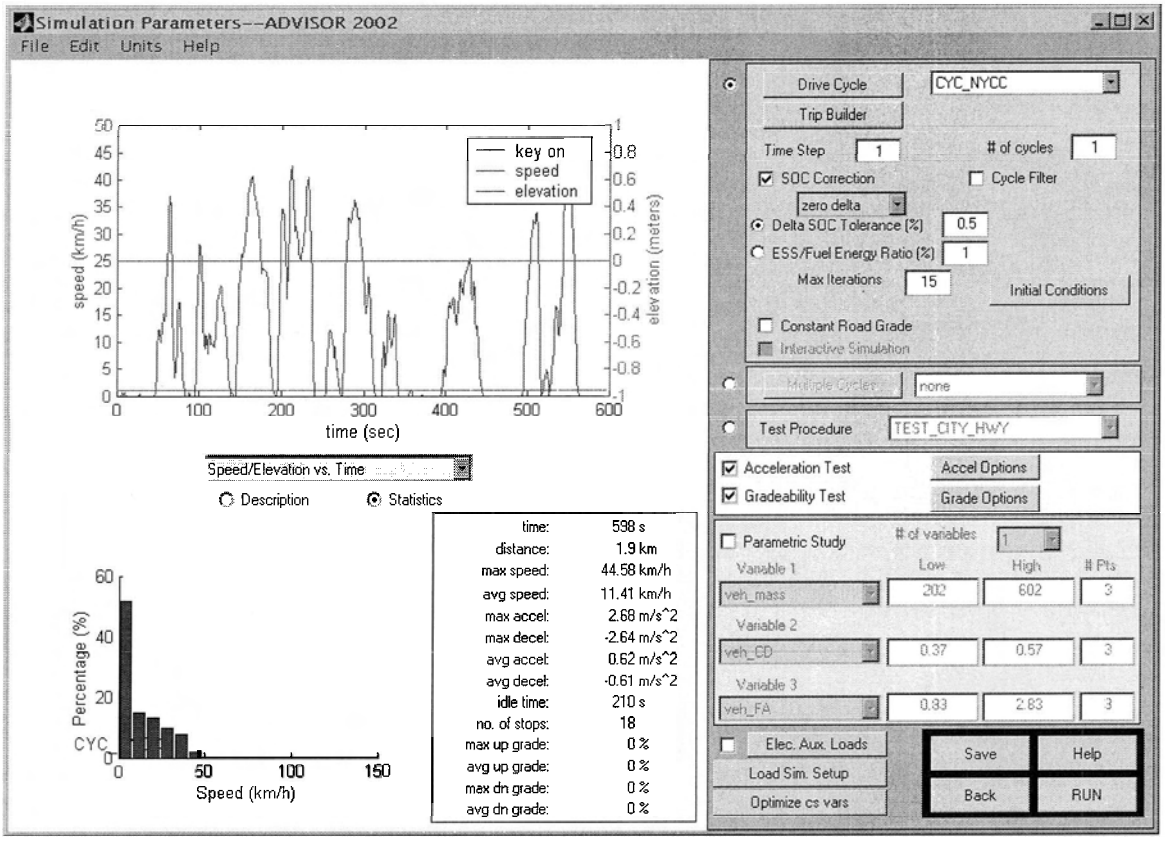

Figure 4.4: ADVISOR drive cycle selection screen

4.2.2. Simulation Window & Results

When the test has finished running, the results are displayed as a series of graphs. Initially the top graph shows an overlay of the tested drive cycle and the achieved velocity of the vehicle during the same time, while the second graph shows the level of

the energy storage system SOC over the test. The two lower graphs are initially blank, however any parameter that is recorded at each time step can be displayed on the graphs. This includes values such as component requested and achieved power outputs, efficiencies, temperatures etc. If acceleration or grade tests were also run the results are displayed along with fuel economy values expressed in terms of liters of fuel used and an approximately equivalent gasoline mileage value. Any problems with the vehicle model during the run are also indicated, such as an inability to achieve the requested velocity at any point along the drive cycle.

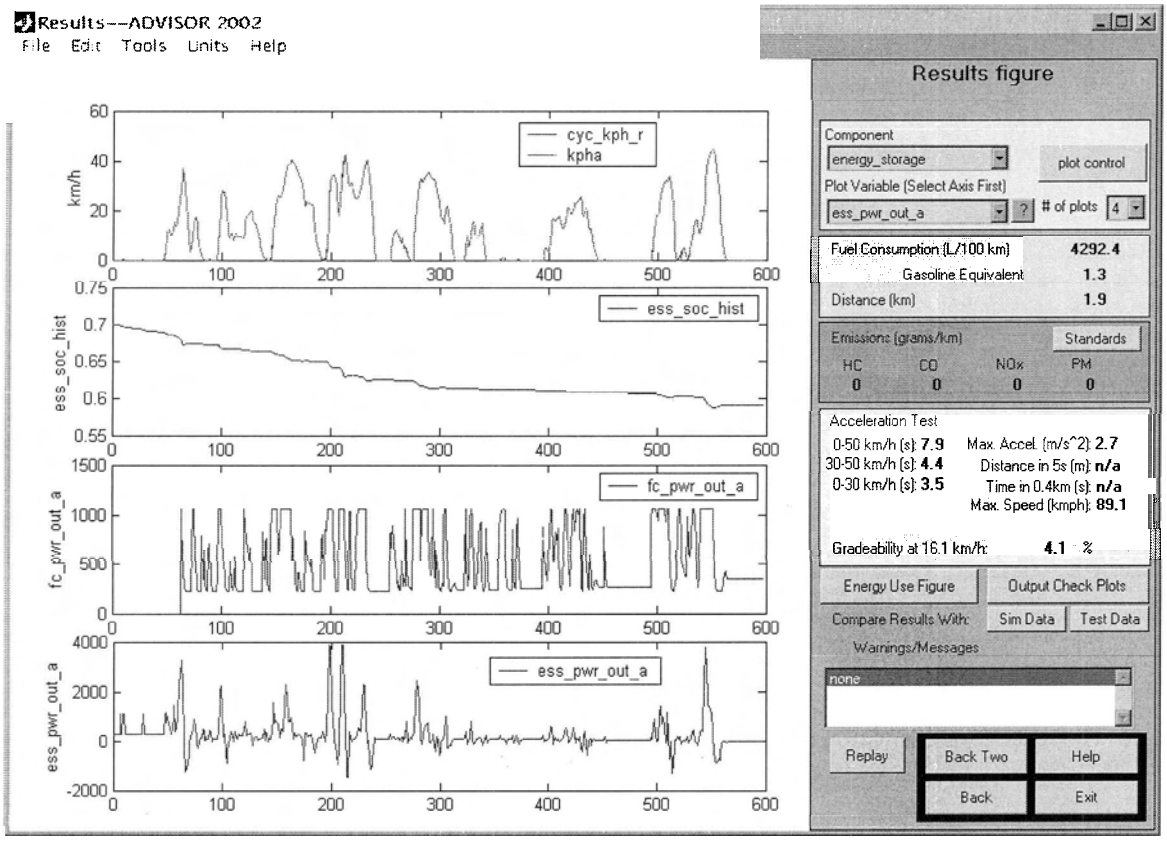

Figure 4.5: ADVISOR drive cycle simulation results screen

Further dialogs can be accessed from the results screen to report more detailed information about the vehicle and component models during the drive cycle. This includes efficiency maps and breakdowns of the losses incurred throughout the system. The results from the simulation can be saved to a data file for later redisplay or comparison with subsequent simulations.

4.3. Vehicle Parameters

The design of the ADVISOR model is broken down into many different modules for the many subsystems simulated in the vehicle.

4.4. Chassis

The chassis of the vehicle is specified in terms of parameters that primarily have an influence on the dynamic performance of the vehicle while driving. This includes basic physical dimensions and weight, as well as more complex measurements such as aerodynamic drag coefficient and the location of the vehicle's centre of gravity. The values given are primarily used by ADVISOR to determine how much power is required for a given velocity request. Because this power request is then propagated throughout the remaining vehicle model, the accuracy of the values is important.

The mass of the vehicle is a particularly important characteristic, impacting on many factors including inertia, rolling resistance and grade climbing ability. In this work, the weight of the chassis itself plus the additional weight of a typical passenger is used as the mass of the vehicle.

4.5. Fuel Converter Model

The fuel converter is an all-encompassing term for the device in the vehicle that converts chemical energy of a fuel into mechanical or electrical energy. This definition includes both conventional internal combustion engines connected to a generator, as well as alternatives such as fuel cells. From the perspective of the overall vehicle model these different technologies can be handled in essentially the same way, since the primary output parameters are the available power output and fuel required to achieve that power for both. However despite sharing a common external interface the internal structure of the fuel converter models varies widely to accurately simulate the different technologies involved.

For the low-speed vehicles being studied the fuel converter is a PEM fuel cell stack of between 1 and 3 kW. The component is based on a semi-empirical model obtained from previous work performed by Dr. Zuomin Dong at the University of Victoria and experimental data from tests performed on a 1500 W fuel cell stack.

ADVISOR offers two options for simulating the fuel cell, one based on lookup tables indexed to the polarization curve and an interface to external modelling programs. The internal polarization curve option is the easiest to use while remaining fast and reasonably accurate. To use the model either the existing 50 kW model can be scaled to the desired size, or polarization curve and accessory data obtained from experimental results can be used to create a new model. Although the option of scaling the existing model is feasible for some vehicles, for low-speed vehicles the scaling factor produces unacceptable inaccuracy in the simulated behavior of the model.

Using a new polarization curve with the model is relatively straightforward; the curve is discretized into a set of points specified by current density and stack voltage. From this data the gross power output of the fuel cell stack can be calculated at the given operating points. To determine the net power of the stack the parasitic losses to accessories required to operate the stack need to be deducted. These parasitic losses are considered to be dynamic and load-dependent, and are inputted as power requirements indexed to the current density of the stack polarization curve. By using these separate gross power and accessory lookup tables the model is very flexible and informative about the magnitude of parasitic losses under changing operating conditions. As well, by discretizing all of the operating data, the stack model requires very little computational power. The main disadvantage with the use of lookup tables is the inaccuracy due to the resolution of the data. However since the resolution is flexible it can be adjusted to match the accuracy of the experimental data on which the model is based.

In addition to the lookup-table based component models, ADVISOR also offers a theoretical fuel cell model which is based on a separate and standalone simulation program. Since the complexity of a completely theoretical model is outside the scope of a vehicle simulator, the easiest way of providing access to that type of model is through

external program linkages. ADVISOR currently includes code for integrating the theoretical fuel cell stack model called GCTool from the Argonne National Laboratory. Despite the additional complexity and computational power required, the theoretical model does provide the ability to model fuel cell stacks for which there is no available experimental data. It also provides the ability to use ADVISOR as a tool to optimize both the overall vehicle by manipulating component sizes and the fuel cell stack by modifying specific parameters of the stack design.

4.6. Fuel Storage Model

The fuel storage system is only considered in limited detail by any of the models in ADVISOR. Although the initial static mass of the fuel and fuel storage system is accounted for in the fuel converter model, all dynamic changes during vehicle operation are ignored. The additional complexity of attempting to model the mass reduction was not considered necessary given the small mass of fuel relative to the overall mass of the vehicle (approximately 1:360 ratio) for the vehicles being studied.

In addition to the physical parameters of the fuel storage system, the energy requirements associated with recovering the fuel from the storage systems are accounted for as a parasitic loss from the fuel converter. This energy requirement is designed to represent a fuel pump or similar mechanism required to transfer fuel from the storage system to the fuel converter in usable form. As a parasitic load, the fuel storage is generally dynamic, changing along with the power demands placed on the fuel converter, although the specific mechanism for calculating the energy requirement varies between model types.

4.7. Energy Storage Model

The energy storage system is important to the overall performance of the vehicle, necessitating an accurate model. ADVISOR has many different energy storage system models available for the variety of technologies available and the numerous approaches to simulating their behavior.

4.7.1. Battery Models

Batteries are currently the most common type of energy storage device used in hybrid vehicles, so there are many different types of models available to simulate them. In addition, the electrical behavior of batteries is very complex and is related to numerous factors, many of which can be difficult to measure in a working cell. Largely because of this complexity, along with the large variety of battery types, there are several different approaches that are used by the models in ADVISOR to attempt to accurately simulate their behavior. Similarly to the fuel converter models, the energy storage components generally require experimental data to produce an accurate model, although there is a basic theoretical model of a lead-acid battery provided as well.

Internal Resistor

The internal resistor approach is the most basic type of model used for batteries, since it is conceptually easy to understand and is relatively straightforward to code. The method models battery performance using a charge reservoir and voltage source with an internal resistance.

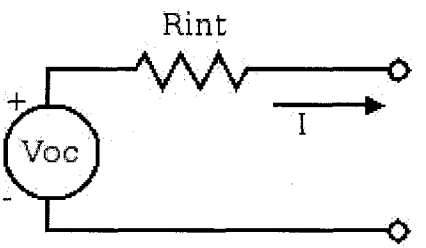

Figure 4.6: Internal Resistance model schematic

The circuit determines the output voltage and current based on the load, while calculations internal to the model attempt to estimate the rate at which this power level depletes the charge reservoir. Maximum and minimum voltage limits are enforced on the model to charge and discharge at realistically safe rates. Due to the non-linear behavior of batteries, the parameters of the simulation circuit are determined from experiments and used based on a lookup table indexed to the level of the charge reservoir. At each time step, the net current into or out of the battery is then used to estimate the change in State of Charge (SOC) of the battery. Finally, efficiency factors and the battery thermal model

are used to estimate the heat generation and transfer, along with the resultant change in the temperature of the battery.

The thermal model assumes forced air-cooling on generic stacked cylinder geometry, with homogeneous internal heat generation in the cells. The air flow rates and inlet air temperature can be specified, along with parameters like the approximate aggregate specific heat of the cell materials.

The greatest areas of inaccuracy of the model come from the estimation of the battery charge, which is dependent on many empirical parameters but not directly measurable during experiments. In addition, the model does not take into account dynamic effects caused by rapidly loading or charging the battery, as it is based on steady-state calculations. However it provides a reasonable approximation of battery behavior with minimal experimental data requirements and limited computational resources. As a result of being the first energy storage system model integrated into the ADVISOR system, there are a wide variety of battery sizes and types available. The majority of the low-speed vehicle models tested used this energy storage system model.

Resistance-Capacitance

The Resistance-Capacitance model simulates the behavior of a battery by using an equivalent circuit diagram made up of three resistors and two capacitors. The bulk capacitance (C_b) and end resistance (R_e) represent the large-scale charge storage and bulk resistance of the battery, while the surface capacitance (C_c) and capacitor resistance (R_c) represent the small scale surface effects in the battery which primarily affect the dynamic performance. The terminal resistance (R_t) represents another portion of the bulk resistance which is not as dynamically affected by the state-of-charge (SOC) of the battery.

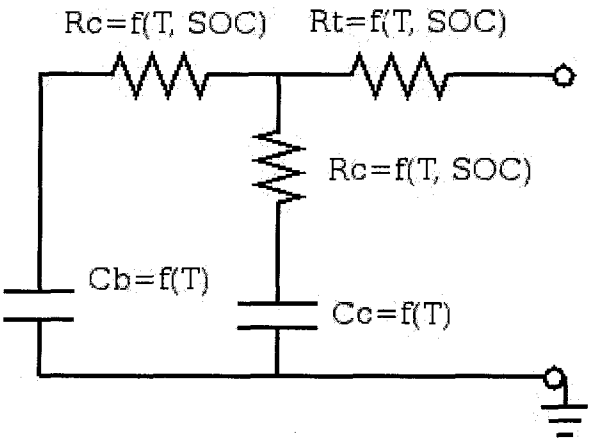

Figure 4.7: RC model schematic

The values for all of the above components were calculated from experimental results and indexed to both temperature and SOC of the battery. The temperature of the battery is determined using the same thermal model used for the internal resistance approach listed above. Although newer and more complex than the internal resistance model, it can accurately model the dynamic behavior of a battery in addition to steady state modes.

Fundamental Lead Acid

Another approach in contrast to the external performance modelling used by the previous models is to attempt to simulate the physical reactions that occur within a battery and extrapolate the external performance from those factors. However a fundamental model has only been developed for lead acid battery designs, limiting its usefulness for vehicle models that use any other battery technology. Due to weight and performance considerations the hybrid designs considered here tend to utilize more advanced types of battery such as NiMH and LiIon.

Neural Network

Another unique approach utilizes at sophisticated neural network to simulate the performance of a battery. The neural network acts as a non-linear multi-dimensional curve fit to sets of experimental data. Although the function to describe the many interrelated parameters of an operating battery is extremely complex, neural networks are "trained" to adapt to changing inputs and outputs, which it can then emulate. The

difficulty with this model comes from having limited predictive value as the function is most accurate only within the range it was trained, which limits its general applicability. Only a limited variety of batteries have been modelled using this method in ADVISOR, likely due to its recent addition and the significant amount of experimental data required to train the neural network.

4.7.2. Ultracapacitor Model

Ultracapacitors generally have much simpler models than batteries, as many of the complex temperature and state-of-charge effects are not present. The model used by ADVISOR uses an equivalent circuit of capacitor and resistor in series. The capacitor component represents the storage capacity of the ultracapacitor, while the resistor represents the internal resistance. Parameters for these equivalent components are dependent on both temperature and current, again determined from experimental data. Similarly to the battery models, voltage limits are enforced to control the charge and discharge rates at realistic levels.

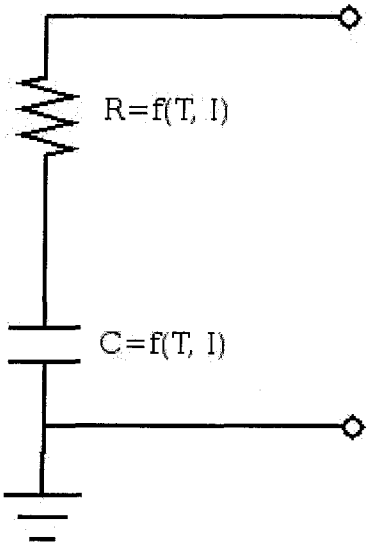

Figure 4.8: Ultracapacitor model schematic

The same thermal model used for the battery models is also used for the ultracapacitor model, with a simplified geometry.

4.8. Motor Model

The motor of a vehicle plays a large role in determining the overall performance of a vehicle, as a result the motor model is an equally important component of the vehicle model. ADVISOR contains numerous models that encompass a wide variety of types and sizes of AC and DC motors. However despite this diversity they are all based on a common modelling approach. To fit within the backwards-facing approach used by the entire vehicle model, the desired speed and torque requests propagated from the transmission are translated by the motor model into a power request. This transformation includes losses from the motor and controller, as well as dynamic effects such as rotor inertia and speed-dependent torque.

The model itself is entirely based on empirical data, which is utilized via a series of lookup tables for quick access. Controller blocks within the simulation ensure that the maximum current is not exceeded and shuts the motor down when it is not needed (such as braking or idling).

4.9. Accessories Model

An accessory load is an auxiliary mechanical or electrical load that is required on the modelled vehicle but not directly included in the powertrain. This accounts for electrical components such as lights and instruments as well as mechanical components such as a Power-Take-Off (PTO). Accessory loads for low-speed vehicles are usually strictly electrical and far less substantial than for conventional vehicles, due to their reduced size and generally utilitarian design. Often there are no heating or cooling requirements for the driver, nor are there substantial instrumentation loads. However even a minimal set of lights and electronics can constitute an intermittent load of several hundred watts.

For modelling purposes, the accessory load was characterized as a constant electrical load on the system which was active whenever the ignition was on. Although the actual accessory loads are likely intermittent to some degree, this aspect is difficult to deterministically simulate. The flexibility of ADVISOR does allow for variable accessory loads via customizable subsystems in Simulink, however a simulation

parameter to which the load can be indexed is not readily apparent. Instead, the use of a constant load is an approximation to produce a worst case estimate of the expected vehicle performance.

4.10. Test Parameters

Objectively measuring the performance of a vehicle can be a difficult operation, as there are many different aspects that are of varying importance depending on its intended use. There are many simple metrics that are commonly used to distinguish conventional vehicles such as acceleration time, fuel economy and engine power output, which are all relative easy to measure. In addition, there are more complex measurement techniques that attempt to replicate the real-world demands that may be placed on the vehicle.

4.10.1. Acceleration Tests

Acceleration test results are commonly used to compare conventional vehicle performance, since quick acceleration is important to most types of driving. The tests are easily performed, with a fixed distance and stopwatch all that is required.

4.10.2. Grade Tests

Grade tests measure the ability of a vehicle to maintain a certain speed while climbing the steepest grade possible. This is similar to a more intuitive form of the power to weight ratio of the vehicle in question, and provides a useful and objective insight into the suitability of a vehicle to different applications. However it is a difficult test to perform on an actual vehicle in a standardized fashion, since it would require that each testing agency have an identical grade available. Due to this difficulty it is not a test performed on vehicles on a regular basis, but it can be a valuable measure for computer simulated vehicles, or test on a chassis or vehicle dynamometer.

4.10.3. Drive Cycle Tests

Drive cycle tests are a more complicated test to perform, however they are capable of providing more realistic information about a vehicle's performance. Drive cycles are a velocity vs. time profile, which is obtained from recording actual driving situations or created to approximate a particular duty cycle. A drive cycle test consists of measuring the performance of the vehicle as it attempts to follow a given velocity profile. Although this type of test can provide large amounts of detailed information about the performance of a vehicle, they are much more complicated than acceleration and grade tests.

The advantage of managing the complexity of the tests is that they can offer more detailed and useful information into the performance of a vehicle. By selecting a drive cycle which matches a typical desired duty cycle for a vehicular application, the relative merits of different designs for that application can be measured and compared. Factors like state-of-charge of the energy storage system over a typical duty cycle, the efficiency of the power plant and use of regenerative braking are all measurements that are useful for evaluating the vehicle and not easily obtainable by other means.

4.11. Modification of the ADVISOR Vehicle Model

Several major modifications to the vehicle model were required to create a basic framework from which to simulate low-speed fuel cell hybrid electric vehicles. The prototype vehicle used as a basis for these modifications was a fuel cell hybrid scooter, designed to have similar performance as a 50cc motor scooter. Initially the model was based on a prototype vehicle from Palcan.

Figure 4.9.11: Prototype Palcan FC-HEV scooter

4.11.1. Vehicle and Chassis Component Models

The first modifications required were to the vehicle and chassis component subsystems. These were based on the physical dimensions of the scooter and so it was relatively easy to obtain new values. For the vehicle subsystem a new file was created, following ADVISOR component model naming conventions called VEH_SCOOTER.m to represent a baseline FC-HEV scooter.

Measurements of the approximate frontal area of the scooter were taken to calculate the aerodynamic drag, which worked out to 0.8 m^2. The drag coefficient for that area was obtained from Arne Laven's Masters thesis on fuel cell scooter design [18], though given the predominantly low speeds at which the scooter operates it is not vital to the model's accuracy.

The weight distribution of the vehicle was obtained by using a digital scale to measure the force exerted by each wheel of the Palcan scooter. This gave values of 45.4 kg for the front wheel and 68.0 kg for the rear, which translates to a 40%/60% front/rear weight distribution figure for the modelled scooter. A Wheelbase measurement of 118 cm was obtained from the Palcan scooter at the same time by measuring the distance between the center of the front and rear tire contact patches using a tape measure.

The mass of the vehicle chassis is also required for the model, however this was not measurable due to the inability to disassemble the scooter due to time and intellectual property constraints. However with the total vehicle mass known to be 113 kg and the major component weights known it was possible to make a reasonable estimate. The fuel converter with all required accessories and fuel storage was estimated to be approximately 42 kg, which is high mainly due to the presence of metal-hydride hydrogen storage tanks. The energy storage system was estimated to weigh 10 kg using nickel-MH batteries, while the motor and transmission were estimated at 22 kg [10]. Miscellaneous systems such as the power bus and auxiliary lights are not accounted for in any of the component models, so their weight is lumped with the chassis. This leads to an approximate chassis weight of 39 kg, which generally agrees with the weight of a 50cc scooter chassis obtained by Laven of 40 kg.

The inclusion of a driver in the mass of the overall vehicle is required, so a hypothetical rider was postulated to have a mass from the 50^{th} percentile of the CDC body mass index survey [19] for a driver aged between 20-29 of 78.3 kg. The inclusion of a miscellaneous cargo mass of 10 kg brings the final simulated vehicle mass to 201.3 kg.

4.11.2. Wheel/Axle Model

The wheel model is primarily used to account for the rolling resistance and inertial effects of the wheels of the vehicle. Rolling resistance is specified by two coefficients, a first-order value for low speed rolling resistance and a second-order coefficient for high speed (above ~70 km/h). Values for these resistances were obtained from Arne Laven's thesis, since they also came from a 50cc electric scooter similar to the one being modelled. More precise values could be obtained through further testing, however for a first approximation these values were deemed sufficient.

The other modification to the wheel model was the calculation of the wheel mass moment of inertia. This was calculated based on the Pirelli 120/80-10 SL38 model tire on a solid aluminum rim.

Values for the proportion of braking performed by the drivetrain and friction brakes were taken from the motorcycle wheel model which represented the closest wheel model available in ADVISOR. Although this solution is less than ideal, the instrumentation required to make useful measurements about the braking system *in situ* was unavailable.

4.11.3. Motor Model

Due to the small size of the scooter chassis and a desire to limit the expense of the vehicle, a permanent magnet DC electric motor was used to propel the vehicle. Although AC motors are generally used in hybrid vehicles due to their higher efficiency, this also requires a DC-AC converter and additional power conditioning circuits. The electronics increase both the size and the cost of the drivetrain, both of which are at a premium with a smaller vehicle. To model the DC motor, an existing module for a motor with a peak power of 16 kW included with ADVISOR was scaled to 3.5 kW and used for the scooter vehicle model.

4.11.4. Fuel Converter Model

Due to the existing fuel converter models being unsuitable for simulating a scooter sized fuel cell, a new model was developed that would more closely resemble the behavior of such a powerplant. This took the form of a fuel cell model that combined an external partially empirical fuel cell model with the existing ADVISOR polarization curve fuel cell model. The collection of experimental data and integration of that data into a new fuel cell component model was previously described in Chapter 3.

Integrating the separate fuel cell model into ADVISOR required a new fuel converter component model to act as an intermediary. This component model is based on the polarization curve model type from ADVISOR, however instead of using static curves stored in the data file, they are obtained from the new external model obtained from the experimental data. The data is then used by the polarization curve model as if it were static data. Although this approach is somewhat convoluted it has the benefit of quickly integrating a more dynamic model with a minimum of changes to the existing code.

4.11.5. Energy Storage Model

No data was available for the specific batteries used in the Palcan scooter, so the model for a generic widely used NiMH battery distributed with ADVISOR was selected instead. The model used is based upon test data obtained from the 6V NiMH cells used in the Toyota Prius hybrid car, so they represent high-quality energy storage devices already used in hybrid transportation applications. Since the test data is for an individual cell rather than the battery stack as a whole it is a simple matter to scale the energy storage model to the smaller sizes used in low speed applications.

4.11.6. Auxiliary Models and Other Work

In addition to the modules for the major powertrain components, changes were also made to the auxiliary component models such as the accessories or power control blocks. Most of the changes involved changes to static parameters governing the behavior of these generic models. Also, during the process of creating the model, several bugs were encountered and fixed in the ADVISOR modelling code and the fuel converter component model. These included the thermal modelling of the fuel cell model which was not correctly accounting for heat-removal via the radiator. Additionally, the small scale of the vehicles being considered for this work caused stability problems due to insufficient resolution between simulation time steps. To fix this a parameter was added to the command line ADVISOR interface allowing a user-specified interval for each model.

Aside from changes made to the model itself, work was put into developing more thorough data-analysis tools with which to evaluate the results obtained from ADVISOR. Although significant amounts of information are available from each simulation run, it is not collected into an easily analyzed format. To remedy this, a separate program called adv_analyze was created that could generate a detailed report from the simulation output. The report includes many quantities that are not calculated by ADVISOR directly:

- The total energy required by the vehicle: This is obtained by integrating the energy demand from the motor and accessories modules over the length of the

drive cycle. This is also broken down into the separate amounts so the relative size of the accessory and drive loads can be compared.

- The deviation from the requested motor energy to the amount of power provided by the fuel converter and energy storage system. A large shortfall can help indicate an undersized powertrain for the vehicle on the tested drive cycle.
- Total energy produced by the fuel cell, as well as how much of that energy went into driving the vehicle and how much went into running accessories/charging the ESS.
- Time average fuel cell efficiency: By default ADVISOR calculates the overall thermodynamic efficiency by comparing the total energy out of the fuel cell to the energy of the fuel used. The time average calculates the same efficiency for each time-step and averages them, but does not include time steps where the fuel cell is off and not producing power. This gives a more accurate value for the fuel cell performance, especially for stop-and-go drive cycles.
- The contribution from regenerative braking relative to the other energy flows in the powertrain is also calculated. Although ADVISOR simulates the effect of regenerative braking, the results provide very little direct information on the contribution. By visualizing braking performance in this way it is possible to gauge how the intermittency of a given duty cycle would affect the range of a hybrid vehicle.
- The ability of the vehicle to achieve the desired speed(s): Although the simulated vehicle will attempt to follow the requested velocity profile, there is no guarantee it will succeed. Measuring how closely the vehicle was able to match the desired velocity enhances the comparison of different vehicle designs on similar drive cycles. Calculated values include the percentage of time during the cycle that the vehicle was unable to meet the requested velocity, the average and maximum difference between the requested and achieved velocity when it was missed.
- Overall vehicle thermodynamic efficiency

- The total distance traveled during the simulated test and the resulting fuel economy for the vehicle. It is reported in terms of both hydrogen and gasoline for easier comparison between hybrid and conventional vehicles.

These values add to the basic performance picture provided by the default interface, and provide a convenient method of roughly comparing different vehicle designs and driving conditions. Many of the parameters attempt to quantify the contribution each of various subsystems make towards achieving the drive cycle with the intent of creating a clearer picture of how the components interact under load. This information is valuable when using the model to evaluate a design that may not yet exist.

CHAPTER 5 DESIGN OPTIMIZATION USING ADVISOR

Optimization is an important tool in modern design engineering, especially for products as complex as hybrid-electric vehicles. It can greatly assist in creating a design to meet a particular specification at minimum cost or producing the maximum performance from a given amount of resources. An important requirement for any design optimization approach to be successful is an accurate mathematical model of the problem. In the case of low speed fuel cell hybrid electric vehicles, the ADVISOR model developed above is well suited for this application for a variety of reasons. The model is flexible both in terms of the range of vehicles which it can reasonably approximate and the wide variety of duty cycles that can be simulated.

One of the benefits of ADVISOR being based on the MatLab/Simulink platform is the ability to easily integrate it with existing MatLab optimization routines. However although those algorithms are readily available they have problems with the complexity of the full vehicle model, often being unable to converge to a global minimum. Fortunately ADVISOR is not restricted in which optimization algorithms it can interoperate with and it is relatively straightforward to change to an approach more suited to handling this complex problem.

Before an optimization algorithm can be successfully applied to the model the problem must be clearly formulated. The typical method of organizing an optimization problem involves defining an objective function which describes the design in such a way that it can be minimized. This minimization is then constrained to reasonable design values using a series of constraint functions, creating a complex multi-dimensional problem.

5.1. Objectives

The primary objective in optimizing a low speed fuel cell hybrid electric vehicle depends largely on the intended duty cycle. Both the duty cycle in which it is intended to be used and the market to which it will be presented are important. Aspects generally common to all vehicle designs include adequate performance, low cost and good fuel economy. However the degree to which each is emphasized is in turn dictated by the design objectives. It is the problem of the designer formulating the optimization problem to accurately represent this emphasis using the objective function.

For the scooter prototype considered here the primary focus is on low cost and high fuel economy, with aspects such as performance and mass receiving secondary emphasis. To emphasize this objective function is formulated as a cost function, with major component sizes related to an approximate expense coefficient. The fuel economy can also be factored into the cost function to attempt to partially account for the lifetime costs of fuelling the vehicle.

5.2. Constraints

It is important to place bounds on the objective function that reflect the critical features of an optimized design. These constraints often consist of both minimum and maximum performance requirements as well as limiting dimensions so that the optimized design is physically feasible. It is important that the constraints be broad enough to explore a variety of designs while constraining the search-space to the general area of a feasible design.

The constraints used in the optimization problem for the scooter prototype include a sustainable cruising speed at or above the posted speed limit in urban areas. Also, sufficient acceleration to cruising speed to safely move with urban traffic. A top speed at or above highway speed would ensure that the scooter could traverse short sections of highway or freeway safely. A minimum grade climbing ability is also important to ensure the scooter does not get stuck on common inclines. Physical constraints include a

maximum and minimum fuel cell, battery and motor size, along with limits on the maximum and minimum vehicle weight.

5.3. The DIRECT Algorithm

Solving an optimization problem once it has been formulated requires the application of an algorithm designed to find the global minimum of a function with unknown characteristics. Although many methods have been found for finding a local minimum of an arbitrary function, they often provide no guarantees that the found minimum is the minimum for the entire function. In order to find the global minimum more complex methods must be employed. The ADVISOR software package includes an algorithm for performing global optimization on vehicle models called DIRECT (DIviding RECTangles) [14, 15]. As presented, the algorithm focuses on stability and accuracy over speed, which is desirable for the optimization problem presented by complex numerical vehicle models.

DIRECT eschews an analytical approach that requires gradient calculations for a more numerical approach. It is based on Lipschitz optimization methods, however with modifications to allow for more than two dimensions and the elimination of parameter tuning. The search-space for the objective function is partitioned into three equal regions, then the median point of each area is evaluated using the objective function. The ratio of the median values to the longest side length of the sub-divided area containing the median is calculated and used to compare the likelihood of each region containing the optimal value. One or more of the most likely regions are selected for further subdivision and sampled in a recursive fashion. Because the algorithm relies exclusively on sampling it is very stable, however depending on the shape of the objective function it may require an exhaustive and computation-intensive search to converge on the global optimum.

Despite the lack of speed the DIRECT algorithm is useful because of its stability, which allows it to capably deal with "black-box" functions that have unknown characteristics. In this it is well suited to ADVISOR model optimization, since the precise behavior of the objective function over the design space is unpredictable.

5.4. Sample Problem

To evaluate the suitability of the low-speed ADVISOR model for design optimization, a theoretical design optimization problem is posed. The optimization problem was formulated to determine the configuration of fuel cell size, motor size and battery capacity that could satisfy a given duty cycle with the least projected cost. For the purposes of the test the duty cycle was composed of a set of maximum acceptable acceleration times to different speeds, a minimum grade climbing ability and the ability to perform the New York City Cycle driving cycle.

To represent a typical duty cycle, the New York City Cycle (NYCC) was used as it represents a short commute in heavy traffic. It was recorded during a drive through Manhattan in New York, and as such there are many accelerations and decelerations due to the stop and go nature of traffic. The cycle contains peak speeds of 44 km/h, with an average speed of 11 km/h over the approximately 10 minute cycle. Other common urban cycles such as the Urban Dynamometer Drive Sequence (UDDS) were considered, but the NYCC was selected since it has relatively low peak speeds in addition to its average speed that one could reasonably expect a scooter to achieve. Additionally, its relatively short duration was attractive for reducing the computation time required for design optimization.

The cost-based objective function was used to approximate the investment costs of the three major powertrain components: fuel cell, motor and energy storage system. Estimated cost on a per kW or per Ah basis were used along with the scaling factor. The simulated mileage value for the scooter was also incorporated to partially account for fuel expenses over the lifetime of the vehicle as well. Although this objective function likely does not produce a realistic cost estimate for the actual production of a scooter given today's technology, it serves as an estimate for the major components cost assuming that they would represent the majority of the cost of the vehicle.

For our sample prototype optimization the objective function of the vehicle system investment cost is:

$$f(\boldsymbol{X}) = 1000 \times 1.049 \times x_1 + 300 \times 16 \times x_2 + 500 \times 6 \times x_3 + x_4 \qquad (5.4.1)$$

where $\boldsymbol{X} = \{x_1, \ldots, x_4\}$ is the vector of a number of generic design variables; and x_1 is the size of the fuel cell, x_2 is the size of the motor and motor controller, x_3 is the capacity of the energy storage system, and x_4 is the fuel economy.

These sizes are scaled to reflect the assumed costs of $1,000 per kW of net fuel cell power, $500 per amp-hour of battery capacity and $300 per kW of motor output. Although this function neglects other major costs of constructing an actual vehicle such as the chassis and accessory systems, the powertrain represents a large percentage of the overall vehicle expense and the primary area of difference from conventional scooters.

For the sample optimization, the acceleration and grade climbing requirements were determined from performance requirements outlined by Palcan [16] and existing literature [17]. A maximum time of 5 seconds to 30 km/h was the acceleration benchmark, which represented the requirement for decent low-end performance to safely maneuver with traffic. Additional acceleration requirements were imposed for the 0-50 km/h and 30-50 km/h times of 10 and 5 seconds respectively. The vehicle also had to be able to climb a minimum of a 15% grade. Both the acceleration and grade tests were simulated assuming an initial energy storage system state of charge of 80%.

With the problem so defined, it was optimized using the DIRECT global optimization algorithm. The final result was a design with a fuel cell of 0.89 kW net output, a motor size of 4.32 kW and a storage capacity of 3.2 Ah for the batteries. This was able to perform the NYCC with a sustainable energy storage state-of-charge (SOC) of 0.2, at an estimated 90.9 mile per gallon gasoline equivalent (mpgge) fuel economy Under acceleration simulation it was able to achieve times of 9.7 and 4.9 seconds for the 0-50 and 30-50 km/h tests, satisfying the given constraints. Finally the grade climbing ability of the design was predicted to be 15.7%. These results took 24 iterations and 679 total function evaluations, which amounted to nearly 9 days of computation on a 600 MHz computer. As shown in Figure 5.1, the search can be terminated after 10 iterations, and

the computation can be completed in 3.75 days on this modest PC if a looser stopping rule is used.

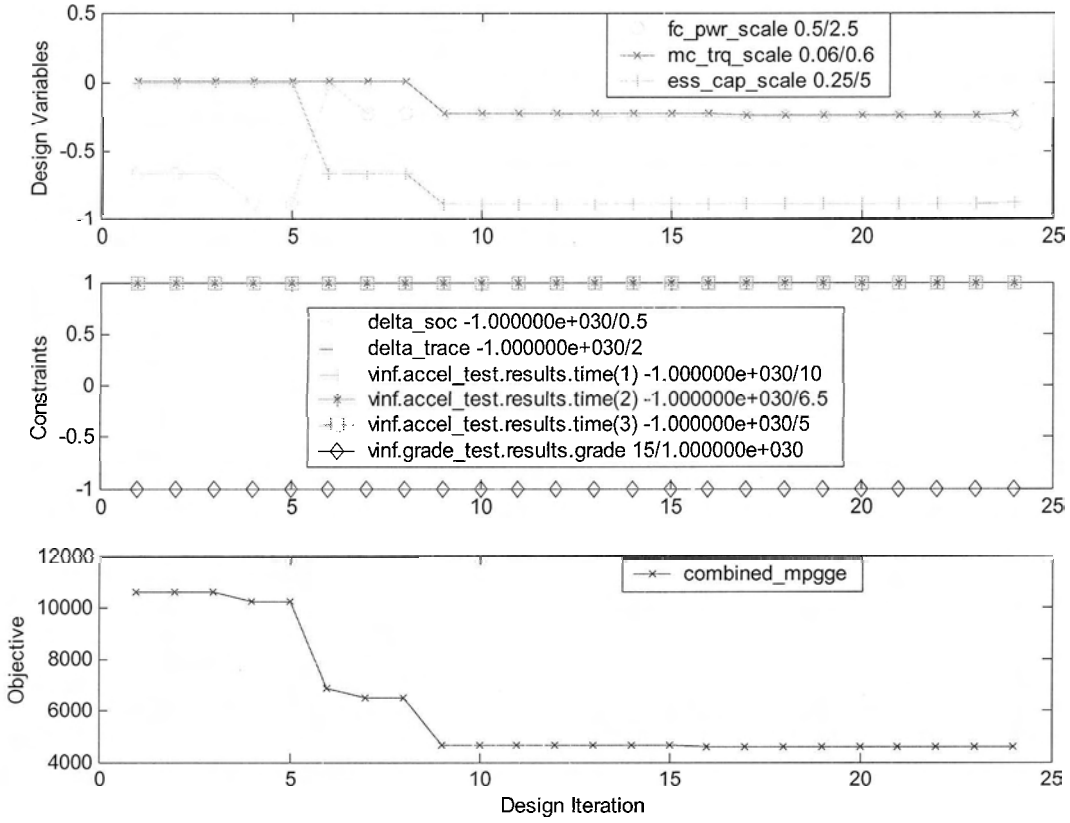

Figure 5.1: Optimization of scooter design over 24 iterations

Compared to the initial scooter design, this optimum had a 60% reduction on the value of the objective function of the optimization, achieving similar performance with a smaller fuel cell and more battery power. Although the larger fuel cell size of the initial design gave it superior endurance grade-climbing ability, the addition of battery capacity meant that the burst speed performance was similar and sustainable for long enough periods of time that a reasonable charge could be maintained in the batteries during use.

Table 5.1: Results of Design Optimization

Design Variable	Initial Value	Optimum
Size of the fuel cell, x_1	1.05 (kW)	0.89 (kW)
Size of the motor & motor controller, x_2	3.5 (kW)	4.28 (kW)
Capacity of the energy storage system, x_3	3 (Ah)	3.20 (Ah)
Fuel economy, x_4	111.4 (mpgge)	90.9 (mpgge)

CHAPTER 6 CONCLUSIONS

The development of the model for the fuel cell – battery hybrid electric scooter was more complicated than initially estimated due to the general lack of component models in ADVISOR at the appropriate scale. However with the dedicated fuel cell model along with modified models of ancillary devices, an adequate simulation of scooter performance was possible. Further testing of various system components to create a broader variety of candidate models at appropriate scale would improve the ability to model low-speed vehicles substantially.

The results from the model optimization showed some interesting trends with the scooter performance. The benefit of hybridization is easily visible as it allows for a smaller fuel cell by increasing the motor and energy storage system size. Especially for urban use where average speeds are slow but burst speeds can be high the downsides of shrinking the fuel cell relative to the energy storage are minimal. As long as the fuel cell is of sufficient size to provide a constant recharge to the energy storage this can be a sustainable arrangement. However this method of reducing the overall cost does come at the loss of some overall flexibility, limiting sustained cruising speeds and effectively barring the scooter from safe highway use. This limitation is not as critical due to the intended usage of these scooters and the fact that conventional internal combustion scooters do not tend to perform well in highway traffic either. It is also not a major factor for utility vehicles which tend to spend most of their time well away from highways.

The cost reductions available from using a hybrid design are also visibly significant. Due primarily to the large disparity between the cost of the fuel cell and the rest of the powertrain major savings are possible. These cost savings create more feasible opportunities for introduction of fuel cell vehicles into the commuter fleet, and lower the barrier to entry for doing research on fuel cell based vehicles.

Fuel cell hybrid low-speed electric vehicles are a potentially versatile and economical approach to solving mass transportation emissions problems in much of the world. The use of computer-aided design tools to reduce the size and major source of cost for these vehicles is imperative if they are to be introduced to market in a timely manner. Our work has shown that these tools are relatively easy to develop and powerful for performing initial design exploration before a more expensive prototyping stage or complex dynamic simulation is undertaken.

6.1. Research Contributions

The work in this thesis forms the basis for further research into the design of fuel cell hybrid electric vehicles. Data obtained from a small fuel cell was used to create an appropriately-sized model that could be integrated into the ADVISOR vehicle simulator. Combined with the development of additional component models for ADVISOR the ability of the vehicle simulator was expanded to model low-speed electric vehicles. A data analysis tool was created to obtain useful insights from the vehicle simulator. Preliminary optimization attempts demonstrated the flexibility and usefulness of the vehicle model as a preliminary design tool.

6.2. Future Work

Several avenues of further work based on the accomplishments detailed in this thesis are planned. The construction and calibration of a dynamometer/test platform is underway and will be used to validate the presented scooter model. Based on an dual-roller assembly and eddy-current brake system capable of dissipating up to 15 kW, it is designed to work in concert with a computer control system to provide a dynamically variable load. This control system allows low-speed vehicles to be tested using the same drive cycles as implemented in ADVISOR, providing the capability to verify the model outlined in this thesis and conduct further work on fuel cell vehicle design.

Figure 6.1: Electric and FCHEV scooters on lab dynamometer

Using the data obtained from the testing we hope to improve the accuracy of the model and expand to variety of vehicles under consideration to more powerful low-speed vehicles. In conjunction with this, there are also plans to work on enhancing the accuracy of the fuel cell model used in the vehicle simulation. By incorporating the parametrically-varied curves what were obtained during the fuel cell testing into a more sophisticated model, it is hoped to improve the accuracy of the model over a broader scale of operating conditions. Finally, we also plan to expand the scope of the model to account for fuel cell aging during use. This will allow the incorporation of the effects of different duty cycles on long term vehicle performance.

REFERENCES

1. Dockery, M., *An Association Between Air Pollution and Mortality in Six US Cities*, The New England Journal of Medicine, December 1993.

2. Houghton, J.T., Meira Filho, L.G., Callender, B.A., Harris, N., Kattenberg, A. and Maskell, K. (Eds.), *Climate Change 1995: The Science of Climate Change*, Cambridge University Press, UK. 1995, pp.572.

3. Scott, David S., "Energy Currencies," *International Journal of Hydrogen Energy*, v.19, n.3, 1994, pp.199-201.

4. Scott, David S., "The Energy System," *International Journal of Hydrogen Energy*, v.19, n.6, 1994, pp.485-490.

5. Amphlett, J.C., Farahani, M, et al., "Operation of a solid polymer fuel cell. A parametric model," *Proceedings of the Intersociety Energy Conversion Engineering Conference*, v 3, 1991, pp.624-629.

6. *Ballard Nexa Power Module Users Manual*, June, 2003, pp 11-12.

7. Staschewski, D., and Mao, Z.-Q., "Hydrogen-air PEMFC operation with extraordinary low gas pressures and internal humidification - concept and experimental prototype stack," *International Journal of Hydrogen Energy*, v.24, 1999, pp.543-548.

8. Hamelin, J., Agbossou, K., *et. al.,* "Dynamic behavior of a PEM fuel cell stack for stationary applications," *International Journal of Hydrogen Energy*, v.26, 2001, pp.625-629.

9. Wipke, K., Cuddy, M., and Burch, S., "ADVISOR 2.1: A User-Friendly Advanced Powertrain Simulation Using a Combined Backward/Forward Approach." *IEEE Transactions on Vehicular Technology: Special Issue on Hybrid and Electric Vehicles*, 1999.

10. Ortiz F., Buisset R., and Ades C., "VEDELEIC: New Technologies for Electric Vehicles, Results of Tests and Demonstration," *Proceedings of the 15th Electric Vehicle Symposium*, Brussels, October 1998.

11. Lindstrom, J., *et. al.* "Guidelines Fuel Cell Testing," University of Victoria, 2003.

12. Wipke, K., Cuddy, M., and Burch, S., "ADVISOR 2.1: A User-Friendly Advanced Powertrain Simulation Using a Combined Backward/Forward Approach," *IEEE Transactions on Vehicular Technology: Special Issue on Hybrid and Electric Vehicles*. 1999.

13. Markel, T., and Wipke, K., "Modelling Grid-Connected Hybrid Electric Vehicles Using ADVISOR," *Proceedings of the Annual Battery Conference on Applications and Advances*, 23-29. 2001.

14. Perttunen, C.D., Jones, D.R. and Stuckman, B.E., "Lipshitzian optimization without the Lipschitz constant," *Journal of Optimization Theory and Application*, v.79, n.1, 1993, pp.157-181.

15. Finkel, D. E., "DIRECT Optimization Algorithm User Guide," Center for Research in Scientific Computation, North Carolina State University. 2003.

16. Dong, Z., "Palcan-Uvic Fuel Cell Battery Hybrid Electric Scooter Technical Specifications," November, 2004.

17. Lin, B., "Conceptual design and modeling of a fuel cell scooter for urban Asia," *Journal of Power Sources*, v86, 1999, pp.202-213.

18. Laven, A., *Development of a Prototype Fuel Cell Powered Motor Scooter*, Masters Thesis, University of Nevada, 1999.

19. National Center for Health Statistics, National Health and Nutrition Examination Survey. *Anthropometric Reference Data, United States, 1988-1994*. Table 5. Hyattsville, Maryland: Public Health Service. 1996.

20. Venkataraman, P., *Applied Optimization with MATLAB Programming*, John Wiley & Sons, New York. 2002.

21. Wang, G. G., and Dong, Z., "Design Optimization of a Complex Mechanical System Using Adaptive Response Surface Method," *Transactions of the CSME*, v.24, n.1B, 2000, pp.295-306.

22. Laramie, J., Dicks, A., *Fuel Cell Systems Explained,* John Wiley & Sons, New York. 2002.

APPENDIX A: ADVISOR CODE

```
% fc_scooter_palcan_in.m
%
% By: Matthew Guenther <mguenthe@me.uvic.ca>
%
% First pass at a model for a hybrid electric/fuel cell powered
% scooter.  Attempt to achieve similar performance and form factor
% to a 50cc two-stroke scooter.

global vinf

vinf.name='FC/HEV Scooter';
vinf.drivetrain.name='fuel_cell';

vinf.fuel_converter.name = 'FC_model_palcan_advisor_H2';
vinf.fuel_converter.ver='fcell';
vinf.fuel_converter.type='polar';

vinf.motor_controller.name='MC_PM16evs';
vinf.energy_storage.name='ESS_NIMH6';
vinf.energy_storage.ver='rint';
vinf.energy_storage.type='nimh';
vinf.transmission.name='TX_1SPD';
vinf.transmission.ver='man';
vinf.transmission.type='man';
vinf.wheel_axle.name='WH_SCOOTER';
vinf.wheel_axle.ver='Crr';
vinf.wheel_axle.type='Crr';
vinf.vehicle.name='VEH_SCOOTER';
vinf.exhaust_aftertreat.name='EX_FUELCELL';
vinf.powertrain_control.name='PTC_FUELCELL';
vinf.powertrain_control.ver='fc';
vinf.powertrain_control.type='man';
vinf.accessory.name='ACC_HYBRID';
vinf.accessory.ver='Const';
vinf.accessory.type='Const';
% Scale components to scooter sizes
vinf.variables.name{1}='fc_pwr_scale';
vinf.variables.value(1) = 1.0;
vinf.variables.default(1) = 1.0;
vinf.variables.name{2}='fc_trq_scale';
vinf.variables.value(2) = 1.4;
vinf.variables.default(2) = 1.0;
vinf.variables.name{3}='mc_trq_scale';
vinf.variables.value(3)=0.21875;
vinf.variables.default(3)=0.21875;
vinf.variables.name{4}='ess_module_num';
vinf.variables.value(4)=20;
vinf.variables.default(4)=20;
vinf.variables.name{5}='ess_cap_scale';
vinf.variables.value(5)=0.5;
vinf.variables.default(5)=0.5;
vinf.variables.name{6}='fd_ratio';
vinf.variables.value(6)=1;
vinf.variables.default(6)=1;
vinf.variables.name{7}='fd_mass';
vinf.variables.value(7)=10;
vinf.varialbes.default(7)=10;
```

```
vinf.variables.name{8}='tx_mass';
vinf.variables.value(8)=10;
vinf.variables.default(8)=10;
vinf.variables.name{9} = 'acc_elec_pwr';
vinf.variables.value(9) = 300;
vinf.variables.default(9) = 300;
```

```
% FC_model_palcan_advisor_H2.m
%
% TERS model wrapper
%
% Call the model function to set the important parameters, use this
file
% to set the other (mostly irrelevant) constants
%


%%%%%%%%%%%%%%%%%%%%%%%%%%%%%%%%%%%%%%%%%%%
% FILE ID INFO
%%%%%%%%%%%%%%%%%%%%%%%%%%%%%%%%%%%%%%%%%%%
fc_description = 'PalCan PalPac Model - 1500 W (gross) Ambient Pressure
Hydrogen Fuel Cell System';
fc_version = 2002; % version of ADVISOR for which the file was
generated
fc_proprietary = 0; % 0=> non-proprietary, 1=> proprietary, do not
distribute
fc_validation = 2; % 0=> no validation, 1=> data agrees with source
data,
% 2=> data matches source data and data collection methods have been
verified
disp(['Data loaded: FC_model_palcan_advisor_H2.m - ',fc_description]);

%%%%%%%%%%%%%%%%%%%%%%%%%%%%%%%%%%%%%%%%%%%
% POLARIZATION CURVE
%%%%%%%%%%%%%%%%%%%%%%%%%%%%%%%%%%%%%%%%%%%

% Set values for fuel cell parameters used by empirical model
fc_cell_num = 25;
fc_cell_area = 384.0e-6; % (m^2)
fc_tstat = 45; % (deg C)
fc_coolant_cp = 4.182; % (J/gK)

% Execute theoretical/empirical model
model_palcan_advisor;

% For sane interpolation, cannot have any portion of the power curve
beyond maximum
% power, truncate all maps here?

% Select polarization curve model
fc_fuel_cell_model = 1;

fc_stack_num = 1; % number of stacks per parallel string
fc_string_num = 1; % number of parallel strings

fc_fuel_type = 'Hydrogen';
fc_fuel_den = 0.08181; % (g/L), density of the fuel
fc_fuel_lhv = 119.7*1000; % (J/g), lower heating value of the fuel
%fc_fuel_utilization_map = ones(size(fc_fuel_map)) * 0.8333333;


%%%%%%%%%%%%%%%%
% ACCESSORIES
%%%%%%%%%%%%%%%%
```

```
% fuel pump
fc_fuel_pump_map = fc_fuel_map * fc_cell_num; % (g/s)
fc_fuel_pump_pwr = ones(size(fc_fuel_pump_map)) * 50; % (W), estimated

% Use median as opposed to mean, OCV values usually screw the average
up
fc_fuel_air_ratio = median((fc_fuel_map * fc_cell_num) ./
fc_air_comp_map);

% Theoretical value, results in incorrect flow rate
%fc_fuel_air_ratio = (1.2 * 2.02) / (2.5 * 0.5 * 28.97); % (g/g)

% Theoretcial value, doesn't tend to work well
%fc_fuel_air_ratio = 1.2 / 2.5;

% FIXME [MBG]: Fixed coolant flow rate in g/s
fc_coolant_flow_rate = 140; % (g/s)

% FIXME [MBG]: May need values for this pump, unknown for purpose
(humidification, liquid fuels?)
fc_water_pump_map = [0, 1000]; % (g/s)
fc_water_pump_pwr = [0, 0]; % (W)
fc_fuel_water_ratio = 32/1000; % (g/g), should not be needed, does not
work without a value


%%%%%%%%%%%%%%%%%
% EMISSIONS
%%%%%%%%%%%%%%%%%

fc_emis = 0;       % boolean 0=no emis data; 1=emis data

% (g/s), engine out HC emissions indexed vertically by fc_map_spd and
% horizontally by fc_map_trq
fc_hc_map = zeros(size(fc_fuel_map));

% (g/s), engine out HC emissions indexed vertically by fc_map_spd and
% horizontally by fc_map_trq
fc_co_map = zeros(size(fc_fuel_map));

% (g/s), engine out HC emissions indexed vertically by fc_map_spd and
% horizontally by fc_map_trq
fc_nox_map = zeros(size(fc_fuel_map));

% (g/s), engine out PM emissions indexed vertically by fc_map_spd and
% horizontally by fc_map_trq
fc_pm_map = zeros(size(fc_fuel_map));

% (g/s), engine out O2 indexed vertically by fc_map_spd and
% horizontally by fc_map_trq
%fc_o2_map = zeros(size(fc_fuel_map));

fc_o2_map = fc_fuel_map * fc_cell_num * 9.9; % (g/s)


%%%%%%%%%%%%%%%%%%%%%%%%%%%%%%%%%%%%%%%%%%%
```

```
% COLD ENGINE MAPS                    %
%%%%%%%%%%%%%%%%%%%%%%%%%%%%%%%%%%%%%%%%%%%%%%%%%%%%%%%%%%%%%%%%%%%%%%%%%%%%%%%%%%%%%%%%%%%%%%%%%%%%%%%%%%%%%%%%%%%%%%%%%%%%%%%%%%%%%%%%%%%%%%%%%%%%%%%%%%%%%%%%%%%%%%%%%%%%%%%%%%%%%%%%%%%%%%%%%%%%%%%%%%%%%%%%%%%%%%%%%%%%%%%
%%%%%%%%%%%
fc_cold = 0;      % boolean 0=no cold data; 1=cold data exists
fc_cold_tmp = 20; %deg C
fc_fuel_map_cold = zeros(size(fc_fuel_map));
fc_hc_map_cold = zeros(size(fc_fuel_map));
fc_co_map_cold = zeros(size(fc_fuel_map));
fc_nox_map_cold = zeros(size(fc_fuel_map));
fc_pm_map_cold = zeros(size(fc_fuel_map));
%Process Cold Maps to generate Correction Factor Maps
names = {'fc_fuel_map', 'fc_hc_map', 'fc_co_map', 'fc_nox_map',
'fc_pm_map'};
for i = 1:length(names)
    %cold to hot raio, e.g. fc_fuel_map_c2h = fc_fuel_map_cold ./
fc_fuel_map
    eval([names{i},'_c2h=',names{i},'_cold./(',names{i},'+eps);'])
end


%%%%%%%%%%%%%%%%%%%%%%%%%%%%%%%%%%%%%%%%%
% DEFAULT SCALING                     %
%%%%%%%%%%%%%%%%%%%%%%%%%%%%%%%%%%%%%%%%%%%%%%%%%%%%%%%%%%%%%%%%%%%%%%%%
%%%%%%%%%%%
fc_pwr_scale = 1.0;   % --  scale fc power
%the following variable is not used directly in modelling and should
always be equal to one
%it's used for initialization purposes
fc_eff_scale = 1.0; % -- scale the efficiency
fc_trq_scale = 1.0; % -- required only for autosize and optimization
routines
fc_spd_scale = 1.0; % -- required only for autosize and optimization
routines
%%%%%%%%%%%%%%%%%%%%%%%%%%%%%%%%%%%%%%%%%%%%%%%%%%%%%%%%%%%%%%%%%%%%%%%%
%%%%%%%%%%%


%%%%%%%%%%%%%%%%%%%%%%%%%%%%%%%%%%%%%%%%%
% FUEL CELL MASS                      %
%%%%%%%%%%%%%%%%%%%%%%%%%%%%%%%%%%%%%%%%%%%%%%%%%%%%%%%%%%%%%%%%%%%%%%%%
%%%%%%%%%%%
%fc_base_mass=5.0*fc_max_pwr;        % kg   mass of the fuel cell
stack, assuming mass penalty of 5 kg/kW (DOE 2000 status)
%fc_base_mass = 1.50;          % kg   mass of the fuel cell stack,
assuming mass penalty of 2.5 kg/kW (DOE 2004 target)
fc_acc_mass = 1.20;          % kg   mass of fuel cell accy's, electrics,
cntrl's - assumes mass penalty of 0.5 kg/kW ESTIMATE

% FIXME [MBG]: don't know if this is still applicable, gets overriden
by ADVISOR internal
% calculation regardless
fc_max_pwr = (max(fc_pwr_map) / 1000) * fc_pwr_scale; % (kW)     peak
engine power

% calculate the mass of fuel for the fuel cell
target_range = 100; % (km)
target_fe = 200; % (mpgge)
```

```
gasoline_lhv = 42.6; % (kJ/g)
gasoline_density = 749; % (g/L)
L_to_gal = 3.785;
kJ_to_kWh = 277.777e-6;
fc_elec_density = 19.95; % (kWh/kg)
tank_storage_fraction = 0.015; % (kg H2/kg Tank) for FeTi-H2
%tank_storage_fraction = 0.073; % (kg H2/kg Tank) for MgH

fuel_energy = ((target_range/1.6093) / target_fe) * gasoline_lhv *
gasoline_density * L_to_gal * kJ_to_kWh; % (kWh)
fuel_mass = fuel_energy / fc_elec_density; % (kg)
tank_mass = fuel_mass / tank_storage_fraction; % (kg)

% set the final mass variables
fc_fuel_mass = fuel_mass + tank_mass; %(kg)
fc_mass = fc_base_mass + fc_acc_mass + fc_fuel_mass; %(kg)

% clear temporary calculation variables
clear target_range target_fe gasoline_lhv gasoline_density L_to_gal
kJ_to_kWh fc_elec_density;
clear tank_storage_fraction fuel_energy fuel_mass tank_mass;

% user definable mass scaling function
fc_mass_scale_fun =
inline('(x(1)*fc_trq_scale+x(2))*(x(3)*fc_spd_scale+x(4))*(fc_base_mass
+fc_acc_mass)+fc_fuel_mass','x','fc_spd_scale','fc_trq_scale','fc_base_
mass','fc_acc_mass','fc_fuel_mass');
fc_mass_scale_coef = [1 0 1 0]; % coefficients of mass scaling function
%%%%%%%%%%%%%%%%%%%%%%%%%%%%%%%%%%%%%%%%%%%%%%%%%%%%%%%%%%%%%%%%%%%%%%%
%%%%%%%%%%%


%%%%%%%%%%%%%%%%%%%%%%%%%%%%%%%%%%%%%%%%%%%%%%%%%%%%%%%%%%%%%%%%%%%%%%%
% OTHER DATA                                                            %
%%%%%%%%%%%%%%%%%%%%%%%%%%%%%%%%%%%%%%%%%%%%%%%%%%%%%%%%%%%%%%%%%%%%%%%
%%%%%%%%%%%
% variables not applicable to a fuel cell but needed for use of engine
block diagram

% set above in call to empirical model code
%fc_tstat = 60;                  % C      engine coolant thermostat set
temperature (typically 80 +/- 5 C)

% Specific heat values from Incropera & DeWitt
fc_cp = 706;                    % J/kgK  ave cp of engine (graphite)
(iron=500, Al or Mg = 1000)
fc_h_cp = 900;                  % J/kgK  ave cp of hood & engine
compartment (carbon fibre) (iron=500, Al or Mg = 1000)

%fc_ext_sarea = 0.3;             % m^2    exterior surface area of
engine
fc_ext_sarea = 2*(0.15*0.21) + 2*(0.15*0.19) + 2*(0.21*0.19);  % m^2
exterior surface area of engine
fc_hood_sarea = 1.5;            % m^2    surface area of hood/eng
compt.
fc_emisv = 0.8;                 %        emissivity of engine ext
surface/hood int surface
```

```
fc_hood_emisv = 0.9;            %        emissivity hood ext
fc_h_air_flow = 0.0;            % kg/s   heater air flow rate (140
cfm=0.07)
fc_cl2h_eff = 0.7;              % --     ave cabin heater HX eff (based
on air side)
fc_c2i_th_cond = 500;           % W/K    conductance btwn engine cyl &
int (carbon 1950 W/mK)
fc_i2x_th_cond = 500;           % W/K    conductance btwn engine int &
ext (carbon 1950 W/mK)
fc_h2x_th_cond = 10;            % W/K    conductance btwn engine &
engine compartment


%%%%%%%%%%%%%%%%%%%%%%%%%%%%%%%%%%%%%%%%%
% EXHAUST DATA                          %
%%%%%%%%%%%%%%%%%%%%%%%%%%%%%%%%%%%%%%%%%%%%%%%%%%%%%%%%%%%%%%%%%%%%%%
%%%%%%%%%%%

% Perform linearization and interpolation to determine wasted power
leaving the
% fuel cell stack as heat in the exhaust

%fc_ex_pwr_frac=[0.40 0.30];                          % --   frac of
waste heat that goes to exhaust as func of engine speed
fc_ex_pwr_frac = [0.20 0.10];                          % --   frac of
waste heat that goes to exhaust as func of power level, (SAE 2000-01-
0373)

%fc_exflow_map=fc_fuel_map*(1+14.5);                 % [g/s]  ex gas
flow map:  for SI engines, exflow=(fuel use)*[1 + (stoic A/F ratio)]
%fc_exflow_map = fc_fuel_map * (1 + 91) * fc_cell_num;  % [g/s]  ex gas
flow map:  for fuel cell  exflow=(fuel use)*[1 + (A/F ratio)], where
1.5*H2 + 2.0*(O2 + 3.774*N2) ==> H20 + 0.5H2 + 0.5O2 + 2.0*3.774*N2,
where 1.5=anode stoich, and 2.0=cathode stoich
fc_exflow_map = fc_fuel_map * fc_cell_num * 71.994;  % [g/s]  ex gas
flow map:  for fuel cell  exflow=(fuel use)*[1 + (A/F ratio)], where
1.2*H2 + 2.5*(O2 + 3.774*N2) ==> H20 + 0.2H2 + 0.75O2 + 2.5*3.774*N2,
where 1.2=anode stoich, and 2.5=cathode stoich

fc_waste_pwr_map = fc_fuel_map .* fc_fuel_utilization_map * fc_fuel_lhv
* fc_cell_num - fc_pwr_map;   % W    tot FC waste heat = (fuel pwr) -
(mech out pwr)
fc_ex_pwr_map = zeros(size(fc_waste_pwr_map));       % W   initialize
size of ex pwr map

for i = 1:length(fc_pwr_map)
    fc_ex_pwr_map(i) = fc_waste_pwr_map(i) * interp1([min(fc_pwr_map)
max(fc_pwr_map)], fc_ex_pwr_frac, fc_pwr_map(i)); % W  pwr map of waste
heat to exh
end

%fc_extmp_map=fc_ex_pwr_map./(fc_exflow_map*1089/1000) + 20;  % W   EO
ex gas temp = Q/(MF*cp) + Tamb (assumes engine tested ~20 C)
fc_extmp_map = fc_ex_pwr_map ./ (fc_exflow_map * 1145 / 1000) + 20;  %
W   EO ex gas temp = Q/(MF*cp) + Tamb (assumes engine tested ~20 C) (cp
based on exhaust composition listed above)
```

```
%%%%%%%%%%%%%%%%%%%%%%%%%%%%%%%%%%%%%%%%%%%%
% REVISION HISTORY
%%%%%%%%%%%%%%%%%%%%%%%%%%%%%%%%%%%%%%%%%%%%
% 05/06/2003 [MBG]: File created
```

```
% model_palcan_advisor.m
%
% Empirical/theoretical fc model based on the Palcan stack test data
% Some functions and data output eliminated, designed to obatin and
return
% required data to the global (i.e. 'base') environment while ADVISOR
is running.

function model
%warning off MATLAB:divideByZero
%warning off

fc_cell_num = evalin('base', 'fc_cell_num');
fc_cell_area = evalin('base', 'fc_cell_area');
fc_tstat = evalin('base', 'fc_tstat');
fc_coolant_cp = evalin('base', 'fc_coolant_cp');


% This routine defines the physical geometry of the stack. All units in
[mm]
% Data is for the Palcan PC 6 Stack
stack.stackW = 175; % Stack width
stack.stackH = 108 ; % Stack height
stack.nCell = fc_cell_num; % Number of cells in stack
stack.aPlateT = 2.25; % Air plate thickness
stack.hPlateT = 2.25; % Hydrogen plate thickness
stack.endPlateT = 4.5; % End plate thickness
stack.meaT = 0.75;    % Including carbon paper
stack.unactT = 8; % Innactive thickness on perimeter of stack

% Stack Length (the '+4' adds an allowance for bus and insulating
plates)
stack.stackL = 2*stack.endPlateT +
stack.nCell*(stack.aPlateT+stack.hPlateT+stack.meaT) + 4;

stack.RodArea = 3.1415*2*2; % Compression Rod Area [mm]2 = Pi*R2
stack.rodL = stack.stackL; % Compression rod length [mm]

dplate.reactChanD = 0.85; % Reaction channel depth [mm]
dplate.plateT = stack.aPlateT; % Plate thickness [mm]

stack.perimeter = 2*(stack.stackH + stack.stackW); % Stack Perimeter
[mm]
dplate.plateArea = stack.stackH*stack.stackW; % Total plate Area [mm2]
stack.activeArea = 9600; % Stack Activation Area [mm2]
stack.activeArea = fc_cell_area * 1e6 * stack.nCell; % [mm2] Stack
activation area

% ------------------------------------------------------------
% Weight [kg]
% This routine calculates the total weight of the stack
% Weight = Density * Volume , density given in g/mm^3
% ------------------------------------------------------------
eDens = 0.96e-3;
meaDens = 1.5e-3; % Membrane Density
gDens = 2.0e-3;    % graphite density
alDens = 2.707e-3;% aluminum
```

```
cDens = 8.93e-3;  % copper
uDens = 1.9e-3;   % ultem density
maniDens = 5e-3;  % manifold density 5e-3 g/mm^3 (medium between metal
and plastics)
SteelDens =7.8e-3;% Compression Rod density

wGraphitePlate =
dplate.plateArea*(dplate.plateT+0.4*dplate.reactChanD)*gDens*stack.nCel
l; % Weight [g] = Plate Volume*nCells*density
wEndPlate = dplate.plateArea*stack.endPlateT*alDens*2; % End Plate
Weight [g]
wRods = (6*stack.RodArea*stack.rodL)*SteelDens; % Compression rod
weight [g]
wMea = dplate.plateArea*stack.meaT*meaDens*stack.nCell; % Membrane
Weight [g]

property.totalWeight = (wGraphitePlate+wEndPlate+wRods+wMea)/1000; %
Total Stack Weight [kg]


% ------------------------------------------------------------------
----
% This routine calculates Voltage vs Current relationship
% ------------------------------------------------------------------
----
cool.airInT = 298;  % Average inlet air temperature

%cool.stackAvgT = 318; % Stack Temperature (deg K)
cool.stackAvgT = fc_tstat + 273; % Stack Temperature (deg K)

air.airAvgT = (cool.airInT + cool.stackAvgT) / 2; % Average air
temperature in the stack
relativeT = air.airAvgT - 300; % 300 K Room T
air.airDen = 1.1774 - 3.588e-3*relativeT;
air.airCp = (1.0057 - 6.600e-5*relativeT) * 1000;
waterCp = fc_coolant_cp * 1000; % Cp of water J/K-kg
air.airVisc = 1.983e-5 + 1.84e-8*relativeT;
air.airThermCond = 0.02624 - 7.58e-5*relativeT;
waterDens = 998; % density of water [kg/m3]

operation.h2Stoich = 1.2;
operation.airStoich = 2.5;
operation.temperature = cool.stackAvgT;
operation.pressureSaturate = 70.434643-
7362.6981/operation.temperature+0.006952085*operation.temperature-
9.000*log(operation.temperature);
operation.pressure = 304000.0; % H2 and air inlet pressure = 3 bar =
300000 Pa
operation.pressureSaturate = exp(operation.pressureSaturate)*100000; %
Saturation pressure of water in Pa


% Experimentally Derived Voltage[V] vs Current relationship----------
---------------
MaxCurrentDensity = 1.0; % Maximum Current Density A/cm2
Increment = 0.1; % Increment between current density data points
Npoint = MaxCurrentDensity/Increment;
```

```
%currentDen = Increment * [1:Npoint]; % Current density from 0-1 A/cm2
%currentDen = [Increment:Increment:MaxCurrentDensity];
currentDen = [0:Increment:MaxCurrentDensity]; % [A/cm2]

% fid = fopen('PolCurve.m','w');
% for j=1:Npoint,
%    voltage(j) = 1.012 - 0.03 * log((currentDen(j) * 1000) ) - 3.1e-4
* currentDen(j) * 1000 - 3.1e-4 * exp((6.0e-3 * currentDen(j) * 1000)
);
%    fprintf(fid,'%f %f\n ', [currentDen(j), voltage(j)]'); %
Experimentally derived V versus I relationship
%    property.tCurrent(j) = currentDen(j)*stack.activeArea/100; %FC
total current [A]
% end
% fclose(fid);
%
% % Empirically/Experimentally Defined Voltage vs relationship(Used for
Ballard Mark V model)
% fid = fopen('PolCurveEmpirical.m','w');
% for j=1:Npoint,
%     Tk=cool.stackAvgT; % Use the stack temperature for calculations
%     pressure.bars = 3; % H2 and air inlet pressure [bars]
%     pressureSaturate = operation.pressureSaturate/100000; %
Saturation pressure of water in bar
%     xn2in  = (1 - pressureSaturate/pressure.bars)*0.79;
%     xn2out = (1 - pressureSaturate/pressure.bars)/(1+
((operation.airStoich-1)/operation.airStoich)*(0.21/0.79));
%     xn2 = (xn2in + xn2out)/2; % Mole fraction of nitrogen
%     xh20 =  pressureSaturate/pressure.bars; % Mole fraction of water
%     ph2 = pressure.bars*(1 - 0.5*xh20); % Interface pressure of H2
[bars]
%     po2 = pressure.bars*(1 - xh20 -
xn2*exp(0.291*currentDen(j)/Tk^0.832)); % Interface pressure of O2
[bars]
%     po2inlet  = 0.21*(pressure.bars - pressureSaturate); % [bars]
%     xo2= po2/pressure.bars; % O2 Stoich Ratio
%     po2outlet = 0.21*(pressure.bars - pressureSaturate)*(1-
1/xo2)/(1-0.21/xo2);  % [bars]
%     po2int = (po2inlet-po2outlet/(log(po2inlet/po2outlet)));
% [bars]
%     co2=po2int/((5.08*10^6)*(exp(-498/Tk)));
%
%     property.tCurrent(j) = currentDen(j)*stack.activeArea/100; % [A]
%     a= 4.3085*(10^-5)*(Tk)*(log(ph2)+0.5*log(po2));
%     E(j)   =  1.229 - 0.85*(10^-3)*(Tk-298.15) + 4.3085*(10^-
5)*(Tk)*(log(ph2)+0.5*log(po2));
%
%     A = stack.activeArea/100;  % Active area of the fuel cell [cm]2
%     l = 0.0178; % Thickness of membrane [cm]
%     Lage = 14; % Membrane water content measure
%     rm(j) = 181.6*(1 + 0.03*(currentDen(j)) +
0.062*((Tk/303)^2)*(currentDen(j))^2.5)/((Lage - 0.634 -
3*(currentDen(j)))*exp(3.25*(Tk-303)/Tk));      % Resistivity of Nafion
Membrane
%     R(j) = rm(j)*l/A; % Resistance [Ohms]
%     nohm(j)= -property.tCurrent(j)*R(j); % Ohmic Voltage
%
```

```
%     nact(j)= -0.9514 +3.12*(10^-3)*(Tk) + 7.4*(10^-5)*(Tk)*log(co2) -
1.87*(10^-4)*(Tk)*log(property.tCurrent(j));
%
%     max_airflowLPM = 150; % Maximum air flow [LPM]
%     max_airflow_kgps = max_airflowLPM*(1/60)*(1/22.4)*(28.97)/1000;
% Maximum air flow [kg/sec]
%     max_current =
max_airflow_kgps/(28.97*operation.airStoich/(4*96484.55*0.21)/1000*stac
k.nCell); % Maximum current [A]
%     econ(j) = (8.31)*(Tk)*log(1 -
property.tCurrent(j)/max_current)/(96500*2); % Concentration voltage
%
%     voltage_emp(j) = E(j)+ nact(j)+ nohm(j)+ econ(j); % [V]
%    fprintf(fid,'%f %f\n ', [currentDen(j), voltage_emp(j)]'); %
Empirically derived V versus I relationship
% end
% fclose(fid);

% Palcan stack experimental data
fid = fopen('PolCurveExperimental.m', 'w');

% Old polarization curve data from Ballard stack
%currentDen = [0.00:0.1:1.30];
%voltage_exp = [1.00, 0.84, 0.79, 0.76, 0.72, 0.71, 0.68, 0.66, 0.64,
0.62, 0.59, 0.55, 0.46, 0.29];

% Polarization curve data from Palcan stack base case
voltage_exp = [24.58, 20.09, 18.84, 17.82, 17.11, 16.27, 15.57, 14.72,
13.66, 12.09, 6.11] / stack.nCell;
%voltage_exp = [20.09, 18.84, 17.82, 17.11, 16.27, 15.57, 14.72, 13.66,
12.09, 6.11] / stack.nCell;

% % Polarization curve data from Palcan stack for 5 psi reactant
pressure
% currentDen = [0:0.1:1.0];
% voltage_exp = [25.25, 20.56, 19.53, 18.50, 17.76, 16.94, 16.14,
15.24, 14.10, 12.12, 6.80] / stack.nCell;
%
% % Polarization curve data from Palcan stack for 6 psi reactant
pressure
% currentDen = [0:0.1:1.1];
% voltage_exp = [25.06, 20.92, 19.61, 18.56, 17.79, 17.01, 16.20,
15.37, 14.49, 13.33, 11.75, 8.50] / stack.nCell;

data = [currentDen; voltage_exp];
fprintf(fid, '%f %f\n', data); % Emprically derived V versus I
relationship
fclose(fid);

% Test polarization curve data to determine points and max current
density
Npoint = length(currentDen);
MaxCurrentDensity = max(currentDen); % Maximum Current Density A/cm2
property.tCurrent = (currentDen .* stack.activeArea) / 100; %FC total
current [A]

for j=1:Npoint,
```

```
    voltage_used(j) = voltage_exp(j); %% Use empirical voltage/current
relationship
    property.tVoltage(j) = voltage_used(j) * stack.nCell; % FC total
voltage [V]
    property.power(j) = property.tVoltage(j) * property.tCurrent(j); %
FC System Power [W]

    % FIXME[MBG] reversible voltage is temperature dependant, this does
not take that into account:
    property.heatProduced(j) = (1.48 -
voltage_used(j))*property.tCurrent(j)*stack.nCell; % Heat produced by
FC [W]
end % 1.48 V = (Change in enthalphy / n x F)  (eqn 3.13 of Michael's
thesis)

% ------------------------------------------------------------
% Flows (Calculates air and H2 inlet flows)
% ------------------------------------------------------------

% Totally made up fuel utilization factor for 100% of stoich hydrogen
used
operation.fuel_utilization = ones(size(voltage_used)) *
(1/operation.h2Stoich);

for i=1:Npoint,
    MH2 = 2.008; Mair = 28.97; % grams/mole of H2 and Air, F=Faradays'
Constant = 96484 C/mole
    operation.h2Flow(i) =
property.tCurrent(i)*MH2*operation.h2Stoich/(2*96484.55)/1000*stack.nCe
ll; % [kg/s] (see p.48 Micheal's thesis)
    operation.airFlow(i) =
property.tCurrent(i)*Mair*operation.airStoich/(4*96484.55*0.21)/1000*st
ack.nCell; % [kg/s] assume 21% O2 at compressor

    operation.prodWater(i) =
property.tCurrent(i)*18.0098/(2*96484.55)/1000*stack.nCell; % [kg/sec]
    operation.h2WaterFlow(i) =
8.937*operation.pressureSaturate/(operation.pressure-
operation.pressureSaturate)*operation.h2Flow(i);%(see p.50 Micheal's
thesis)
    operation.airWaterFlow(i) =
0.6219*operation.pressureSaturate/(operation.pressure-
operation.pressureSaturate)*operation.airFlow(i);
end

% ------------------------------------------------------------
% This routine determines heat loss of stack
% ------------------------------------------------------------
% Energy loss due to radiation (cool.aQRad)
sb = 5.67e-8; % Stefan Boltzmann constant [W m-2 K-4]
aEnd = stack.stackH*stack.stackW/1.0e6; % Area of FC ends [m2]
aSides = (stack.stackL*stack.perimeter)/1.0e6; % Area of FC sides [m2]
cool.aQRad = (2*aEnd*0.85 + aSides*0.70*1.3) *sb*
((cool.stackAvgT^4.0)-(cool.airInT^4.0));

% Energy loss due to natural convection (cool.aQNConv)
% (1) Natural convection for vertical walls
```

```
gravity = 9.81; % [kg/m3]
beta = 1/air.airAvgT;  % [K-1]
ra = gravity*beta*(cool.stackAvgT-
cool.airInT)*((stack.stackL/1000)^3.0)/(air.airVisc/air.airDen)/26.2e-
6; % Rayleigh number
cool.prNumber = 0.705; % Prandtl number for air
cool.nuNumber = ((1.0+ ((0.492/cool.prNumber)^0.5625))^0.4444444444); %
intermediate step
cool.nuNumber = 0.68+0.67*(ra^0.25)/cool.nuNumber; % Nusselt number
(vertical walls). See Michael's Thesis.
cool.aH = air.airThermCond/(stack.stackL/1000)*cool.nuNumber; % Heat
transfer coefficient
cool.aQNConv.wall = 1.15*aSides*cool.aH*(cool.stackAvgT-cool.airInT);
% The coefficient 1.15 is due to increased area due to geomemtry of
manifolds

% (2) Natural convection for top and bottom
aLPrime = aEnd/(stack.perimeter/1000);
ra = gravity*beta*(cool.stackAvgT-
cool.airInT)*(aLPrime^3)/(air.airVisc/air.airDen)/26.2e-6; % Rayleigh
number
aNuUp = 0.15*(ra^0.333); % Nusselt number top
aNuDown = 0.27*(ra^0.250); % Nusselt number bottom
hUp = air.airThermCond/aLPrime*aNuUp; % Heat transfer coefficient top
hDown = air.airThermCond/aLPrime*aNuDown; % Heat transfer coefficient
bottom
cool.aQNConv = cool.aQNConv.wall + (hUp+hDown)*(cool.stackAvgT-
cool.airInT)*aEnd; % Total convenction heat loss

% (3) Evaporative cooling [W]
% latent heat of vaporization [water] = 2.4e6 (J/kg)
for i=1:Npoint,
    operation.pWaterEvap(i) = 0.90; % Fraction of evaporated Product
water ??????
    cool.aQEvap(i) =
2.432e6*operation.pWaterEvap(i)*operation.prodWater(i);
    cool.aQAir(i) = property.heatProduced(i)-cool.aQRad-cool.aQNConv-
cool.aQEvap(i); % Total heat produced by convection [W]
    if (cool.aQAir(i) < 1.0) cool.aQAir(i) = 10.0; end
end

% ---------------------------------------------------------
% Powerdensity Volume[W/m3], Powerdensity Weight [W/kg]
% This routine calculates the power density for the stack
% for volume and weight. (gross power is used)
% Net Power = Gross Power - Parasitic power.
% ---------------------------------------------------------
for i=1:Npoint,
    property.powerVol(i) =
property.power(i)/(stack.stackL*stack.stackW*stack.stackH)*1e6; % Power
Density (Volume)
    property.powerWei(i) = property.power(i)/property.totalWeight; %
Power Density (Mass)

    % FIXME[MBG]: Why is this here?
    %(stack.stackL*stack.stackW*stack.stackH)*1e-9;
end
```

```
%-------------------------------------------------------------
% ParasitePower [Watts]
% This routine calculates the parasite powers
% Pump was selected using method used by (Cowden and Nahon,1996)
% -------------------------------------------------------------
sf = 1.5;  % Safety factor to account for extra pressure losses
pumpEff = 0.5; % efficiency of pump
motorEff = 0.7; % efficiency of motor
Patm = 101325; % Atmospheric pressure at 1 bar [N/m2]
pumpPDropHum  = 100000; % Assumed pump pressure drop [N/m2] (pumping
humidified air) ~ 16 psi
pumpPDropCool = 100000;  % Assumed pump pressure drop [N/m2](pumping
coolant)  ~ 2 psi
compK = 1.4; % constant "k" for isentropic compression
compEff = 0.7; % efficiency of compressor
comp.ratio = 3; % compression ratio of compressor

for i=1:Npoint,
    %% Power required to pump coolant [W]
    cool.waterFlow(i) = property.heatProduced(i) / waterCp /
(cool.stackAvgT - cool.airInT) / 0.1; % Water flow [kg/s]
    cool.wPump(i) = 0.8 * (((cool.waterFlow(i) / waterDens) *
pumpPDropCool * sf) / (pumpEff * motorEff)); % Pump Power [W] (needed
to reject 80% of heat)

    if (cool.wPump(i) < 5.0) cool.wPump(i) = 5; end

    %% Power required to pump humidifier water [W]
    tHumidWater(i) = operation.h2WaterFlow(i) +
operation.airWaterFlow(i)*0.5; % Total flow of water
    fcsystem.pumpPower(i) =
tHumidWater(i)/air.airDen*pumpPDropHum*sf/(pumpEff*motorEff); % Pump
Power [W]

    if (fcsystem.pumpPower(i) < 5.0) fcsystem.pumpPower(i) = 5; end

    % Compressor Power [W]
    fcsystem.compPower(i) = compK/(compK-
1)*Patm*operation.airFlow(i)/air.airDen*((comp.ratio^((compK-
1)/compK))-1)/compEff;

    if (fcsystem.compPower(i) < 10.00) fcsystem.compPower(i) = 10; end

    fcsystem.netPower(i) = property.power(i) - cool.wPump(i) -
fcsystem.pumpPower(i) - fcsystem.compPower(i);
end

% FIXME [MBG]: This is a hack to prevent negative powers in the power
map for ADVISOR compatibility
%fcsystem.netPower(1) = 0;

heatloss = cool.aQRad + cool.aQNConv;
GrossStackPower = (property.tCurrent .* voltage_used)*stack.nCell;

% Take care of divide by zero errors during division by zero power at
open circuit data point
```

```
efficiency = [0, fcsystem.netPower(2:length(fcsystem.netPower)) ./
property.power(2:length(property.power))]; % System efficiency
exergetic.efficiency = [0, (property.power(2:length(property.power)) ./
(operation.h2Flow(2:length(operation.h2Flow)) .*
operation.fuel_utilization(2:length(operation.fuel_utilization)))) *
(MH2/(1000*241826))]; % From ASME Paper also


% Truncate all current density indexed data to be exported so that no
points
% after the peak current density show up, otherwise problems occur
within
% ADVISOR during interpolation
peak_pwr_ind = find(fcsystem.netPower == max(fcsystem.netPower));



% Export data to caller workspace
% (if base used, ADVISOR has problems switching between ICE and fuel
cell models)
assignin('caller', 'fc_cell_num', stack.nCell);
assignin('caller', 'fc_cell_area', (stack.activeArea * 1e-6) /
stack.nCell); % Cell active area in m2
assignin('caller', 'fc_base_mass', property.totalWeight); % Weight in
kg
assignin('caller', 'fc_I_map', (currentDen(1:peak_pwr_ind) * 10000) *
stack.nCell); % Current density [A/m2]
assignin('caller', 'fc_V_map', voltage_exp(1:peak_pwr_ind));
%assignin('caller', 'fc_pwr_map', fcsystem.netPower(1:peak_pwr_ind)); %
Net power is fc elec output - heat losses - compressor losses
assignin('caller', 'fc_pwr_map', GrossStackPower(1:peak_pwr_ind)); %
Net power is fc elec output - heat losses - compressor losses
assignin('caller', 'fc_heat_loss', heatloss); % Heat output from stack
via radiation and convection
assignin('caller', 'fc_evap_loss', cool.aQEvap(1:peak_pwr_ind)); % Heat
out of stack due to liquid product water evaporating

%assignin('caller', 'fc_gross_pwr_map',
GrossStackPower(1:peak_pwr_ind)); % Gross electrical power
assignin('caller', 'fc_eff_map', efficiency(1:peak_pwr_ind));
assignin('caller', 'fc_exergy_eff_map',
exergetic.efficiency(1:peak_pwr_ind));

assignin('caller', 'fc_fuel_map', [0.00005,
operation.h2Flow(2:peak_pwr_ind) * 1000 / stack.nCell]); % Fuel cell
fuel flow at different current densities [g/s]
assignin('caller', 'fc_fuel_utilization_map',
operation.fuel_utilization(1:peak_pwr_ind));
assignin('caller', 'fc_air_comp_map', [0.00005,
operation.airFlow(2:peak_pwr_ind) * 1000]); % Stack air flow rate for
compressor [g/s]
assignin('caller', 'fc_air_comp_pwr',
fcsystem.compPower(1:peak_pwr_ind)); % Compressor power indexed by flow
rate [W]
assignin('caller', 'fc_pump_pwr', cool.wPump(1:peak_pwr_ind) +
fcsystem.pumpPower(1:peak_pwr_ind));
```

```
assignin('caller', 'fc_coolant_pump_map', [0.00005,
cool.waterFlow(2:peak_pwr_ind) * 1000]); % Cooling water flow [g/s]
assignin('caller', 'fc_coolant_pump_pwr', cool.wPump(1:peak_pwr_ind));
assignin('caller', 'fc_tstat', cool.stackAvgT - 273);


% Waste (heat) power, should be calculated from potential power from
fuel subtract gross electrical power
%assignin('base', 'fc_waste_pwr_map', cool.wPump + fcsystem.pumpPower +
fcsystem.compPower);

% fc_pump_map, fc_compressor_map (water, fuel and air flow in g/s)
% fc_coolant_flow_rate, fc_pump_map, fc_pump_pwr
% fc_base_mass, fc_acc_mass, fc_fuel_mass [kg]
%
fc_mass_scale_fun=inline('(x(1)*fc_trq_scale+x(2))*(x(3)*fc_spd_scale+x
(4))*(fc_base_mass+fc_acc_mass)+fc_fuel_mass','x','fc_spd_scale','fc_tr
q_scale','fc_base_mass','fc_acc_mass','fc_fuel_mass');
% fc_mass_scale_coef=[1 0 1 0]; % coefficients of mass scaling function

% emissions

% exhaust waste power (fc_evap_loss?)

% radiation heat transfer data, extra unused fuel converter variables


% ---------------------------------
% Export Data to files for plotting
% ---------------------------------

fid = fopen('PolCurveExperimentalLosses.m', 'w'); % Open file for
writing
data = [currentDen; GrossStackPower; efficiency; fcsystem.compPower;
cool.wPump; fcsystem.pumpPower];
fprintf(fid, '%f %f %f %f %f %f\n', data); % Write data to the file
fclose(fid); % Close the file



% % ------------------------------------------------------------
% % Plotting files
% % Output collected in matlab files: "gaout#.m"
% % ------------------------------------------------------------
% file0 = fopen('gaout0.m','w');
% % 1 currentDen (A/cm2), 2 Voltage (Polarization Curve)
% for i=1:Npoint,
% fprintf(file0, '%.2f %.2f\n', [currentDen(i),voltage_used(i)]');
% end
% fclose(file0);
%
% file1 = fopen('gaout1.m','w');
% % 1 currentDen, 2 netpower, 3 Power/Vol, 4 Power/Weight
% for i=1:Npoint,
% fprintf(file1, '%.2f %.2f %.2f %.2f\n',
[currentDen(i),fcsystem.netPower(i),property.powerVol(i),property.power
Wei(i)]');
```

```
% end
% fclose(file1);
%
% file2 = fopen('gaout2.m','w');
% % 1 currentDen (A/cm2) , 2 netpower, 3 heat power loss, 4 evaporation
power loss (Units: Watts)
% % 5 parasitic power, 6 Gross Stack Power
% for i=1:Npoint,

% fprintf(file2, '%.2f %.2f %.2f %.2f %.2f  %.2f\n',
[currentDen(i),fcsystem.netPower(i),heatloss, cool.aQEvap(i),
parasiticpower,GrossStackPower]');
% end
% fclose(file2);
%
%
% file3 = fopen('gaout3.m','w');
% % 1 currentDen, 2 system efficiency
% % 3 exergetic efficiency of system(from p.7 of Dr.Dong's FC modeling
notes)
% % LHV = 241826 kJ/KMol for H2
% for i=1:Npoint,
% fprintf(file3, ' %.2f %.2f %.2f\n',
[currentDen(i),efficiency(i),exergetic.efficiency(i)]');
% end
% fclose(file3);
```

```
% ADVISOR data file:     VEH_SCOOTER.m
%
% Data source:           Palcan prototype scooter measurements, Arne
Laven Masters Thesis, Vespa/Celco/Honda product
%                        specifications
%
% Data confirmation:     XXX
%
% Notes:                 Defines road load parameters for a hypothetical
E-scooter,
%                        based on measurements of the Palcan prototype
FC hybrid scooter.
%
% Created on:            04/30/2003
% By:                    Matthew Guenther <mguenthe@me.uvic.ca>
%
% Revision history at end of file.
%%%%%%%%%%%%%%%%%%%%%%%%%%%%%%%%%%%%%%%%%%%%%%%%%%%%%%%%%%%%%%%%%%%%%%%%%%%%
%%%%%%%%%

%%%%%%%%%%%%%%%%%%%%%%%%%%%%%%%%%%%%
% FILE ID INFO
%%%%%%%%%%%%%%%%%%%%%%%%%%%%%%%%%%%%
veh_description='Fuel Cell Scooter';
veh_version=2002; % version of ADVISOR for which the file was generated
veh_proprietary=1; % 0=> non-proprietary, 1=> proprietary, do not
distribute
veh_validation=0; % 0=> no validation, 1=> data agrees with source
data,
                  % 2=> data matches source data and data collection
methods have been verified
disp(['Data loaded: VEH_SCOOTER - ',veh_description])


%%%%%%%%%%%%%%%%%%%%%%%%%%%%%%%%%%%%
% PHYSICAL CONSTANTS
%%%%%%%%%%%%%%%%%%%%%%%%%%%%%%%%%%%%
veh_gravity = 9.81;     % m/s^2
veh_air_density = 1.2; % kg/m^3


%%%%%%%%%%%%%%%%%%%%%%%%%%%%%%%%%%%%
% VEHICLE PARAMETERS
%%%%%%%%%%%%%%%%%%%%%%%%%%%%%%%%%%%%
% Note on vehicle mass:
%   The measured curb weight for the Palcan scooter is 113 kg
%   For reference: Vespa ET2 curb weight 98 kg, Suncom 71 kg (excl.
batteries)

veh_glider_mass = 39 + 78.3; % (kg), vehicle mass w/o propulsion system
(fuel converter,
                             % exhaust aftertreatment, drivetrain,
motor, ESS, generator) +
                             % weight of one passenger.  Weight of
passenger determined from
                             % 50th percentile 20-29 year old (78.3 kg)
from the
```

```
                                % NHANES III survey

veh_CD = 0.37;  % (--), coefficient of aerodynamic drag (from Arne
Laven's thesis)
veh_FA = 0.83;    % (m^2), frontal area, including driver, from Palcan
scooter and personal body estimates.

% fraction of vehicle weight on front axle when standing still
veh_front_wt_frac = 0.38;  % from Palcan prototype scooter

% height of vehicle center-of-gravity above the road
veh_cg_height = 0.3;    % (m) from Celco E-Scooter

% vehicle wheelbase, from center of front tire patch to center of rear
patch
veh_wheelbase = 1.30;   % (m)
veh_cargo_mass = 10; %kg  cargo mass

%%%%%%%%%%%%%%%%%%%%%%%%%%%%%%%%%%%%%%%%%%%%
% REVISION HISTORY
%%%%%%%%%%%%%%%%%%%%%%%%%%%%%%%%%%%%%%%%%%%%
% 06/06/2004 [MBG]: Modify to use values from Palcan prototype scooter
% 22/03/2003 [MBG]: Modify mass, wheelbase, CD, FA to be closer to an
actual scooter, using
%   values from Arne Laven's thesis
```

```
% ADVISOR data file:  WH_SCOOTER.m
%
% Data source:
%
% Data confirmation:
%
% Notes:
%
% Created on: 4/25/2003
% By:  Matthew Guenther <mguenthe@me.uvic.ca>, based on WH_CYCLE.m
%      by tony_markel@nrel.gov
%
% Revision history at end of file.
%%%%%%%%%%%%%%%%%%%%%%%%%%%%%%%%%%%%%%%%%%%%%%%%%%%%%%%%%%%%%%%%%%%%%%%%%%%%%%%
%%%%%%%%%


%%%%%%%%%%%%%%%%%%%%%%%%%%%%%%%%%%%%%%%%%%%%
% FILE ID INFO
%%%%%%%%%%%%%%%%%%%%%%%%%%%%%%%%%%%%%%%%%%%%
wh_description='Wheel/axle assembly for scooter';
wh_version=2002; % version of ADVISOR for which the file was generated
wh_proprietary=0; % 0=> non-proprietary, 1=> proprietary, do not
distribute
wh_validation=0; % 0=> no validation, 1=> data agrees with source data,
% 2=> data matches source data and data collection methods have been
verified
disp(['Data loaded: WH_SCOOTER - ',wh_description])


%%%%%%%%%%%%%%%%%%%%%%%%%%%%%%%%%%%%%%%%%%%%
% FORCE AND MASS RANGES over which data is defined
%%%%%%%%%%%%%%%%%%%%%%%%%%%%%%%%%%%%%%%%%%%%
% vehicle test mass vector used in tandem with "wh_axle_loss_trq" to
estimate
% wheel and axle bearing and brake drag
wh_axle_loss_mass = [0 2000];    % (kg)
% (tractive force on the drive tires)/(weight on drive axle), used in
tandem
% with "wh_slip" to estimate tire slip at any time
wh_slip_force_coeff = [0 0.3913 0.6715 0.8540 0.9616 1.0212];  % (--)

%%%%%%%%%%%%%%%%%%%%%%%%%%%%%%%%%%%%%%%%%%%%
% LOSS parameters
%%%%%%%%%%%%%%%%%%%%%%%%%%%%%%%%%%%%%%%%%%%%
% drag torque applied at the rear (drive) axle, used with
"wh_axle_loss_mass"
wh_axle_loss_trq = [4 24]*.1;    % (Nm)
% slip=(omega * r)/v -1; used with "wh_slip_force_coeff"
wh_slip = [0.0 0.025 0.050 0.075 0.10 0.125];  % (--)


%%%%%%%%%%%%%%%%%%%%%%%%%%%%%%%%%%%%%%%%%%%%
% OTHER DATA
%%%%%%%%%%%%%%%%%%%%%%%%%%%%%%%%%%%%%%%%%%%%
%wh_radius=23.8/39.37/2; % bridgestone and ecycle websites, Front Tire:
MT 75, 110/70-17 Rear Tire:  MT 75, 130/70-17
```

```
%wh_radius=0.207 % Vespa 100/80-10 Pirelli SL38 front tire
wh_radius = 0.223; % Vespa 120/80-10 Pirelli SL38 rear tire
wh_inertia = 0.21854;  % (kg*m^2) Estimated via wheel_inertia.xls

% fraction of braking done by driveline, indexed by wh_fa_dl_brake_mph
% remainder of braking performed by friction brake system
wh_fa_dl_brake_frac=[0 0 0.7 0.8 0.8];  % (--)

% fraction of braking done by front friction brakes,
% indexed by wh_fa_fric_brake_mph
% remainder of braking performed by rear friction brakes
wh_fa_fric_brake_frac = [0.6 0.6 0.3 0.2 0.1];  % (--)
wh_fa_dl_brake_mph = [-1 0 10 60 1000];   % (mph)
wh_fa_fric_brake_mph = wh_fa_dl_brake_mph; % (mph)

wh_1st_rrc = 0.0157; % (--), rolling resistance coefficient, estimate
from Arne Laven's Masters thesis
wh_2nd_rrc = 0; % (s/m) This is assumed to be zero as scooters are
generally slow vehicles.  Speed does
              % not significantly affect rolling resistance below 45
mph

wh_mass = 0;

%%%%%%%%%%%%%%%%%
% Error checking
%%%%%%%%%%%%%%%%%
% dl+fa_fric must add up to <= 1 for all speeds.  Give user warning if
in error
temp_total_braking=wh_fa_dl_brake_frac+wh_fa_fric_brake_frac;
if any(temp_total_braking>1)
    disp('Warning: Driveline and Front Friction Braking need to add to
less than or equal to 1 for')
    disp('         all speeds.  Please edit either wh_fa_dl_brake_frac
or wh_fa_fric_brake_frac');
    disp('         in WH_*.m.  See Chapter 3.2.4, Braking of the
documentation for more info.');
end
clear temp_total_braking

%%%%%%%%%%%%%%%%%%%%%%%%%%%%%%%%%%%%%%%%%%%%
% REVISION HISTORY
%%%%%%%%%%%%%%%%%%%%%%%%%%%%%%%%%%%%%%%%%%%%
% 4/25/2003: file created
```

APPENDIX B: OPTIMIZATION PROBLEM CODE

```
% optim_scooter.m
%
% Script to exercise the DIRECT optimization Algorithm with ADVISOR.
%
% 1) initialize workspace
% 2) define the problem
% 3) run optimizer
% 4) save results
%

% initiate timer
tic

diary thesis_optim_direct_log.txt;
start_time = sprintf('Start Time: %s\nStart CPUTime: %g\n',
datestr(clock,0), cputime);
disp(start_time);

% initialize the workspace
if 1% 1=initialize, 0=don't initial - for continuation runs
    input.init.saved_veh_file='thesis_optim_scooter_in';
    input.init.time_step = 0.1;
    [a,b]=adv_no_gui('initialize',input);
end

dv_names={'fc_pwr_scale','mc_trq_scale','ess_cap_scale'};
resp_names={'combined_mpgge'};
con_names={'delta_soc','delta_trace','vinf.accel_test.results.time(1)',
'vinf.accel_test.results.time(2)','vinf.accel_test.results.time(3)','vi
nf.grade_test.results.grade'};

% define the problem
cont_bool=0;
p_f='obj_fun_thesis_scooter';
p_c='con_fun_thesis_scooter';
x_L=[0.5,  0.06,   0.25]';
x_U=[2.5,   0.6,    5]';
A=[];
b_L=[];
b_U=[];
c_L=[-1e30; -1e30;  -1e30;  -1e30;  -1e30;  15];
c_U=[0.5;   2;      10.0;    6.5;    5.0;   1e+30];
I=[];
PriLev=2;
MaxEval=618;
MaxIter=31;
GLOBAL.epsilon=1e-4;
prev_results_filename='thesis_optim_direct_results';

if cont_bool==1
   eval(['load(''',prev_results_filename,''')'])
   GLOBAL = direct_opt_results.GLOBAL;
   GLOBAL.MaxEval = MaxEval;
   GLOBAL.MaxIter = MaxIter;
else
   GLOBAL.MaxEval = MaxEval;
   GLOBAL.MaxIter = MaxIter;
```

```
end

plot_info.var_label=dv_names;
plot_info.var_ub=num2cell(x_U);
plot_info.var_lb=num2cell(x_L);
plot_info.con_label=con_names;
plot_info.con_ub=num2cell(c_U);
plot_info.con_lb=num2cell(c_L);
plot_info.fun_label=resp_names;

% start the optimization
direct_opt_results = gclSolve(p_f, p_c, x_L, x_U, A, b_L, b_U, c_L,
c_U, I, GLOBAL, PriLev, plot_info, dv_names, resp_names, con_names);

% save the results
eval(['save(''',prev_results_filename,''',',''''direct_opt_results'');']
)

% save the vehicle
input.save.filename='thesis_scooter_optim_result';
[a,b]=adv_no_gui('save_vehicle',input);

% plot the optimization results
plotoptimresults(direct_opt_results.GLOBAL.f_min_hist, plot_info)

end_time = sprintf('Finish Time: %s\nFinish CPUTime: %g\n',
datestr(clock,0), cputime);
disp(end_time);
diary off;

% end timer
toc
```

```
% obj_fun_thesis_scooter.m
function obj=obj_fun(x,varargin)

% x is design vector, for this problem
%   x(1) is fc scaling factor
%   x(2) is motor scaling factor
%   x(3) is number of battery modules

% initialize
error=0;
obj=0;
txt_error=0;

[stat_text,txt_error] = sprintf('FC Size (kW): %g\nMotor Size (kW):
%g\nESS Ah Capacity: %g\n', x(1)*0.749, x(2)*16, x(3)*6);
disp(stat_text);

% update parameter settings
input.modify.param=varargin{1}; % parameter names are stored in the
first optional argument
input.modify.value=num2cell(x); % assign corresponding values
[error,resp]=adv_no_gui('modify',input);

% run test procedure
if ~error
   input.cycle.param={'cycle.name', 'soc', 'socmenu', 'SOCiter',
'SOCtol', 'number'};
   input.cycle.value={'CYC_NYCC', 'on', 'linear', 15, 0.5, 3};
   [error,resp]=adv_no_gui('drive_cycle',input);
end

% assign objective value, if an error occurred penalize the objective
function?
if ~error
    % subtract mpgge so that when we minimize obj we attempt to
maximize the mileage
    %   $1000/kW of fuel cell
    %   $300 per motor kW
    %   $500 per battery
    %   $1 per mpg
    obj = 1000*0.749*x(1) + 300*16*x(2) + 500*6*x(3) -
resp.cycle.mpgge;

    [stat_text, txt_error] = sprintf('MPG(GE) Estimate: %g\nDelta SOC:
%g\nDelta trace: %g', resp.cycle.mpgge, max(abs(resp.cycle.delta_soc)),
max(resp.cycle.delta_trace));
    disp(stat_text);
else
    obj=100000;
end

[stat_text, txt_error] = sprintf('Objective Function F(%g, %g, %g, %g):
%g\n', x(1), x(2), x(3), resp.cycle.mpgge, obj);
disp(stat_text);

% assign constraint value (what to do for error situation?)
if ~error
```

```
   assignin('base','con',[max(abs(resp.cycle.delta_soc));
max(resp.cycle.delta_trace)])
end

return
```

```
% con_fun_thesis_scooter.m
function [con, con_e]=con_fun(x,varargin)

con=evalin('base','con');

offset=length(con);

% run acceleration test
input.accel.param={'spds'};
input.accel.value={[0 31.06; 18.64 31.06; 0 18.64]}; % speeds for
acceleration test in mph
[error, resp]=adv_no_gui('accel_test',input);
if ~error&~isempty(resp.accel.times)
   con(offset+1,1)=resp.accel.times(1);
   con(offset+2,1)=resp.accel.times(2);
   con(offset+3,1)=resp.accel.times(3);
else
   con(offset+1:offset+3,1)=100;
end

accel_str = sprintf('Accel Test (0-50, 30-50, 0-30)(km/h): %g, %g,
%g\n', con(offset+1,1), con(offset+2,1), con(offset+3,1));
disp(accel_str);

% run grade test
input.grade.param={'duration','ess_init_soc','ess_min_soc','disable_sys
tems','add_mass','speed'};
input.grade.value={30, 0.8, 0.1, 0, 0, 15}; % speed for grade test in
mph always
[error, resp]=adv_no_gui('grade_test',input);
if ~error&~isempty(resp.grade.grade)
   con(offset+4,1)=resp.grade.grade;
else
   con(offset+4,1)=0;
end

grade_str = sprintf('Grade Test: %g\n', con(offset+3,1));
disp(grade_str);

% matlab only
if length(varargin)>3
    for i=1:length(con)
        % varargin(4) is lower constraint bounds,
        % varargin(5) is the upper constraint bounds
        if varargin{4}(i)>-1e29
            con(i)=varargin{4}(i)-con(i);
        elseif varargin{5}(i)<1e29
            con(i)=con(i)-varargin{5}(i);
        end
    end
end
con_e=0;
% ****

return
```